The Relation of Geology to Stress Changes Caused by Underground Excavation in Crystalline Rocks at Idaho Springs, Colorado

---

GEOLOGICAL SURVEY PROFESSIONAL PAPER 965

U.S. DEPARTMENT OF THE INTERIOR

March 3, 1849

The Relation of Geology to Stress Changes Caused by Underground Excavation in Crystalline Rocks at Idaho Springs, Colorado

By FITZHUGH T. LEE, U.S. GEOLOGICAL SURVEY, JOHN F. ABEL, JR., COLORADO SCHOOL OF MINES, *and* THOMAS C. NICHOLS, JR., U.S. GEOLOGICAL SURVEY

GEOLOGICAL SURVEY PROFESSIONAL PAPER 965

A study to understand the effects
of geology and rock stresses on
mining in complexly deformed
anisotropic metasedimentary rocks
using theoretical, laboratory,
and field investigations

U.S. DEPARTMENT OF THE INTERIOR
March 3, 1849

UNITED STATES GOVERNMENT PRINTING OFFICE, WASHINGTON : 1976

UNITED STATES DEPARTMENT OF THE INTERIOR

THOMAS S. KLEPPE, *Secretary*

GEOLOGICAL SURVEY

V. E. McKelvey, *Director*

Library of Congress Cataloging in Publication Data
Lee, Fitzhugh T.
The relation of geology to stress changes caused by underground excavation in crystalline rocks at Idaho Springs, Colorado.
(Geological Survey Professional Paper 965)
Bibliography: p.
1. Rock mechanics. 2. Rocks, Crystalline.
I. Abel, John F., joint author. II. Nichols, Thomas C., joint author. III. Title: The relation of geology to stress changes caused by underground excavation... IV. Series: United States Geological Survey Professional Paper 965.
TA706.L43 557.3'08s [622'.2] 76-16054

For sale by the Superintendent of Documents, U.S. Government Printing Office
Washington, D.C. 20402
Stock Number 024-001-02916-2

CONTENTS

ILLUSTRATIONS

TABLES

METRIC-ENGLISH EQUIVALENTS

Metric unit	English equivalent	Metric unit	English equivalent
Length		**Stress**	
millimetre (mm)	= 0.03937 inch (in)	kilonewtons per square meter (kN/m^2)	= 0.145 pound per square inch (lb/in^2)
metre (m)	= 3.28 feet (ft)		
kilometre (km)	= .62 mile (mi)		

THE RELATION OF GEOLOGY TO STRESS CHANGES CAUSED BY UNDERGROUND EXCAVATION IN CRYSTALLINE ROCKS AT IDAHO SPRINGS, COLORADO

By FITZHUGH T. LEE, JOHN F. ABEL, JR.[1] and THOMAS C. NICHOLS, JR.

ABSTRACT

A comprehensive rock-mechanics study, including theoretical, laboratory, and field investigations, was performed to better understand the influence of certain geologic features and excavation procedures on the stress changes and deformations induced by excavations in a faulted and altered crystalline rock mass. The geologic and excavation factors considered included the structural geologic framework, the tectonic and residual components of the in situ stress field, and the sequence and orientation of excavations. The field results are based upon three-dimensional measurements of geologic features, stress changes, and the nature of the excavation.

Part of the study consisted of developing a basis for interpreting stress data obtained with the U.S. Geological Survey solid-inclusion borehole probe. For this purpose, extensive theoretical analysis and testing in models were required before field data from the probe could be adequately interpreted. These preliminary investigations established the theoretical basis for the probe and developed the confidence necessary for its use. No complete theoretical three-dimensional elastic analysis exists for the complex geometry and stress-strain relations of the borehole probe-host material system. However, two approximate methods were used to analyze the response of the probe to changes of stress. These involved the mathematical combination of two plane-strain elastic analyses of planes parallel to and perpendicular to the probe axes and the elastic evaluation of the probe using axisymmetric finite-element models of the probe. Results from the two approaches were in close agreement; average stress-concentration factors (SCF) were calculated for a range of rock and sensor properties. The SCF is necessary to convert strains measured on the spherical sensor of the probe to stress changes in the host-rock body.

In the field study we recognized discrepancies between measured stresses and those predicted on the basis of simple gravity-loading and elastic behavior. Geologic discontinuities, especially faults and foliation as well as excavation procedures, control the orientation and magnitude of stresses in granitic and metasedimentary rocks at the field site at Idaho Springs, Colo. Stress changes, determined at several locations in the mine at an average depth of 107 m (350 ft), were not satisfactorily predicted by simple gravity loading through elastic analysis. The magnitudes of the in situ stresses, determined by the overcoring method, and of stress changes induced by excavating a crosscut and two rooms greatly exceeded the stresses predicted using elasticity relations and overburden loading; the average horizontal stress components and the average vertical stress component of the in situ stress field are three times and twice as large, respectively.

Reasons for such discrepancies, in some instances, could be identified. If not near a fault, two of the in situ principal stresses are commonly parallel to the pervasive foliation and the other principal stress is commonly normal to foliation. The principal stress orientations vary approximately with the foliation attitude. Adjacent to faults, however, major and minor principal stress changes either were coincident with the fault normal or were in the plane of the fault. Strain energy, naturally concentrated along faults, was further concentrated in rock adjacent to both faults and underground openings; vertical decompression of 7,000 lb/in^2 was triggered in one place by excavation through a fault. Stresses determined by overcoring were unequal in opposite walls of faults, differing by a factor of 2.

The excavation process also contributed to changes in the magnitudes and directions of the principal stresses in the vicinity of the excavation. The direction of the greatest decompressive stress changed during excavation so that it remained perpendicular to the greatest room cross section.

Stress changes occurred some 7 diameters ahead of the advancing crosscut driven in the jointed and closely foliated gneiss and gneissic granite. Instrumentation placed ahead of three model tunnels detected compressive stress changes 4 diameters in concrete, and 2 diameters in granite. These findings are far different from a theoretical elastic estimate of the onset of detectable stress change at 1 tunnel diameter ahead of the face. In addition, minor compressive stress peaks were detected about 6 diameters ahead of the crosscut, 2 diameters ahead of the face in acrylic, 1.25 diameters in concrete, and 1 diameter in granite. These subsidiary stress peaks are not explained by available theory. Such rock-mass behavior, if not anticipated, might result, especially in a complex (multiple-opening) underground operation, in damage of support systems owing to overloading.

Laboratory and field data suggest that the stress field may have both residual (locked-in) and tectonic or gravity components. The release of residual strain energy is principally brought about by excavation through excavation-induced fault movements. Disturbances of the stress field caused by the intermittent excavation in the mine in part were time dependent, with stabilization requiring weeks to months.

INTRODUCTION

The laboratory and field investigations described in this report were started by the U.S. Geological Survey in July 1965 and completed in August 1971. The investigation was conducted as part of a continuing program in rock mechanics research whose main purpose is to examine rock behavior with respect to engineering problems associated with surface and underground excavation in rock.

The literature contains very few studies that recognize or demonstrate the importance of three-dimensional information in the analysis of rock deformation due to tunneling or mining. Because this problem is three-dimensional, an appropriate solution should logically be expressed in this form. In the past, the lack of adequate instrumentation together with inadequate geologic data has

---

[1] Colorado School of Mines, Golden, Colo.

greatly restricted interpretations and conclusions of rock-mass behavior.

The response of a rock mass to excavation is commonly analyzed by assuming: that the in situ stress field is gravitational, the rock mass is elastic, the excavation techniques are uniform, and the excavation is instantaneous. This approach cannot take into account a number of factors which could be important; namely, the geologic framework, tectonic and residual components of the in situ stress field, the variability of excavation techniques, and the sequential nature of excavation. The purpose of this investigation was to determine the importance of these factors to the response of a specific rock mass to the excavation of geometrically simple tunnels and rooms.

The scope of the investigation included: (1) the development and application of a borehole probe to determine the initial in situ stress field and the stress changes induced by excavation, (2) a detailed investigation of the site geology, and (3) deformation analyses to discover shortcomings of conventional analytical methods and the nature and importance of the effects of commonly neglected factors.

The initial in situ stresses and the excavation-induced stress changes were monitored with the three-dimensional stress probe described by Nichols, Abel, and Lee (1968). Also, at some of the underground locations, other instruments were used.

To provide an adequate basis for interpreting probe measurements, detailed theoretical and controlled laboratory studies of the probe's behavior were conducted. The theoretical studies consisted of finite-element analyses of probe geometry and boundary conditions, which were compared with other mathematical solutions. The laboratory studies consisted of testing the probe under known applied stresses in three models of known physical properties: acrylic, concrete, and Silver Plume Granite. Also, each probe was tested and was calibrated under hydrostatic pressure. The results of these preliminary investigations of the probe were further verified by driving (drilling) model tunnels into the three laboratory models. Stress changes were monitored during the course of model-tunnel driving. These stress distributions and magnitudes were compared with theoretical elastic predictions and with field data available from other sources, and the probe-stress values were found to be reasonable and reliable.

The field investigations described in this report were performed at the Colorado School of Mines experimental mine at Idaho Springs, Colo. The geologic framework—a faulted sequence of metasedimentary rocks intruded by granitic and pegmatitic rocks—is characterized by faults, foliation, and joints. These geologic structural features, often ignored in practice, largely controlled the behavior of the stress field and the deformation of the excavation.

In addition to geologic mapping, the field investigation included the installation of 17 borehole probes at various times in conjunction with the excavation of two rooms and a central connecting crosscut; 16 of these probes produced useful data. Seven were employed to obtain in situ stress-field information, and nine were used to monitor stress changes for periods of up to 4 years. These stress changes resulted from the excavation of the rooms and the central crosscut connecting them. The borehole extensometer measurements of other investigators at the field location contributed to our understanding of rock-mass response.

ACKNOWLEDGMENTS

The investigations benefited from the assistance of several individuals whose help is gratefully acknowledged. R. A. Farrow, U.S. Geological Survey, performed or supervised the many laboratory deformation tests and assisted us in the model investigations. G. S. Erickson fabricated the borehole probes and assisted valuably in collecting readings from the several monitoring probes. We thank R. S. Culver and R. N. Cox, then at the Colorado School of Mines, who supervised the underground excavations and made available to us other rock-strain data from the experimental mine. Cox also was responsible for the finite-element analyses of the borehole probe. J. J. Reed, Samuel Shaw, and Martin Forsmark, all of the Mining Engineering Department, Colorado School of Mines, generously made available appropriate sites in the experimental mine and provided necessary logistical services at the mine. Michael Haverland, U.S. Bureau of Reclamation, furnished in situ stress data from a borehole in the underground study area. We are indebted to D. J. Varnes, H. W. Olsen, A. T. F. Chen, and R. H. Moench for their thought-provoking and enlightening comments and criticism.

INSTRUMENTATION ANALYSES

The borehole probe (Nichols and others, 1968) measures host-rock stress changes in three dimensions in terms of strains induced in the surface of the incapsulated spherical metal sensor. The relation between measured strains and host-rock stresses varies with the geometry and material properties of the probe-rock system. The operation of this complex system, not previously investigated, had to be explained before the desired information, stress in the rock, could be determined.

With its incapsulated spherical sensor, the borehole probe acts as a welded cylindrical inclusion within a semi-infinite elastic rock mass (fig. 1). In addition to these geometric influences on strain measurements, the strain of the sensor is also influenced by differences in the elastic properties of the three materials. These two factors induce stress concentrations about the sphere and about the cylinder when the host body is stressed. (Stress concentration is the ratio of the stress at any point to the applied stress.) The configuration and magnitude of these stress

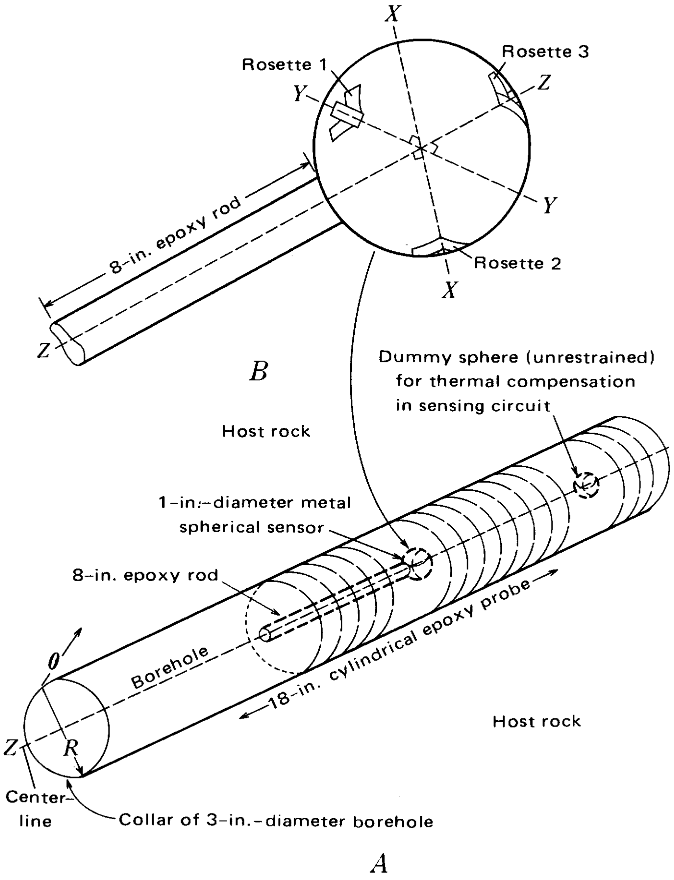

FIGURE 1.—U.S. Geological Survey three-dimensional borehole probe. *R*, radial direction; *Z*, axial direction; *θ*, tangential direction.

A, Relationship of spherical sensor to cylincrical epoxy probe and host rock.

B, Location of strain-gage rosettes on spherical sensor.

concentrations had to be determined in order to obtain the composite stress concentration factor (SCF) needed for the calculation of stresses in the host material. The borehole probe initially contained a steel sensor; subsequent probes utilized other more sensitive metals, including aluminum and brass. The test results are sufficiently general to apply to the other metal sensors.

In this report the maximum principal stress is the most compressive (or least tensile) and compression is positive.

This section describes the analytical bases developed to calculate host-rock stress changes from measurements of sensor strain changes. Three approaches were used: (a) adaptation of exact mathematical solutions for a cylinder and a sphere within a semi-infinite medium, (b) a finite-element representation of the probe-host-rock system, and (c) the analysis of stress changes in model tunnels. This laboratory study of model tunnels was also helpful in checking theoretically predicted probe behavior and in understanding the results of the field investigations.

The following assumptions were required in order to proceed with these analyses:

1. The rock mass, epoxy grout, and sphere are elastic, homogeneous, and isotropic.
2. The stress field is hydrostatic, compressive, and equal to unity.

In summary, the problem was to relate the strain in a semirigid spherical inclusion to the host-rock stress, where the spherical inclusion is enclosed within a cylinder of different material and the cylinder is bonded to and bounded by bedrock.

STRESS CONCENTRATION CALCULATIONS

In order to obtain stresses in the rock, the sensor-strain readings must be corrected for the stress-concentrating effects of geometry (sphere and cylinder) and of the different materials (rock, epoxy, metal). These effects interact simultaneously when the rock mass is subjected to a stress change. Further, the analysis must consider concentrations in both the *R* and *Z* directions (fig. 1).

Changes in σ_R in the host rock are modified near and within the probe as follows: (1) the stresses in the rock mass near the probe are modified by the epoxy cylinder and the spherical sensor, and (2) at the same time, the stresses in the epoxy cylinder are modified by the presence of the spherical sensor (fig. 2*A*).

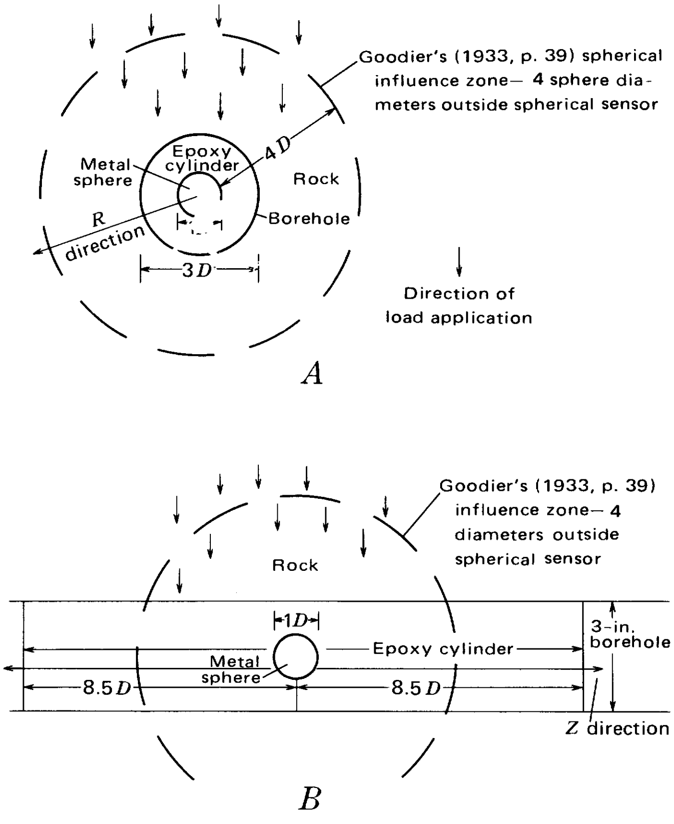

FIGURE 2.—Cross sections of borehole probe showing dimensions and geometric relationships

A, *R* direction—Perpendicular to centerline of borehole probe.

B, *Z* direction—Parallel to centerline of borehole probe.

Changes in σ_Z in the host rock are modified only by the epoxy cylinder (fig. 2*B*). In this direction there is sufficient epoxy (greater than 4 sphere diameters beyond the spherical sensor) so that there is no significant effect produced in the rock by the spherical sensor (Goodier, 1933, p. 39).

Stress changes in the host rock acting at angles greater than 20.5° from the *Z* direction will have less than 4 sphere diameters of epoxy between the sensor and the epoxy-rock interface. Within an intermediate angular zone, from 20.5° to 90° to the *Z* direction, the overall stress concentration will lie between the *R*- and *Z*-direction analyses. The greater the thickness of epoxy between the spherical sensor and the epoxy-rock interface the more closely the sensor will follow the analysis in the *Z* direction. Conversely, the smaller the thickness of epoxy between the spherical sensor and the epoxy-rock interface the more closely the sensor will follow the analysis in the *R* direction. A flow diagram illustrating the mathematical calculations used to determine the SCF in the two directions is shown in figure 3.

MATHEMATICAL CALCULATION OF STRESS CONCENTRATIONS

STRESS CONCENTRATIONS PERPENDICULAR TO BOREHOLE AXIS (*R* DIRECTION)

The stress-concentrating effects of the sphere and of the cylinder were calculated separately; these results were then superposed to obtain the composite SCF (fig. 3).

The stress changes occurring in the rock and the epoxy cylinder at the boundary of a rock mass and in the epoxy cylinder can be calculated from the stress concentration

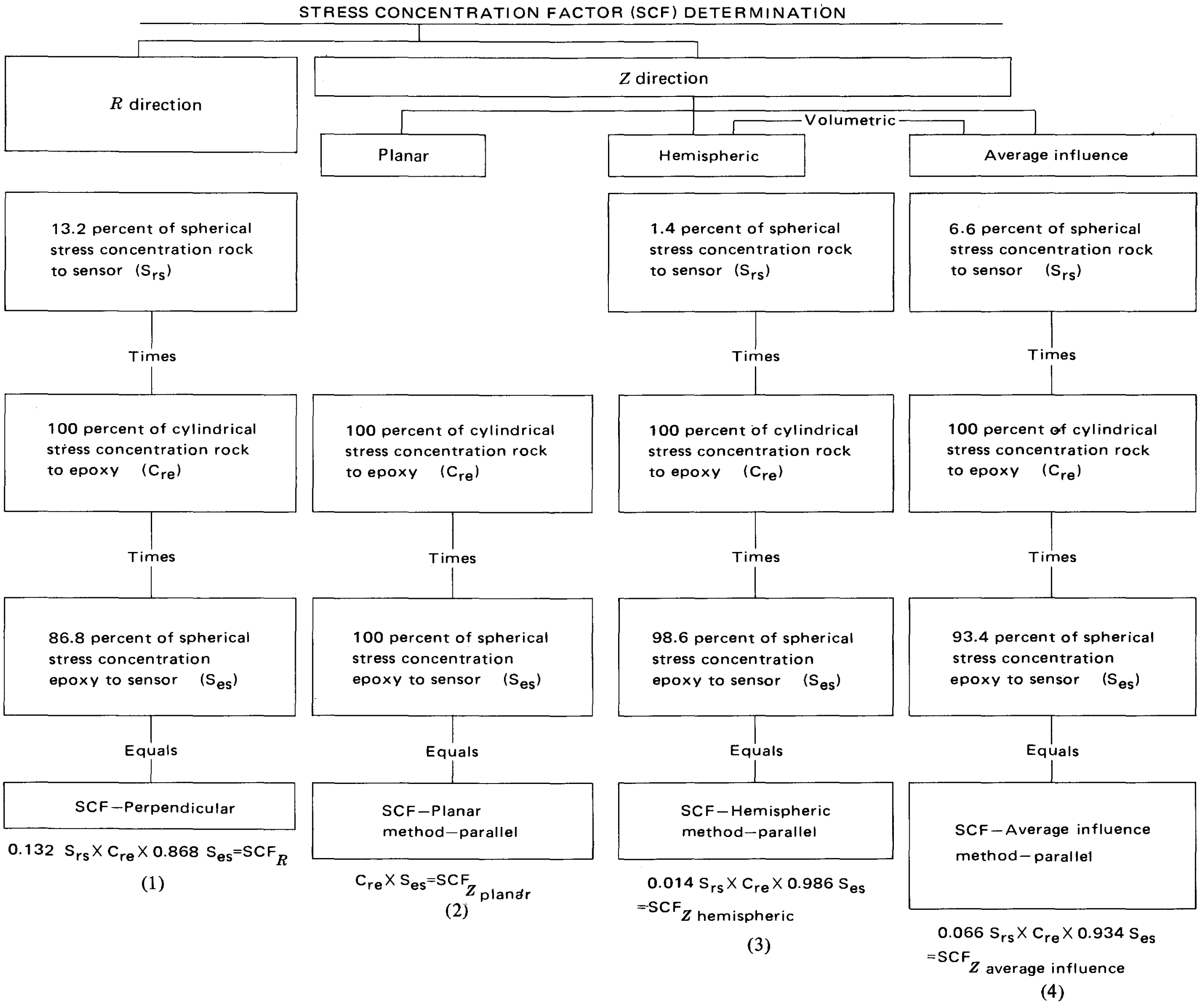

FIGURE 3.—Flow diagram of mathematical methods for calculation of stress concentration factor (SCF).

equation of N. J. Muskhelishvili (in Leeman, 1964, p. 55) and are dependent on the relative stiffness and Poisson's ratios of the rock and of the epoxy. This cylindrical stress concentration is actually a ratio:

$$\frac{\sigma'}{\sigma} = (1-\nu^2)\left[\frac{1}{(\nu+1)+E/E'(\nu'+1)(1-2\nu')} + \frac{2}{E/E'(\nu'+1)+(\nu+1)(3-4\nu)}\right], \qquad (5)$$

where

σ'=stress in cylindrical epoxy inclusion
σ=stress in rock mass (applied stress)
E'=stiffness of epoxy (Young's modulus)
E=stiffness of rock mass (Young's modulus)
ν'=Poisson's ratio of epoxy
ν=Poisson's ratio of rock mass.

For example, the cylindrical stress concentration in an epoxy cylinder with $E'=0.45\times10^6$ lb/in^2 and $\nu'=0.28$ within a rock mass with $E=4.5\times10^6$ lb/in^2 and $\nu=0.25$ is 0.26 or $\sigma'=0.26\sigma$.

A spherical stress concentration is produced at the boundary and within a sphere surrounded by an infinite elastic body that is a function of the relative stiffness (E) and Poisson's ratio (ν) of the sphere and the host. This relationship has been determined mathematically by Goodier (1933) and Edwards (1951) and is shown in figure 4. For a steel sphere surrounded by an infinite body of elastic epoxy—that is, a cylinder greater than 4½ diameters larger than the sensor diameter and with values of $E=0.45\times10^6$ lb/in^2 and $\nu=0.28$, the spherical stress concentration at the boundary and in the steel sphere is approximately 1.9, or $\sigma'=1.9\sigma$,

where

σ'=stress in spherical steel inclusion
σ=stress in infinite mass of epoxy

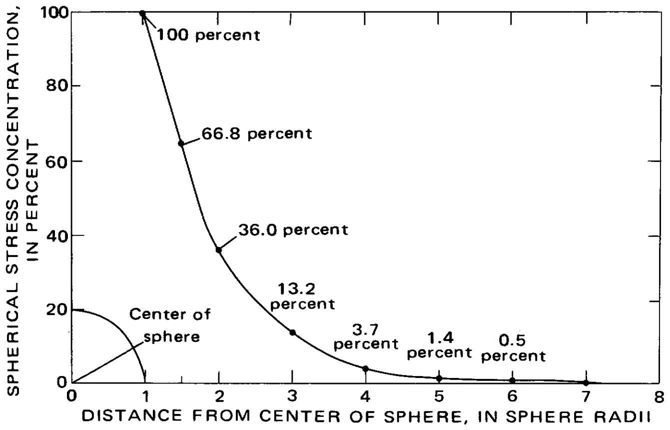

FIGURE 4.—Spherical stress concentration. Percent of total concentration at various diameters from center of sphere. (From Goodier, 1933, p. 41.)

However, the epoxy cylinder extends only 1½ sphere diameters beyond the center of the spherical sensor, so the epoxy is not an infinite body. According to information in figure 4, the spherical stress concentration more than 1½ sphere diameters from the center of the sphere (the rock mass-epoxy boundary) is approximately 13 percent. The remaining 87 percent of the spherical stress concentration takes place between the rock-epoxy boundary and the sphere-epoxy boundary.

Following the principle of superposition, the stress-concentrating effects of the spherical sensor may be combined with the stress-concentrating effects of the epoxy cylinder. For the example shown in figure 5*A*, the calculation of the spherical stress concentration in the rock at the rock mass-epoxy boundary (S_{rs}) in the *R* direction is

$$1+0.68(0.132)=1+0.09,$$

where

1+0.68 is the maximum spherical stress concentration in the rock mass as determined graphically by Edwards' method (1951, p. 27),

and

0.132 is the percent spherical stress concentration more than 1½ diameters from the center of the sphere (fig. 4).

This stress is simultaneously acted upon by a cylindrical stress concentration in the rock mass due to the epoxy cylinder, C_{re},

$$(1+0.09)(0.259)=0.282$$

(Leeman, 1964, p. 55). The epoxy between the rock and the steel sphere then produces another increment of stress concentration at the steel-epoxy boundary (S_{es}). This increment is equal to 1+spherical stress concentration from the epoxy cylinder to the spherical steel sensor times the remaining theoretical spherical stress concentration for a perfectly rigid sphere. This result is multiplied by the cylindrical stress concentration in the epoxy cylinder.

$$[1+0.132(0.68)](0.259)[1+(1-0.132)(0.90)]=0.50=\mathrm{SCF}_R. \qquad \text{(eq 1, fig. 3)}$$

Therefore, in this example the steel sphere should sense 0.50 lb/in^2 for 1 lb/in^2 stress change occurring in the *R* direction. Figure 5*B* shows the steps in the stress concentration which have taken place.

STRESS CONCENTRATIONS PARALLEL TO BOREHOLE AXIS (*Z* DIRECTION)

We must now determine the stress concentrations in the host material in the *Z* direction and compare these with the stress concentrations in the *R* direction, and then we determine the required composite stress concentration factor (SCF).

The stress acting in the *Z* direction (σ_Z) is influenced

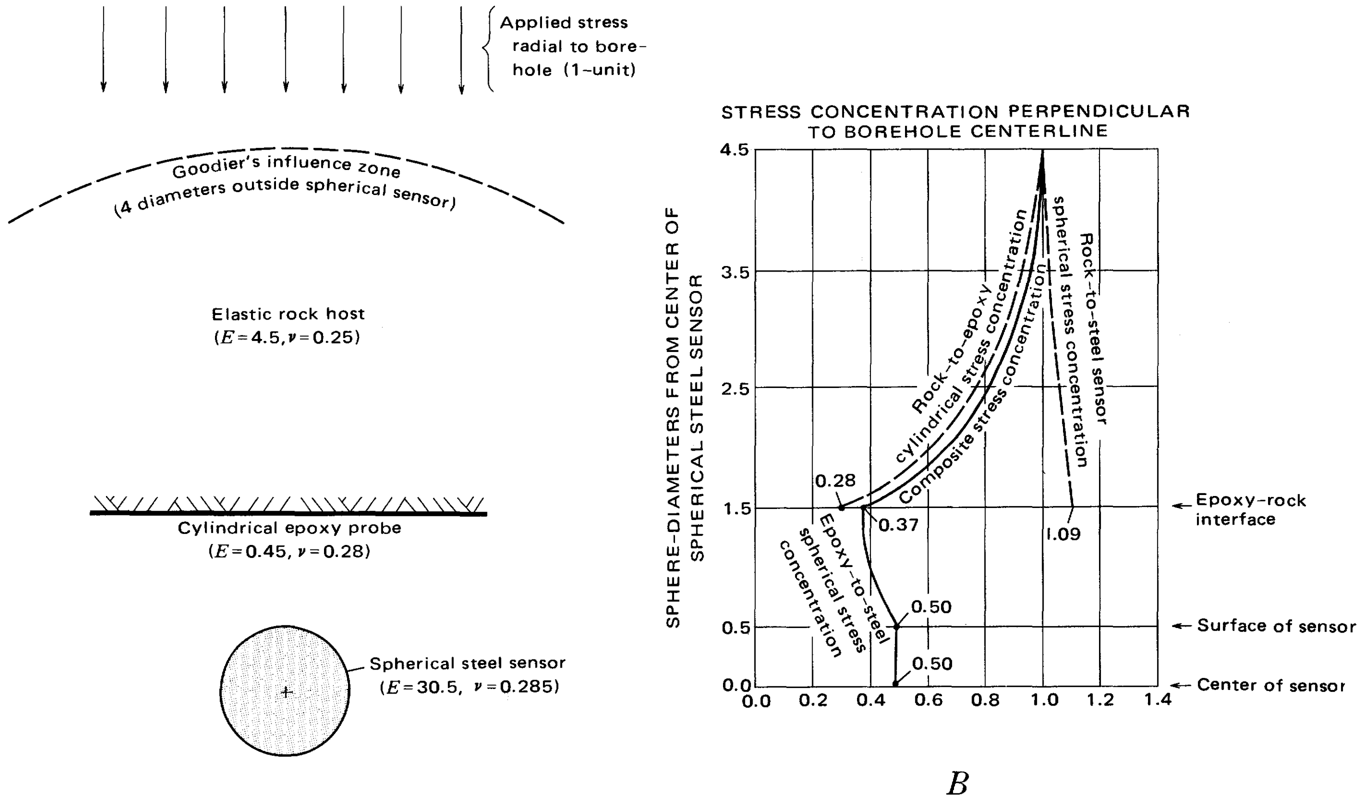

FIGURE 5.—Stress concentrations for example conditions in the R direction. *A*, Goodier's (1933) spherical influence zone. *B*, Superposition of stress concentrations in rock mass.

less by the spherical stress concentration within the rock mass than is the stress acting in the R direction (σ_R), as mentioned previously. Three different approximations for estimating σ_Z concentrations were made (fig. 6).

In the first method, the adjacent rock was assumed to have no significant influence on σ_Z because more than 4 sphere diameters of epoxy are present in that direction (fig. 6*B*). Strain changes in the Z direction are transmitted across the epoxy-rock interface by the bond between the rock and epoxy. This is referred to as the planar method of approximation because the stress is assumed to be transmitted in a plane in the Z direction and confined to the epoxy. This method does not consider any spherical stress concentration from the rock to the spherical sensor.

In the second method, the cylinder of epoxy is replaced by a hemisphere whose volume equals half the volume of the epoxy cylinder (fig. 6*C*). This method assumes that there is a constant spherical stress concentration produced by the spherical sensor on the rock regardless of the angle the stress change makes with the Z direction.

The third method assumes that the spherical stress concentration (rock to spherical sensor) in the rock has an average influence, or effectiveness, which ranges from 13.2 percent to 0.0 percent in the R direction (fig. 6*D*).

For the planar method, the overall stress concentration is equal to the cylindrical rock-to-epoxy stress concentration times the full spherical stress concentration of the epoxy acting upon the steel sphere. For the example, this stress concentration is equal to

$$0.259(1+0.90)=0.49=SCF_Z. \quad \text{(eq 2, fig. 3)}$$

The hemispheric method is nearly the same as the method of calculation of σ_R, once the radius of the hemisphere has been calculated (fig. 6*C*). Because of the finite geometry of the probe, only 1.4 percent of the total spherical stress concentration of the rock on the steel sensor would occur beyond the calculated 6.35-cm (2.5 in.) sphere-radius hemisphere:

$$1+(0.68)(0.014)=1.01.$$

This concentration is also acted upon by the cylindrical stress concentration of the rock on the epoxy.

$$1.01(0.259)=0.26.$$

A further spherical concentration occurs at the epoxy-steel interface, as follows:

$$0.26[1+0.90(1-0.014)]=[1+0.90(0.986)]0.26=0.49=SCF_Z. \quad \text{(eq 3, fig. 3)}$$

The average influence method represents a compromise which should approximate the average conditions in the Z and R directions. This method follows the same calculation as for σ_R except that the average stress concen-

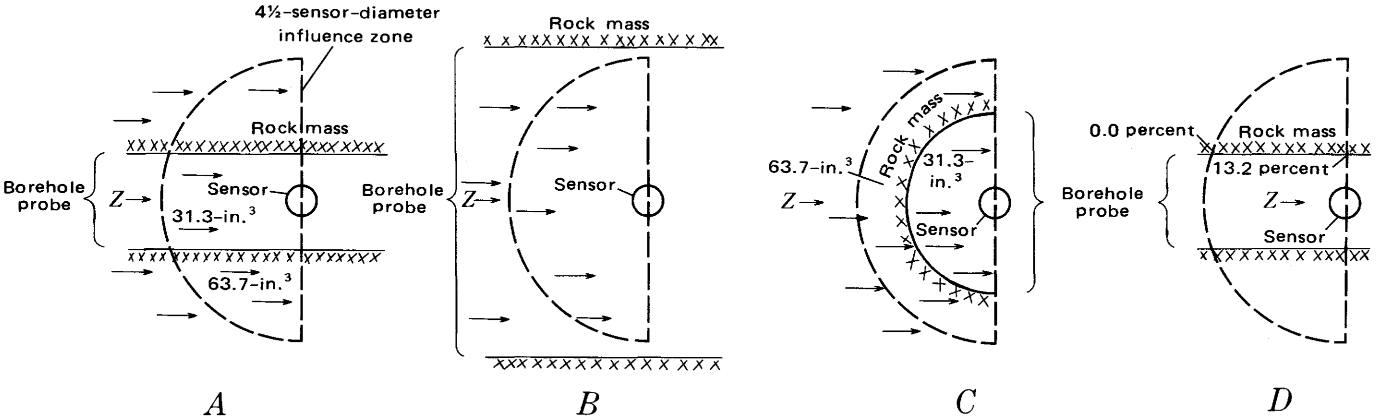

FIGURE 6.—Determinations of stress concentrations in the Z direction. Arrows indicate direction of stress application. Volumes are explained in text (p. 5).

A, Actual case.

B, Planar method (assumes that diameter of borehole probe exceeds diameter of influence).

C, Hemispheric volume method (assumes that cylindrical volume of epoxy is replaced by equal-volume hemisphere).

D, Average influence method (assumes that only average stress concentration in rock mass is effective; that is, 13.2 percent of theoretical normal stress).

tration effect is reduced from 13.2 percent to 6.6 percent. This results in an overall σ_Z concentration of 0.50, the same as that calculated for σ_R. The calculations for the average influence method proceed as follows:

Spherical stress concentration (rock on steel sensing sphere)

$$1+0.68(0.066)=1.04,$$

Cylindrical stress concentration (rock on epoxy cylinder)

$$1.04(0.259)=0.27,$$

Spherical stress concentration (epoxy on steel sensing sphere)

$$0.27[1+0.90(0.934)]=0.50=SCF_Z. \text{ (eq 4, fig. 3)}$$

SUMMARY OF MATHEMATICAL CALCULATIONS OF STRESS CONCENTRATIONS

Table 1 gives calculated percentage differences between the stress magnitudes that should be sensed by the probe, perpendicular to and parallel to the probe axis, for various host-rock and sensor properties using the methods just described.

The close correspondence between the mathematical analyses (table 1) indicated that a composite SCF value could be expressed by any of the equations (1-4) in figure 3. Equation 4 was used for the parallel concentration factor because it is closer to the actual geometry. An appropriate SCF value is applied to all stress calculations using borehole-probe strain measurements.

FINITE-ELEMENT ANALYSES OF STRESS CONCENTRATIONS

The finite-element analytical method provided an independent check on the SCF developed in the preceding section. The symmetry of construction of the borehole probe was appropriate for analysis by finite-element techniques. The principles of this method were outlined by Medearis (1974, p. 219-266). The U.S. Geological Survey contracted with R. M. Cox, then (1969) a graduate student in mining engineering at the Colorado School of Mines, to perform these analyses. The results agreed closely with the

TABLE 1.—*Differences between theoretical stress concentrations perpendicular to and parallel to the borehole axis*

[E=Young's modulus (10^6 lb/in^2); ν=Poisson's ratio; epoxy grout: E=0.45, ν=0.28; steel sphere: E=30.5, ν=0.285; brass sphere: E=15.0, ν=0.285; aluminum sphere: E=10.6, ν=0.33. +, exceeds stress concentration perpendicular to borehole axis. -, less than stress concentration perpendicular to borehole axis]

Elastic host rock		Stress concentrations perpendicular to borehole axis	Percent difference in stress parallel to borehole axis[1]		
E	ν		Linear method	Hemispheric method	Average influence method
		Steel sphere			
0.5	0.25	1.94	-4.4	-3.8	-2.0
1.0	.25	1.44	-4.0	-3.4	-1.9
1.5	.25	1.14	-3.7	-3.2	-1.6
3.0	.25	.70	-2.9	-2.3	-1.2
4.5	.25	.50	-1.8	-1.8	- .6
6.0	.25	.40	-1.5	-1.0	- .5
		Brass sphere			
0.5	0.25	1.90	-4.0	-3.5	-1.8
1.0	.25	1.40	-3.7	-3.3	-1.6
1.5	.25	1.11	-3.3	-2.9	-1.4
3.0	.25	.67	-1.6	-1.3	-.6
4.5	.25	.48	-.2	.0	+.2
6.0	.25	.38	+1.1	+1.1	+.8
		Aluminum sphere			
0.5	0.25	1.89	-3.7	-3.2	-1.4
1.0	.25	1.39	-3.4	-2.9	-1.4
1.5	.25	1.10	-2.7	-2.3	-1.3
3.0	.25	.66	.0	+.6	+.3
4.5	.25	.47	+2.1	+2.3	+1.6
6.0	.25	.37	+2.7	+2.7	+2.2

---

[1] Stress in axial direction of probe.

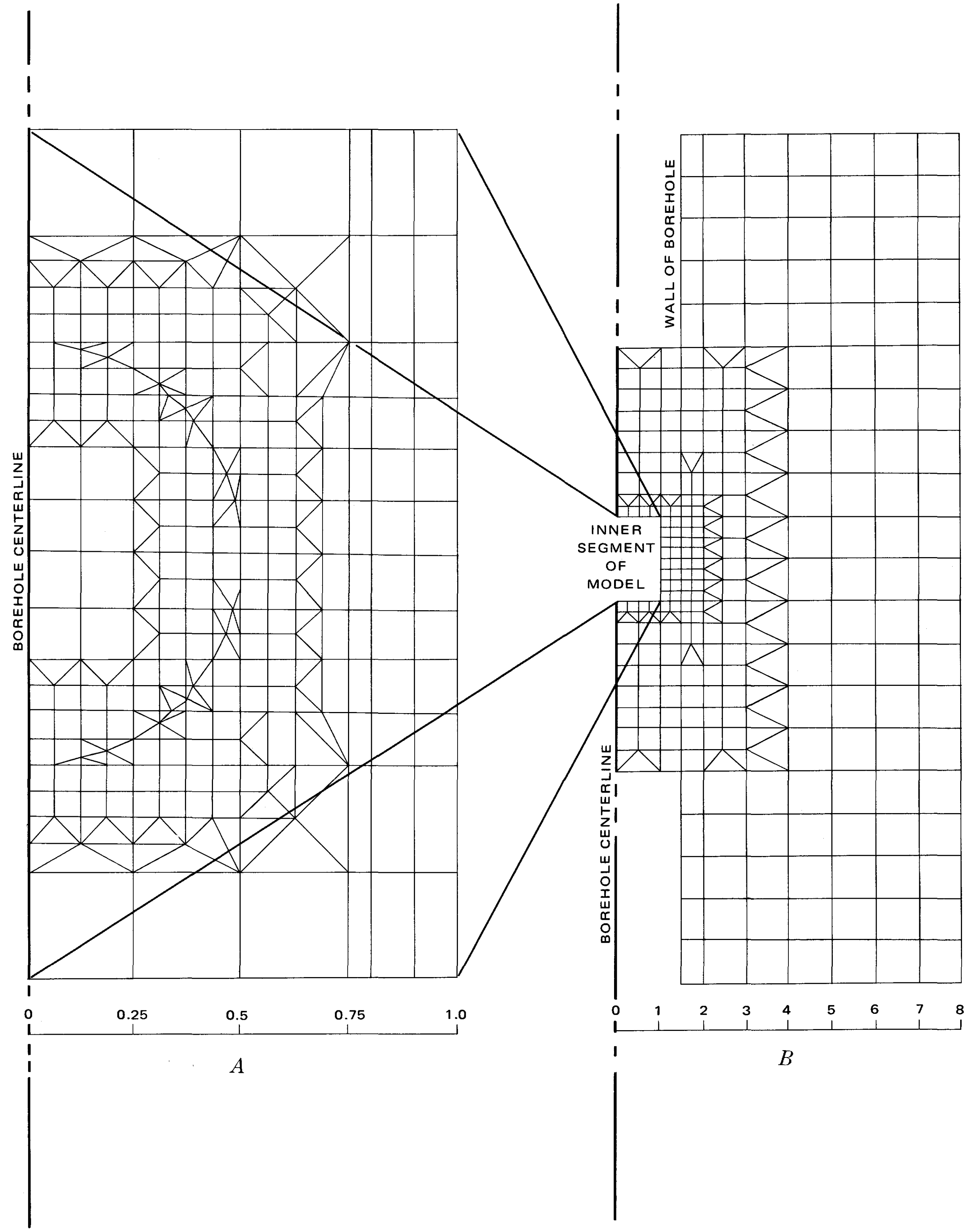

FIGURE 7.—Basic mesh for finite-element model. The mesh contains 665 elements and 573 nodal points. *A*, Mesh for inner segment *B*, Mesh for outer segment. Scales are sphere diameters from center of sphere.

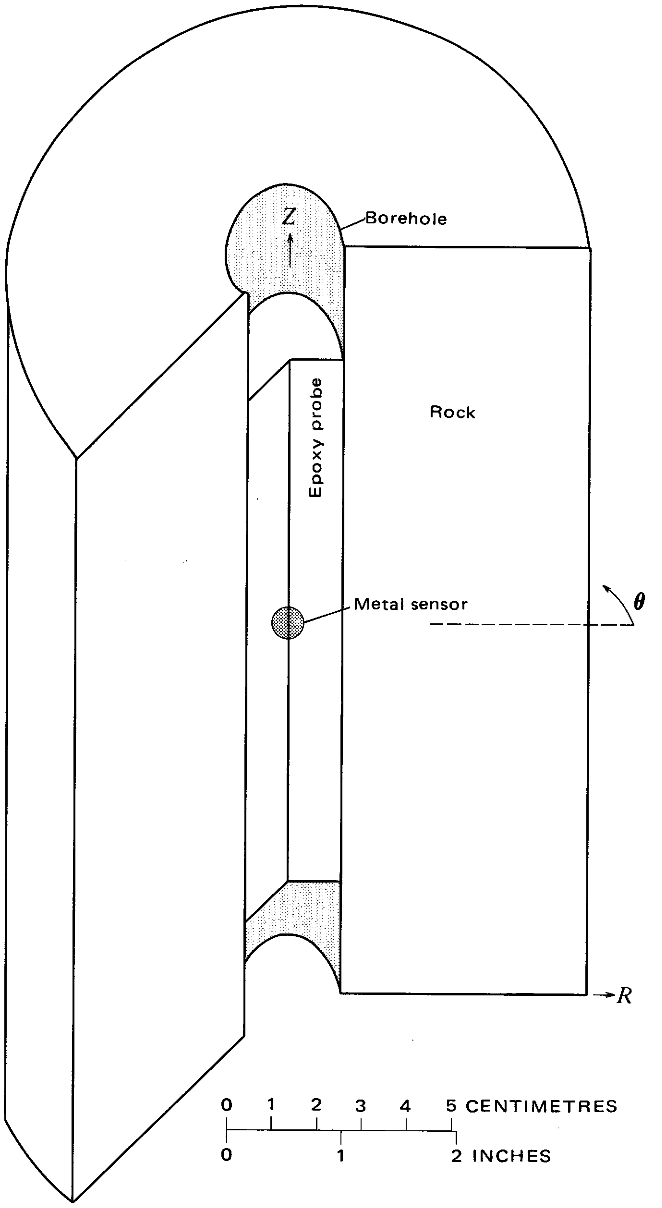

FIGURE 8.—Schematic diagram of axisymmetric problem. *R*, radial direction; *Z*, axial direction; *θ*, tangential direction.

mathematically derived SCF. The following presentation is taken in part from the report by R. M. Cox (written commun., 1969).

A finite-element model was constructed to facilitate the solution of a variety of problems concerned with stress distributions in the probe with a minimum number of changes (fig. 7). Element size was determined by proximity to critical stress areas. The model, when appropriately modified, could be used to study the effects of changes in rock properties, epoxy grout properties, and sensor properties on various loading conditions.

Two types of analyses have been made using the finite-element method: three-dimensional axisymmetric analyses and plane-strain analyses. The axisymmetric analysis, a more general technique, is shown schematically in figure 8. The exterior boundary of the rock mass is far enough from the probe (4½-sensor diameters in the *R* direction) to minimize stress effects on this boundary due to the sphere and cylinder. The plane-strain analysis (fig. 9) permitted estimation of stress distributions in the probe by an alternate method. It also was used to analyze stress-relief by overcoring of the borehole probe.

AXISYMMETRIC ANALYSES

The axisymmetric method was used to study the effects of changes in rock properties, epoxy properties, and spherical sensor properties as well as various load conditions on sensor strains and indicated stresses. After two preliminary analyses were made to test the effectiveness of the axisymmetric method, six additional axisymmetric analyses were made.

PRELIMINARY ANALYSES

Two preliminary finite-element analyses (A and B) were devised to represent two theoretically solved cases of a sphere within a nearly infinite mass under two boundary-loading conditions (fig. 7). Analysis A was subjected to a simulated hydrostatic stress field and analysis B was subjected to a deviatoric stress field. The results were com-

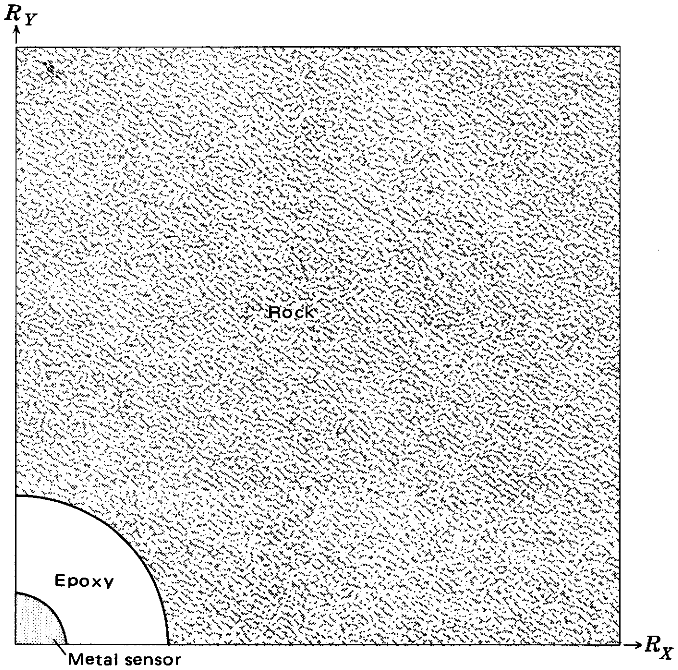

FIGURE 9.—Schematic diagram of plane-strain problem. Metal sensor simulated by cylinder of semi-infinite length.

pared with solutions of Goodier (1933, p. 40). Goodier found the radial stress concentration on such a sphere in a hydrostatic stress field to be

$$\frac{\sigma'}{\sigma''} = 3[(1-\nu)/(1+\nu)] , \qquad (6)$$

where

ν =Poisson's ratio of host material
σ'=stress in steel sphere
σ''=hydrostatic stress

It is apparent from this equation that the radial stress concentration depends on the Poisson's ratio of the host material. For analysis A the epoxy has a Poisson's ratio of 0.28. This value of Poisson's ratio yields a radial stress concentration of 1.69.

Analysis A, with a hydrostatic stress of 1,000 lb/in^2, gives a radial stress of 1,686 lb/in^2 at the steel-epoxy boundary. The radial stress concentration is 1.69, which agrees with the theoretical solution within 0.2 percent. The tangential stress concentration is 1.70 at the locations of rosettes 1 and 2 (rosette locations are shown in fig. 1*B*). The axial stress concentration (parallel to borehole centerline) for these rosettes is 1.64, which is within the probable 4-percent accuracy of the method. At the location of rosette 3, the radial and tangential stress concentrations are 1.77 ± 0.07. A plot of the stress distribution for analysis A is shown in figure 10*A*. The SCF in this case would be 1.72, with a maximum error of 5 percent in any one direction.

The second preliminary axisymmetric analysis (analysis B) had an applied radial stress of 1,000 lb/in^2 and an applied axial stress of 560 lb/in^2. The results of this solution are plotted in figure 10*B*. The radial stress concentration at the steel-epoxy boundary is 1.73, which falls close to the value of 1.69 derived from the mathematical solution of Goodier (1933). The average axial stress concentration is 1.63, with a maximum variation of 6 percent. Again, the axial stress concentration differs only slightly from the radial stress concentration.

From these results we conclude that the finite-element solutions, which can be checked for accuracy by comparing them with other solutions, can be used to estimate the SCF.

PROBE ANALYSES

After verification of the effectiveness of the axisymmetric finite-element method, several analyses of this model were made to study:

1. Distribution of stress in the steel-epoxy probe.
2. Effects of changes in host-rock properties on the stress distribution in the probe.
3. Distribution of stress for boundary-loading conditions present in the laboratory biaxial overcore testing device.

A list of the material properties and boundary-loading conditions used in these analyses is given in table 2.

TABLE 2.—*Finite-element model properties*

Analysis	Sphere		Epoxy cylinder		Host rock		Directions of boundary-loading conditions	
	[1]$E(10^6)$	ν	[1]$E(10^6)$	ν	[1]$E(10^6)$	ν	Radial[1]	Axial
				Axisymmetric analyses				
1	30.5	0.285	0.45	0.28	0.5	0.20	1,000	Fixed.
2	30.5	.285	.45	.28	1.0	.20	1,000	Do.
3	30.5	.285	.45	.28	2.0	.20	1,000	Do.
4	30.5	.285	.45	.28	4.0	.20	1,000	Do.
5	30.5	.285	.45	.28	6.0	.20	1,000	Do.

[1]Units in pounds per square inch.

Any finite-element solution is approximate. The precision of the approximation is dependent on the fineness of the mesh. In the case of the axisymmetric model, the theoretical tangential stress computed for rosettes 1 and 2 should be equal to the radial and tangential stresses computed for rosette 3 (fig. 1*B*). Table 3 shows the variations in these computed values. The indicated variation among the analyses is approximately 4 percent.

TABLE 3.—*Variations in radial and tangential stresses computed from finite element analyses*

[Median maximum variation from mean computed stress =4.1 percent]

Analysis	Host rock		Stresses computed at rosettes[1]				
	[1]$E(10^6)$	ν	1 and 2 (tangential)	3 (tangential)	3 (radial)	Mean[1]	Maximum variation (percent)
1	0.5	0.20	1,832	1,976	1,885	1,898	4.1
2	1.0	.20	1,392	1,497	1,423	1,437	4.2
3	2.0	.20	936	940	934	937	.3
4	4.0	.20	566	607	577	583	4.1
5	6.0	.20	405	434	413	417	4.1

[1]Units in pounds per square inch.

The SCF variation of about 4 percent indicated in table 3 could be reduced to less than 2 percent by using one factor for the tangential stress of rosettes 1 and 2 and radial stress of rosette 3, and another factor for the axial stress of rosettes 1 and 2 and the tangential stress of rosette 3. However, such precision is greater than the precision (about 4 percent) of the finite-element method and an average value for the SCF is used. These SCF's are listed in table 4 and plotted in figure 12*B*.

Over the range of conditions tested, the analyses indicate that the stresses in the metal sensor of the probe vary inversely with the host-rock modulus and that the stress concentration in the host rock at the epoxy-rock contact varies directly with the host modulus.

STRESS DISTRIBUTION

Analyses 1–5 (table 2) were made with the ends fixed (no deformation) and with a radial stress of 1,000 lb/in^2. Results from these analyses were used to construct the stress

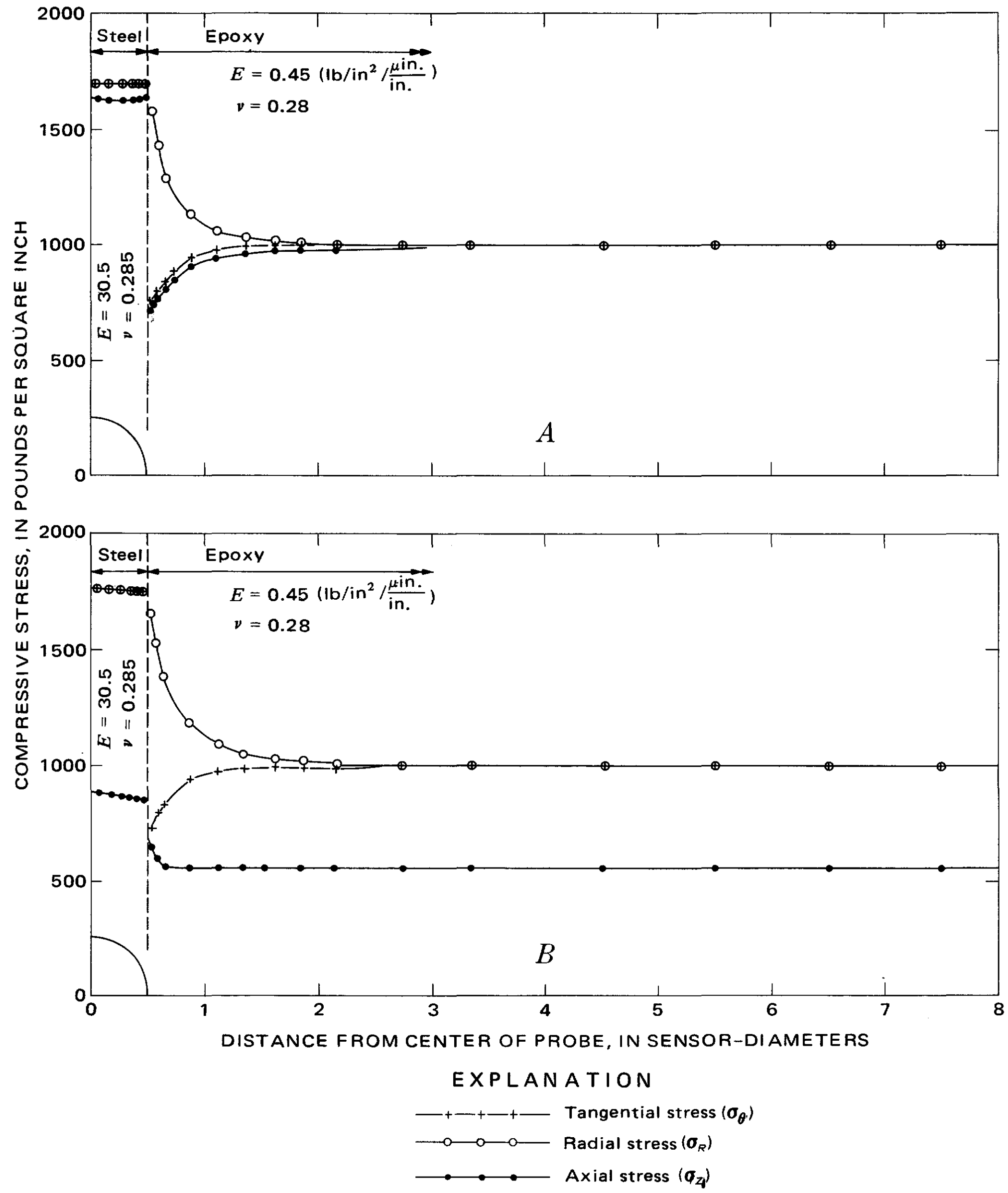

FIGURE 10.—Stress distribution from finite-element analysis along radial line cutting center of probe—steel sensor within epoxy mass.
A, Hydrostatic stress of 1,000 lb/in^2 (analysis A).
B, Triaxial stress of $\sigma_R = \sigma_\theta$ +1,000 lb/in^2, σ_Z=560 lb/in^2 (analysis B).

distributions along a radial line perpendicular to the axis of the borehole probe. The resulting stress distributions are shown in figure 11. Results of the mathematical stress concentration calculations (fig. 5*B*) are in good agreement with those from the finite-element analysis (fig. 11*D*).

SUMMARY OF STRESS CONCENTRATION FACTORS

The locations of the strain-gage rosettes on the probe sensor are shown in figure 1*B*. Because of the axial symmetry of the model, rosettes 1 and 2 should register the same strain (or stress) under uniform radial stress. Stress

TABLE 4.—*Average stress concentration factors (SCF's) for axisymmetric finite-element solution*

[Factor 1 is an average of the parallel tangential stress on rosettes 1 and 2 and the parallel radial stress on rosette 3. Factor 2 is an average of the parallel axial stress on rosettes 1 and 2 and the parallel tangential stress on rosette 3]

Analysis	Host rock		Average factor	Maximum difference (percent)	Factor 1	Maximum difference (percent)	Factor 2	Maximum difference (percent)
	[1]*E*(10^6)	ν						
1	0.5	0.20	1.90	6.5	1.85	1.6	1.95	5.7
2	1.0	.20	1.44	8.0	1.41	1.4	1.47	4.4
3	2.0	.20	.94	7.2	.94	1.1	.93	7.0
4	4.0	.20	.58	6.7	.57	1.7	.58	3.2
5	6.0	.20	.42	7.2	.41	1.2	.43	2.3

[1] Units in pounds per square inch.

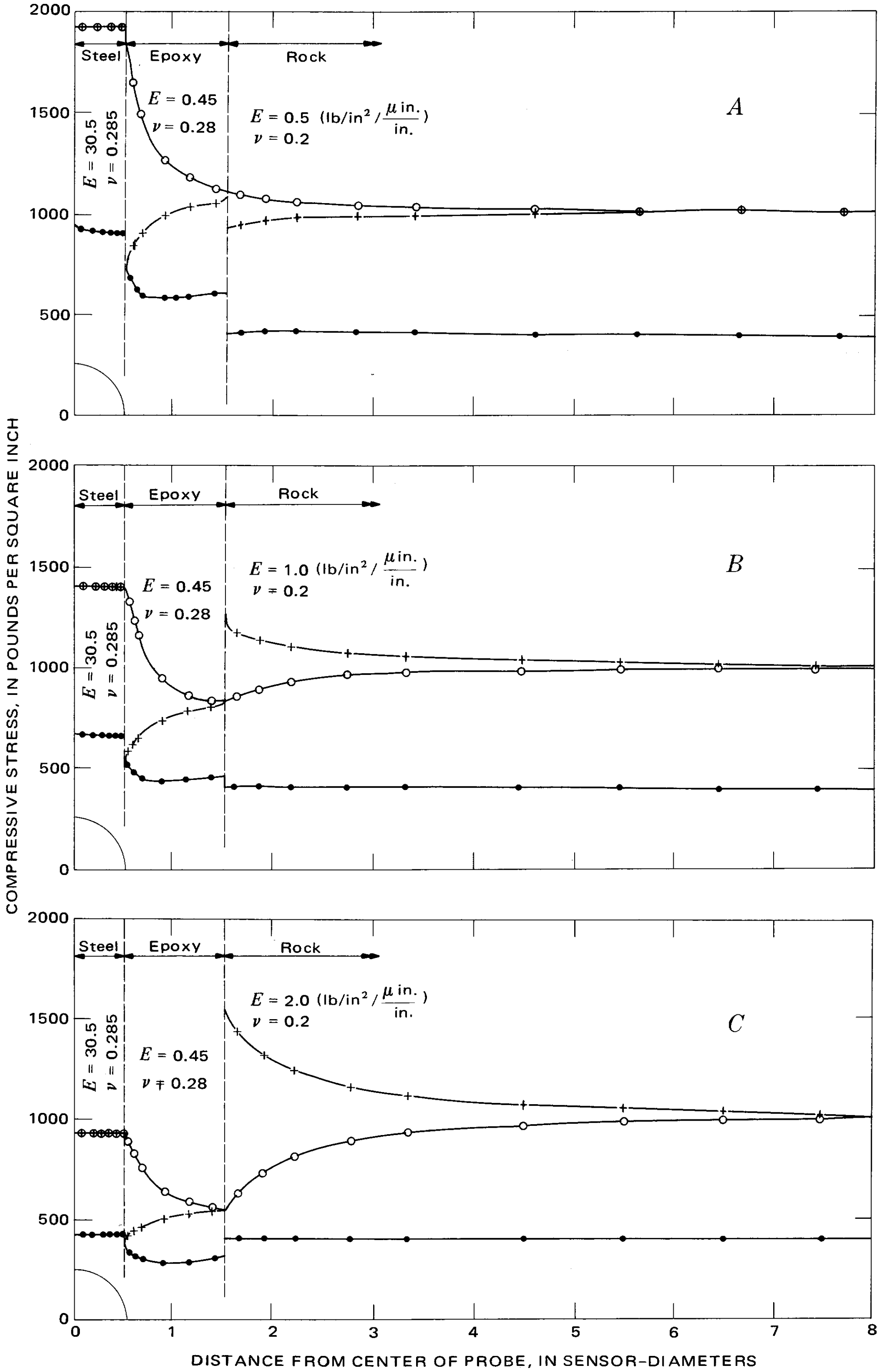

concentration factors determined from finite element analyses for different host-material properties are given in table 4. The radial and tangential stress concentrations are slightly less than the axial stress concentrations (fig. 12*A*). However, an average stress concentration factor (SCF) could be used for calculation of stress in the host material with a maximum error of 8 percent. A plot of this SCF versus the host-rock modulus is shown in figure 12*B*.

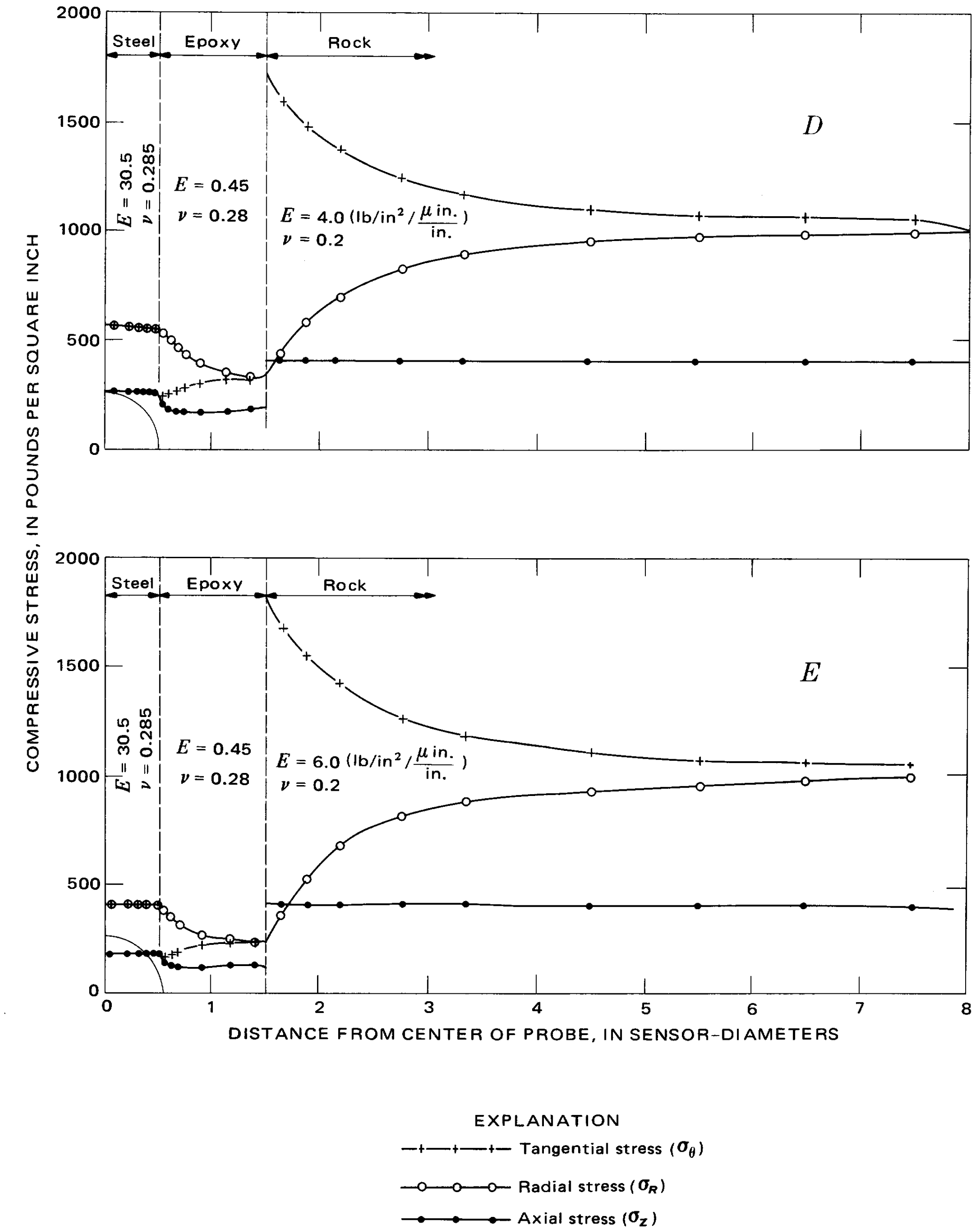

FIGURE 11 (above and facing page).—Stress distribution from finite-element analysis along a radial line cutting the center of the probe (analysis 1).
A, Analysis 1; *B*, analysis 2; *C*, analysis 3; *D*, analysis 4; *E*, analysis 5.

COMPARISON OF STRESS CONCENTRATION FACTORS OBTAINED BY MATHEMATICAL AND FINITE-ELEMENT METHODS

The stress concentrations which were determined for the effect of the geometry on the borehole probe and the rock in which it is placed are given in figure 12*B*. One curve was obtained from the theoretical spherical-cylindrical analysis, which is summarized in table 1, and the other curve is the average stress concentration factor (SCF) computed by the axisymmetric finite-element method, which is summarized in table 4.

In view of the assumptions of elasticity and the approximations needed for both techniques, the agreement is close, and use of the probe in monitoring three-dimensional stress changes in elastic material would appear justified. The stress monitored by the probe sensor is, however, sensitive to the modulus of the host material. For a steel sensor, the SCF ranges from 1.90 to 0.42 as the

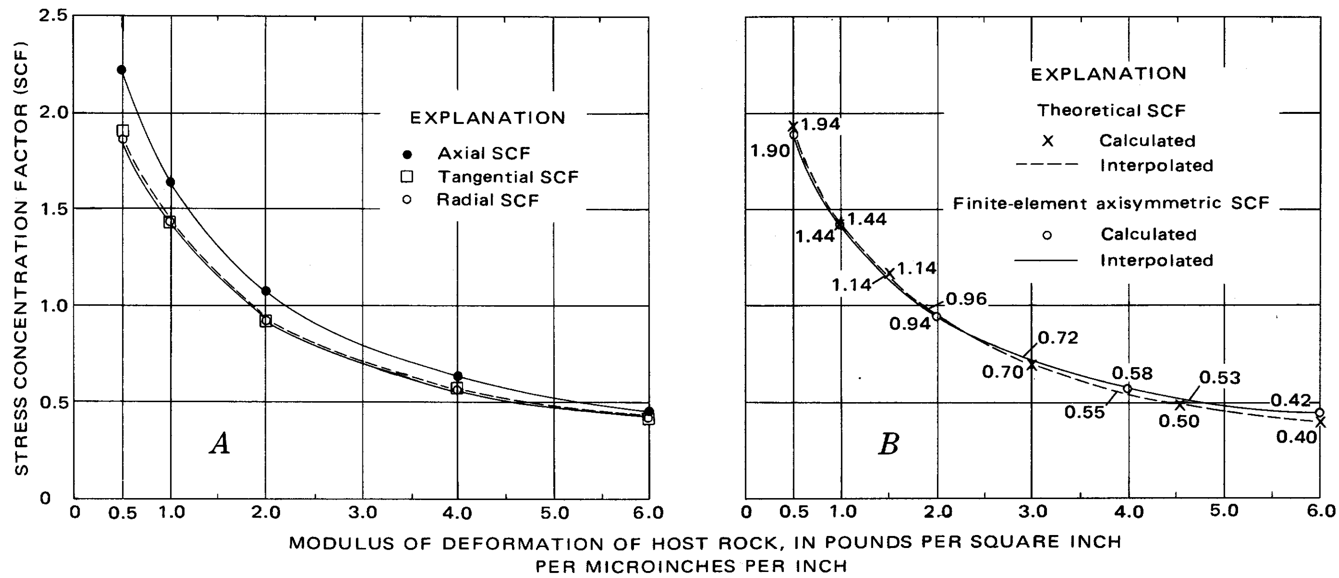

FIGURE 12.—Stress concentration factors (SCF's) for spherical steel sensor surrounded by epoxy cylinder and host rock. Poisson's ratio held constant (0.2).

A, Axial, tangential, and radial stress concentration factors plotted against modulus of deformation of host rock.

B, Averaged radial and tangential stress concentration factors plotted against modulus of deformation of host rock. [Note: A stress change of 1 lb/in^2 in the host rock of modulus 6×10^6 lb/in^2 results in a stress change of approximately 0.4 lb/in^2 on the steel sensor; i.e., SCF ≈ 0.4]

host-rock modulus increases from 0.5×10^6 to 6.0×10^6 lb/in^2. Thus, knowledge of the modulus of deformation of the host rock is essential to accurately determine stress changes.

ANALYSIS OF LABORATORY BIAXIAL TEST

Another use of the axisymmetric finite-element method is in the evaluation of in situ stresses determined by overcoring the borehole probe. Overcoring relieves the rock surrounding the probe from the in situ stress field, causing a stress change in the spherical sensor. This change should allow the calculation of the in situ stress field present in the rock mass. The rock cylinder recovered from the borehole with its enclosed probe can be tested in a biaxial loading device in the laboratory. By virtue of these known applied loads, a check on the theoretically derived SCF can be obtained. The axisymmetric finite-element method is a means of checking laboratory biaxial core-loading results. The results of this analysis (with free end) (analysis 6, fig. 13*A*; table 5), when compared with the results of analysis 4 (similar material properties but fixed end), show that the laboratory biaxial device produces the stress concentration in the radial and tangential directions that would be expected in the field. However, the axial boundary conditions in the field and in the biaxial device are probably different. The axial stress is considerably less in the laboratory biaxial device because no axial stress is applied, whereas some axial component of stress would be anticipated.

TABLE 5.—*Finite-element model properties for biaxial test (axisymmetric analysis)*

Analysis	Sphere		Epoxy cylinder		Host rock		Directions of boundary-loading conditions	
	[1]$E(10^6)$	ν	[1]$E(10^6)$	ν	[1]$E(10^6)$	ν	Radial[1]	Axial
6	30.5	0.285	0.45	0.28	4.0	0.25	1,000	Free

[1] Units in pounds per square inch.

PLANE-STRAIN ANALYSES

Plane-strain finite-element analyses were made primarily to test qualitatively the effectiveness of the probe in estimating in situ stresses. The method was first tested to verify that it would reproduce a theoretical plane-strain problem.

PRELIMINARY PLANE-STRAIN ANALYSIS

The results of the preliminary plane-strain analysis (analysis 7) are shown in figure 13*B* as a plot along a radial line perpendicular to the long axis of the probe (similar to fig. 11). The host-rock properties (table 6) were the same as

TABLE 6.—*Finite-element model properties for plane-strain analysis*

Analysis	Sphere		Epoxy cylinder		Host rock		X[1]	Y[1]
	[1]$E(10^6)$	ν	[1]$E(10^6)$	ν	[1]$E(10^6)$	ν		
7	30.5	0.285	0.45	0.28	2.0	0.20	1,000	1,000

[1] Units in pounds per square inch.

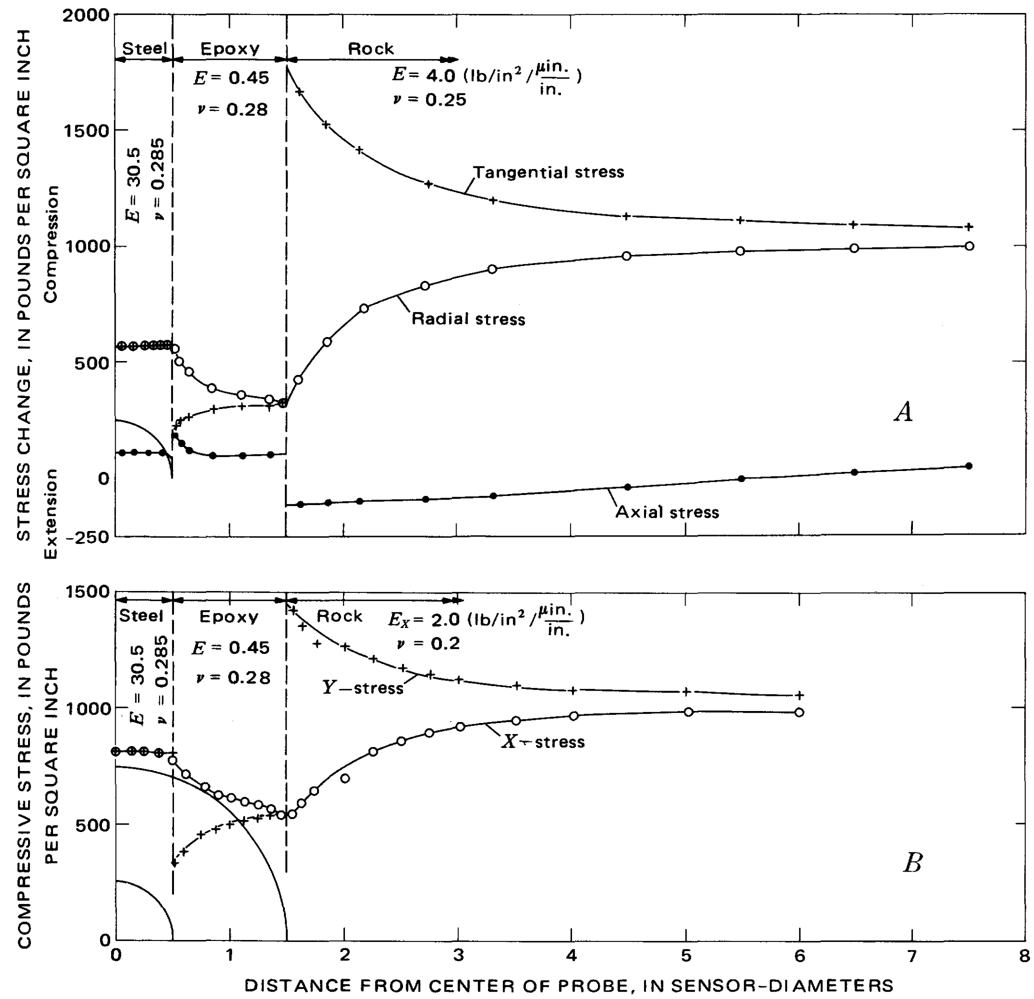

FIGURE 13.—Stress distributions. *A*, Along a radial line cutting the center of the probe (analysis 6, biaxial test). *B*, Along the *X* axis for the plane-strain analysis (analysis 7).

for analysis 3 of the axisymmetric analysis. The resulting stress concentration for this analysis, however, is only 0.8 compared to 0.94 for the similar axisymmetric case. This result was to be expected because the plane-strain analysis is a representation of a cylinder superposed on a cylindrical inclusion, and the magnitude of stress concentration is greater for a spherical inclusion than for a cylindrical inclusion (Goodier, 1933). However, in general the stress distributions are similar to those of the axisymmetric analyses, and qualitative indications of the stress orientations can be obtained using a plane-strain model.

ANALYSIS OF OVERCORING

The plane-strain finite-element method was utilized to analyze simulated stress-relief overcoring procedures in a step-by-step manner using both the U.S. Bureau of Mines deformation gage and the three-dimensional borehole probe. The U.S. Bureau of Mines theoretical biaxial plane-strain solution was used to check the finite-element method. This comparison was desirable because no exact theoretical three-dimensional solution exists for analyzing strain changes produced by overcoring the borehole probe. The analysis of this simulated operation proceeded as follows:

1. The model simulated a rock mass with the boundaries sufficiently removed from the eventual borehole location to minimize the boundary effects of the borehole.
2. The rock was then placed under a biaxial hydrostatic stress of 1,000 lb/in^2; the borehole was then placed in the model and the resulting stress pattern and displacements were determined.
3. The appropriate gage was then installed and the instrument was overcored. The resulting stress pattern and displacements were determined.

The results of the finite-element analysis of the U.S. Bureau of Mines stress-relief procedure show a stress distribution about the borehole prior to overcoring that is identical with the distribution predicted by theoretical solutions. The stress in the rock cylinder (after overcoring) is zero, as predicted by elastic theory.

The radial displacements of the borehole boundary were calculated to be 0.0017 cm (0.00067 in.) after overcoring. This gives a diameter change of 0.0034 cm (0.00134 in.) for the plane-strain finite-element solution.

The theoretical diameter change for plane strain under hydrostatic stress derived from Obert and Duvall (1967, p. 413) is

$$U=2pd(1-\nu^2)/E \text{ (hydrostatic)}, \qquad (7)$$

where

U=the diameter change,
d=the borehole diameter,
ν=Poisson's ratio,
E=Young's modulus, and
p=hydrostatic pressure.

Using the same material properties and loads as in the finite-element solution,

$$E=2\times 10^6 \text{ lb/in}^2,$$

where

ν=0.20,
d=1.5 in., and
p=1,000 lb/in^2,

this equation yields a diameter change of 0.0037 cm (0.00144 in.). Thus, the theoretical and finite-element solutions agree within 6.9 percent. It is not known whether this difference is due to the size of the finite-element mesh or whether a difference actually exists.

The results of a plane-strain finite-element analysis of the borehole-probe overcoring operation are shown in figure 14. The group of curves ***B*** shows the stress distributions around the drill hole before installation of the probe, which are the same stress distributions as those previously determined theoretically. The group of curves ***A*** shows the stress distributions within the probe and the rock overcore after overcoring. The stresses in the probe are tensile, as would be expected from a relieved compressive stress field. The radial stress in the rock overcore is tensile, and the tangential stress is compressive.

The stress concentration in the steel sensor is approximately 0.60, which is lower than the stress concentration of 0.80 predicted in analysis 7, which has the same material properties and load conditions. This is probably due to the use of a plane-strain method of analysis which simulates a cylinder within a cylinder. The results can be applied only qualitatively to the actual three-dimensional problem of a sphere within a cylinder.

REQUIREMENT OF TENSILE STRENGTH

The plane-strain analysis of overcoring assumes adequate tensile strength in the rock mass around the borehole probe. In order to obtain stress-relief information, the rock within the overcore must be capable of transmitting a tensile stress. In the preceding example the rock (E=2.0×10^6 lb/in^2, ν=0.2) was subjected to about 600 lb/in^2 tension when a 1,000-lb/in^2 equal biaxial stress was removed. Field experiments have demonstrated that when overcoring in low-modulus- and low-tensile-strength rocks in a compressive stress field tensile failures can occur in the rock near the rock-epoxy interface, prohibiting meaningful results. The level of the tensile stress generated in the rock by overcoring and by removal of a compressive stress is a function of the ratio of the rock modulus to the epoxy modulus. If the rock modulus is decreased and approaches the modulus of the epoxy grout (0.45×10^6 lb/in^2), the tensile stress rises. Tuffaceous rock under an estimated 1,000-lb/in^2 compression, with a modulus of between 0.7×10^6 and 0.9×10^6 lb/in^2, failed in tension in the rock adjacent to the probe during overcoring. Granitic rock under 2,000-lb/in^2 compression, but with an average modulus of 7×10^6 lb/in^2, did not fail in tension during overcoring. The indicated beneficial effect of reducing the modulus of the epoxy grout for overcoring low-modulus rock will be studied.

LABORATORY MODEL-TUNNEL INVESTIGATIONS

The purpose of the laboratory-model studies was twofold: to evaluate the studies of probe behavior previously described and to define the effects of tunneling in simple systems omitting body loads and geologic factors, such as faults and foliation. The laboratory model-tunnel results were compared with the findings from the field tunnel study.

The materials used in the model-testing program were chosen to represent a range of fabric properties, from an amorphous material (acrylic) to an artificial granular aggregate (concrete) to a natural granular aggregate (granite).

Because the model tunnels were smooth-walled cylindrical boreholes, they would resemble "mole"-drilled tunnels more closely than conventional "drill-and-blast" tunnels. The model tunnel in the acrylic was advanced by a twist drill; the concrete and granite model tunnels required use of a diamond-core drill. The drilling caused a significant thermal disturbance in the acrylic model which necessitated a wait to verify stability after each drilling increment. The loading was adjusted to maintain the same average stress in the models after each increment of tunnel advance. All model testing was done under room temperature and humidity conditions. The probes used to monitor stress changes in the model-tunnel studies differed somewhat from those used in the field. Rather than the 7.6-cm (3 in.) borehole used in the field, we grouted the laboratory probes in a 5.1-cm (2 in.) borehole. Also, the laboratory probe was 15.2 cm (6 in.) long, while the field-borehole probe is 43.2 cm (17 in.) long. The

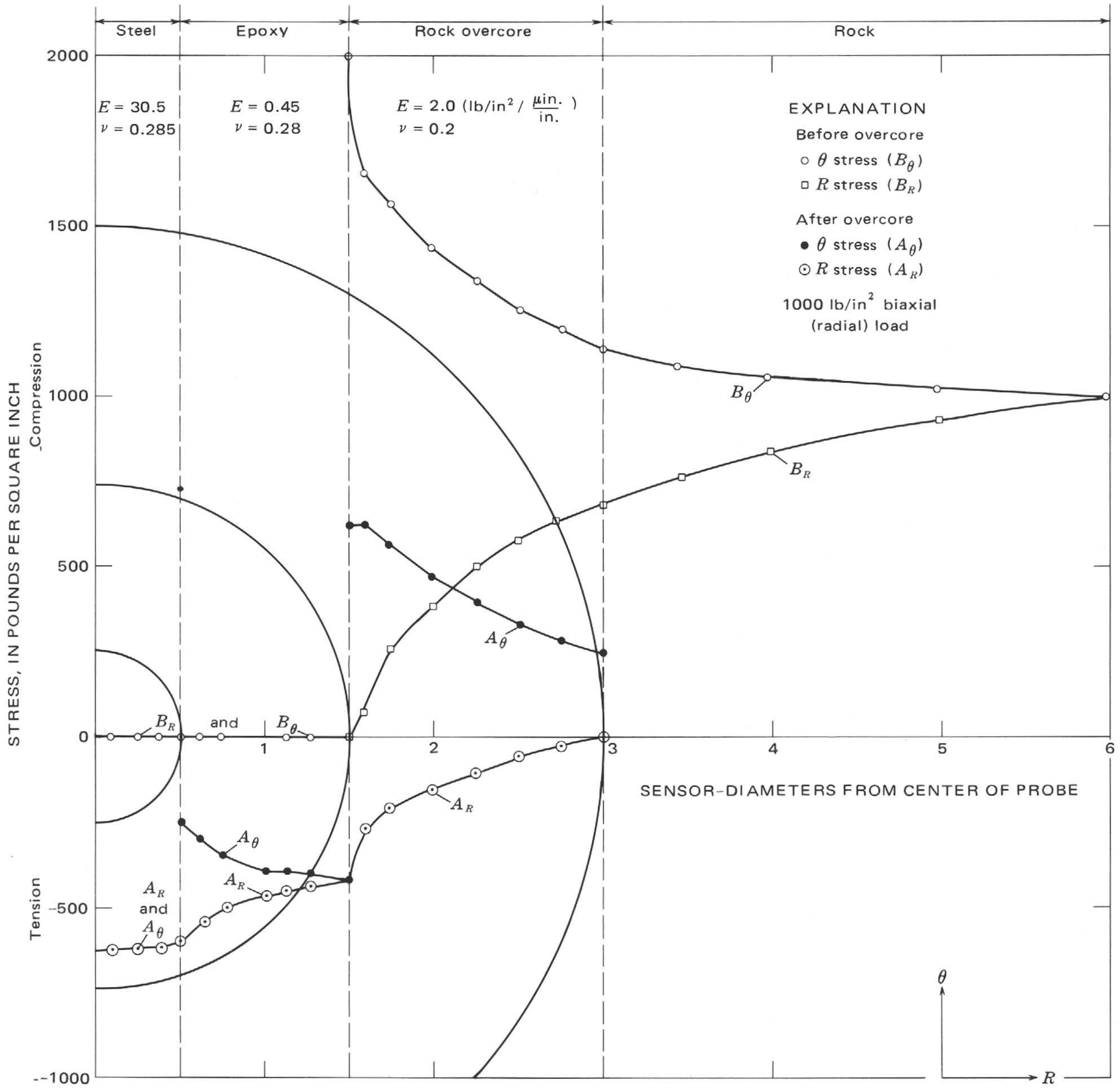

FIGURE 14.—Plane-strain finite-element analysis of stress distribution in borehole probe and rock along R axis. Curves B show stress in rock around drill hole before installation of probe. Curves A show stress in probe and rock overcore after stress relief by overcoring.

diameter of the spherical sensor is 2.5 cm (1 in.) for all applications.

Stress changes were monitored for each increment of tunnel advance. Tunnel advance was accomplished by removing the model from the hydraulic press, drilling the necessary distance, replacing the model in the press, and successively loading and unloading the model. Normally, two cycles were sufficient to demonstrate the repeatability of stress-strain response at the probe location. It was not physically possible, although desirable, to advance the tunnels under load. Changes in stress, however, appear to be consistently related to changes in tunnel length which occurred between loadings. The tunneling methods had no measurable effect on stress changes near the monitoring probe.

ACRYLIC MODEL

The acrylic model containing a centrally located probe (fig. 15) was tested under an average uniaxial stress of 1,950 lb/in² prior to drilling the tunnel. The resulting strains measured by the sensor were equivalent to a compressive stress of 2,100 lb/in² parallel to the vertical loading direction, 1,000 lb/in² in tension horizontal and approximately perpendicular to the axis of the probe borehole,

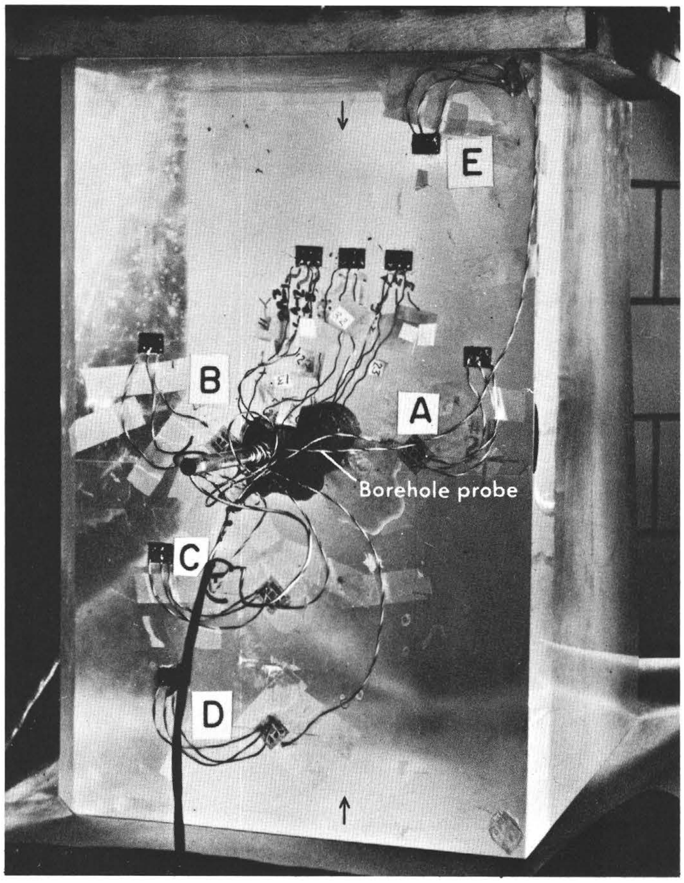

FIGURE 15.—View of acrylic model showing three-dimensional borehole probe grouted into central drill hole. Strain gages (A-E) were used in previous testing (Nichols and others, 1968, p. C14). Tunnel was advanced from rear face. Model measures 48.3 cm (19 in.) high, 33.0 cm (13 in.) wide, and 30.5 cm (12 in.) deep. Arrows indicate loading direction.

and 1,820 lb/in² in tension horizontal and approximately parallel to the axis of the probe borehole.

The 4.78-cm- (1.88 in.) diameter tunnel was advanced by drilling into the side of the acrylic model opposite the sensor implacement hole (in a direction arbitrarily chosen as N. 45° E.).

As the tunnel in the acrylic model was advanced in increments toward the probe, the probe sensed an increase in compression in the direction of loading. The principal stress changes in the plane normal to the direction of loading were very small. The directions of the principal stress changes remained essentially fixed (table 7; figs. 16*A*, 17).

Stresses estimated from photoelastic studies by Galle and Wilhoit (1962), in a smaller but similarly loaded plastic block ahead of a 3.18-cm- (1.25 in.) diameter bore, are in good agreement with the stresses monitored by the probe for a 1.50-tunnel-diameter interval between the probe and the tunnel face (fig. 16*B*). Differences existed, however, when the face was between 1.50 and 2.25 tunnel diameters from the monitoring probe.

TABLE 7.—*Average stresses determined ahead of tunnel face in acrylic model*

[Acrylic properties: E=0.327×10⁶ lb/in², ν=0.39, tensile elastic limit=12,000 lb/in². Probe properties: epoxy grout, E=1.55×10⁶ lb/in², ν=0.39; steel sensor, E=30.5×10⁶ lb/in², ν=0.285; SCF=2.73. Average stress applied=1,950 lb/in² vertical. +, compressive stress; –, tensile stress]

Diameters from sensor center	Maximum principal stress			Intermediate principal stress			Minimum principal stress		
	Magnitude (lb/in²)	Bearing (degrees)	Plunge (degrees)	Magnitude (lb/in²)	Bearing (degrees)	Plunge (degrees)	Magnitude (lb/in²)	Bearing (degrees)	Plunge (degrees)
4.47	+2,100	N. 66 W.	74	-1,000	S. 39 E.	14	-1,820	N. 50 E.	7
3.93	+2,100	N. 65 W.	73	-980	S. 36 E.	15	-1,750	N. 52 E.	8
3.39	+2,170	N. 65 W.	73	-1,040	S. 38 E.	15	-1,820	N. 50 E.	8
2.86	+2,190	N. 66 W.	73	-990	S. 36 E.	15	-1,780	N. 52 E.	8
2.32	+2,260	N. 65 W.	73	-1,020	S. 36 E.	15	-1,790	N. 52 E.	8
2.05	+2,300	N. 63 W.	73	-1,020	S. 36 E.	15	-1,780	N. 52 E.	8
1.51	+2,210	N. 70 W.	73	-1,040	S. 35 E.	14	-1,930	N. 52 E.	10
1.24	+2,180	N. 70 W.	72	-1,000	S. 33 E.	14	-1,860	N. 54 E.	10
.97	+2,290	N. 69 W.	72	-980	S. 32 E.	14	-1,860	N. 55 E.	10
.70	+2,320	N. 66 W.	72	-1,000	S. 30 E.	14	-1,800	N. 57 E.	10
.43	+2,570	N. 65 W.	71	-1,030	S. 25 E.	15	-1,860	N. 62 E.	12

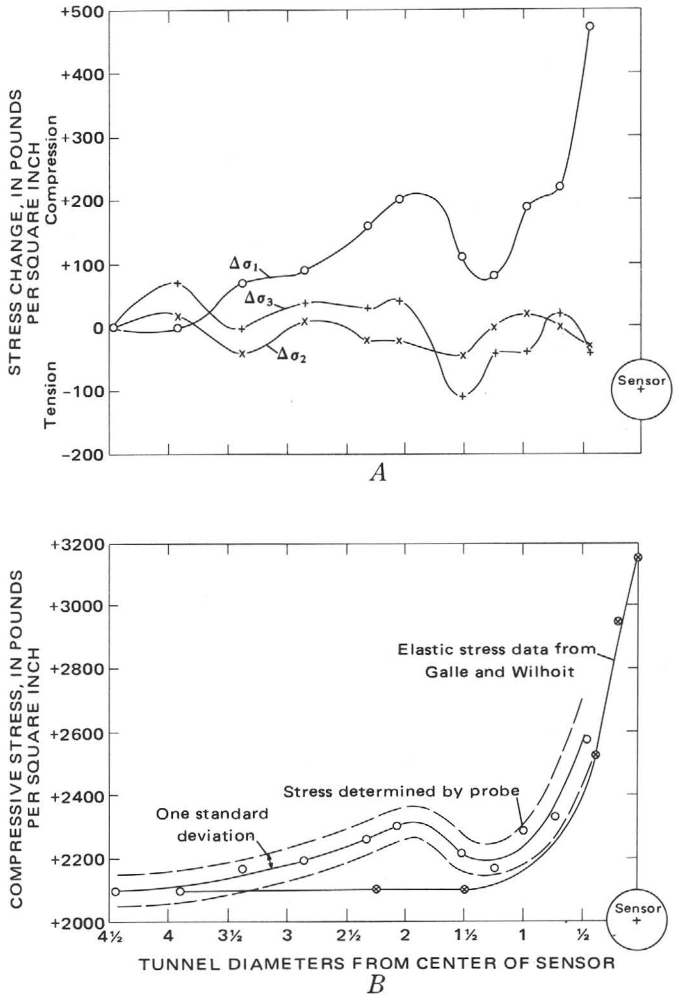

FIGURE 16.—Changes of magnitude in principal stresses (*A*) and maximum principal stress compared to results of Galle and Wilhoit (1962, p. 148, fig. 7b) (*B*) in acrylic model.

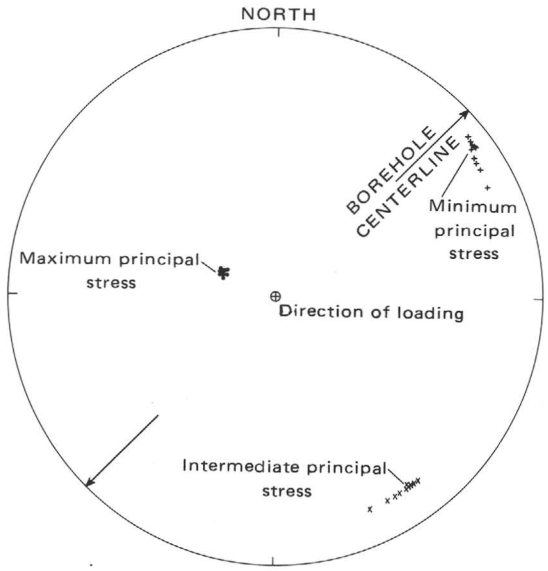

FIGURE 17.—Bearing and plunge of principal stress changes in acrylic model (lower hemisphere equal-area projection).

Specific findings from the acrylic model study requiring further explanation are:

1. The stress before tunneling is 7.7 percent above the average applied uniaxial stress, 2,100 lb/in^2 instead of 1,950 lb/in^2.
2. The tensile stresses present in the model with respect to the loading (maximum principal) stress.
3. The approximate 9-percent peak in the maximum principal stress concentration that occurred at 1.75 tunnel diameters ahead of the advancing model tunnel.

These findings will be evaluated after the presentation of the results obtained from the concrete and granite models.

CONCRETE MODEL

A second model was constructed of high-strength concrete (fig. 18). The concrete model with its grouted sensor was initially tested under an average vertical uniaxial stress of approximately 1,310 lb/in^2 after the 4.78-cm- (1.88 in.) diameter tunnel had been driven 4.44 cm (1.75 in.). The resulting average strains measured by the sensor were equivalent to approximately 1,420 lb/in^2 in compression in the vertical loading direction, 500 lb/in^2 in tension normal to both the vertical loading direction and to the axis of the model tunnel, and 150 lb/in^2 in tension parallel to the horizontal axis of the model tunnel.

The same incremental tunnel-advancing procedure was used with the concrete as had been used for the acrylic tunnel-model experiment. The direction of tunnel advance was arbitrarily denoted east. The stress magnitudes and directions sensed by the probe in the concrete model after each advance of the tunnel are presented in table 8 and in figures 19*A* and 20.

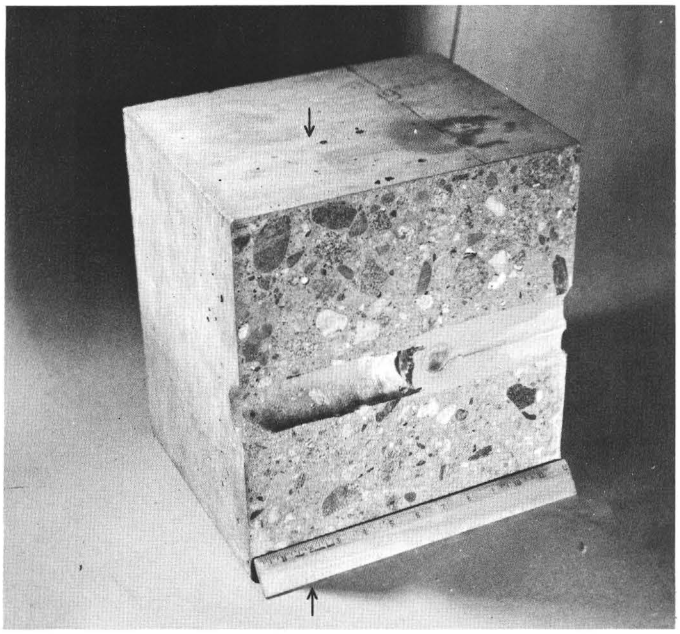

FIGURE 18.—Concrete tunnel model. Block has been sawed parallel to borehole axis, exposing strain sensor. Tunnel was advanced from left to right. Arrows indicate loading direction. Scale in inches.

The results from the concrete model in the direction of applied uniaxial loading (fig. 19*B*) agree rather closely with the photoelastic data in the region less than 1 tunnel diameter ahead of the advancing tunnel face. The stress-strain response of the concrete model as detected by the probe was remarkably similar to that of the acrylic model, as follows:

1. The stress before tunneling is 8.4 percent greater than the applied uniaxial stress—1,420 lb/in^2 rather than 1,310 lb/in^2.
2. The sizable variation between the two tensile principal stresses normal to and parallel to the tunnel axis and (or) the axis of the probe hole that occurred in the acrylic model was also present in the concrete.

TABLE 8.—*Average stresses determined ahead of tunnel face in concrete model*

[Concrete properties: E=3.3×10^6 lb/in^2, ν'=0.26, compressive strength=7,580 lb/in^2. Probe properties: epoxy grout, E=0.45×10^6 lb/in^2, ν=0.28; brass sensor, E=15.0×10^6 lb/in^2, ν=0.285; SCF=0.614. Average stress applied = 1,310 lb/in^2 vertical +, compressive stress; –, tensile stress.]

Diameters from sensor center	Maximum principal stress			Intermediate principal stress			Minimum principal stress		
	Magnitude (lb/in^2)	Bearing (degrees)	Plunge (degrees)	Magnitude (lb/in^2)	Bearing (degrees)	Plunge (degrees)	Magnitude (lb/in^2)	Bearing (degrees)	Plunge (degrees)
2.66	+1,420	S. 31 W.	82	–140	N. 5 W.	7	–510	N. 86 E.	5
2.00	+1,580	S. 30 W.	82	–140	N. 5 W.	7	–540	N. 86 E.	5
1.45	+1,570	S. 30 W.	82	–170	N. 7 W.	6	–610	N. 84 E.	5
1.18	+1,640	S. 32 W.	83	–100	N. 5 W.	6	–580	N. 85 E.	4
.91	+1,610	S. 34 W.	83	–70	N. 6 W.	5	–620	N. 85 E.	5
.64	+1,670	S. 36 W.	82	–170	N. 6 W.	6	–710	N. 84 E.	5
.37	+1,870	S. 42 W.	83	–220	N. 7 W.	4	–740	N. 83 E.	5

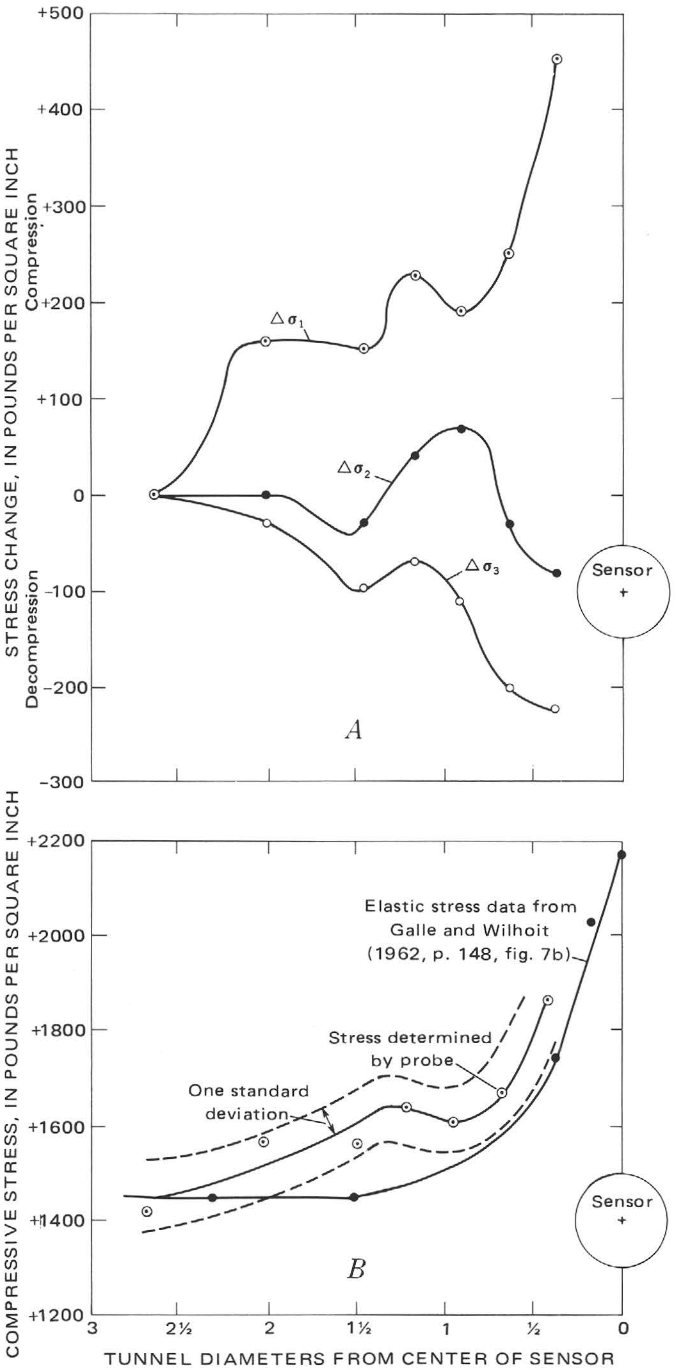

FIGURE 19.—Changes of magnitude in principal stresses (*A*) and maximum principal stress compared to the results of Galle and Wilhoit (1962, p. 148, fig. 7b) (*B*) in concrete model.

3. A minor, but significant, compressive stress concentration in the loading direction was sensed by the probe. In the concrete model this was between approximately 1 and 2.25 tunnel diameters ahead of the advancing tunnel, whereas in the acrylic model the concentration occurred between 1.5 and 2.5 tunnel diameters ahead. A maximum principal stress concentration peak of 9 percent occurred approximately 1.25 tunnel diameters in front of the advancing tunnel in the concrete model (fig. 19*B*). This compares to a similar peak at 2 tunnel diameters in the acrylic model (fig. 16*B*).
4. The minimum principal stress showed a sudden increase when the tunnel was about 1.75 tunnel diameters from the center of the probe. In the concrete model, however, the minimum principal stress did not return to its previous low level, as it had in the nearly elastic acrylic model.

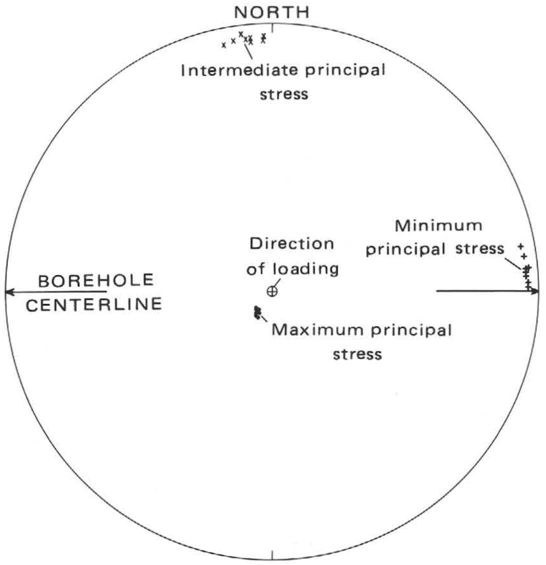

FIGURE 20.—Bearing and plunge of principal stress changes in concrete model (lower hemisphere equal-area projection).

GRANITE MODEL

The third tunnel model (fig. 21) consisted of a block of Silver Plume Granite 30.48 cm (12 in.) high, 43.18 cm (17 in.) wide, and 43.18 cm (17 in.) deep. Concrete platens, 10.16 cm (4 in.) high, 33.02 cm (13 in.) wide, and 30.48 cm (12 in.) deep, were cemented with epoxy to the sides of the granite, extending its height to 50.80 cm (20 in.). The concrete platens were cut from the concrete model, for which E=3.3×10^6 lb/in^2, ν =0.26. The properties of the granite as determined from specimens removed from the block after testing are similar to those of the concrete; namely, E=4.5×10^6 lb/in^2, ν =0.23. The effect of the lower stiffness (E) and higher Poisson's ratio of the concrete platens is to increase the lateral tensile strain in the granite at the granite-concrete interface by approximately 11.7 μin./in., or 53 lb/in^2 per 1,000 lb/in^2 of applied uniaxial (vertical) stress—this in addition to a measured lateral tensile stress of 295 lb/in^2 per 1,000 lb/in^2 applied vertical compressive stress. Any lateral tension due to the mismatch of model and platen materials appears to have been restricted to the immediate vicinity of the platen-rock interface because the probe did not detect such an increase in lateral tensile stress. Therefore, the probe was influenced only by those

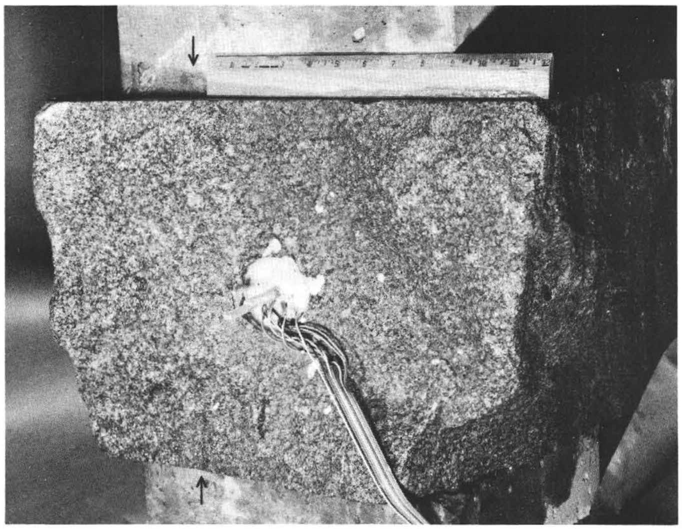

FIGURE 21.—Granite tunnel model showing grouted sensor. A 5.24-cm- (2¹⁄₁₆ in.) diameter tunnel was advanced from the rear side. Arrows indicate loading direction. Scale in inches.

lateral extensional strains resulting from the absence of lateral boundary loads.

The granite model with its grouted sensor was initially tested under an average vertical uniaxial stress of 1,155 lb/in² after the 5.26-cm- (2.07 in.) diameter tunnel had been driven 5.08 cm (2 in.) in a direction arbitrarily designated north. The resulting average strains measured by the sensor were equivalent to 1,380 lb/in² in compression in the vertical loading direction, 90 lb/in² in tension 40° clockwise from the tunnel axis in the horizontal plane normal to the vertical loading direction, and 690 lb/in² in tension 50° counterclockwise from the tunnel axis in the horizontal plane.

An incremental tunnel-advancing procedure was used, as in the previous models. The changes in principal stress magnitudes and directions during tunnel advance in the granite model are presented in table 9. Figure 22*A* presents the principal stress changes and figure 23 the principal stress orientations.

The stress changes near the tunnel face in the granite model differed only slightly in magnitude from the stresses indicated by Galle and Wilhoit (1962). The shape of the applied loading curve is almost exactly the same as that obtained from the acrylic model, except that the percentage concentration of the applied stress ahead of the ad-

TABLE 9.—*Average stresses determined ahead of tunnel face in granite model*

[Granite properties: E=45×10⁶ lb/in², ν=0.23. Probe properties: epoxy grout, E=0.45×10⁶ lb/in², ν=0.28; steel sensor, E=30.5×10⁶ lb/in², ν=0.285; SCF=0.52. Average stress applied=1,155 lb/in² vertical. +, compressive stress; –, tensile stress]

Diameters from sensor center	Maximum principal stress			Intermediate principal stress			Minimum principal stress		
	Magnitude (lb/in²)	Bearing (degrees)	Plunge (degrees)	Magnitude (lb/in²)	Bearing (degrees)	Plunge (degrees)	Magnitude (lb/in²)	Bearing (degrees)	Plunge (degrees)
3.53	+1,390	N. 5 W.	81	–100	S. 43 W.	6	–670	S. 47 E.	7
2.57	+1,370	N. 5 W.	80	–90	S. 44 W.	6	–690	S. 47 E.	7
2.09	+1,380	N. 6 W.	81	–90	S. 42 W.	7	–700	S. 49 E.	6
1.61	+1,400	N. 4 W.	80	–90	S. 41 W.	8	–740	S. 50 E.	7
1.37	+1,440	N. 3 W.	80	–130	S. 41 W.	8	–750	S. 50 E.	7
1.13	+1,470	N. 6 W.	81	–140	S. 41 W.	7	–760	S. 50 E.	7
.89	+1,500	N. 4 W.	80	–170	S. 40 W.	8	–760	S. 51 E.	7
.65	+1,480	N. 12 W.	82	–160	S. 39 W.	5	–830	S. 51 E.	6
.41	+1,560	N. 13 W.	84	–190	S. 39 W.	4	–840	S. 52 E.	5

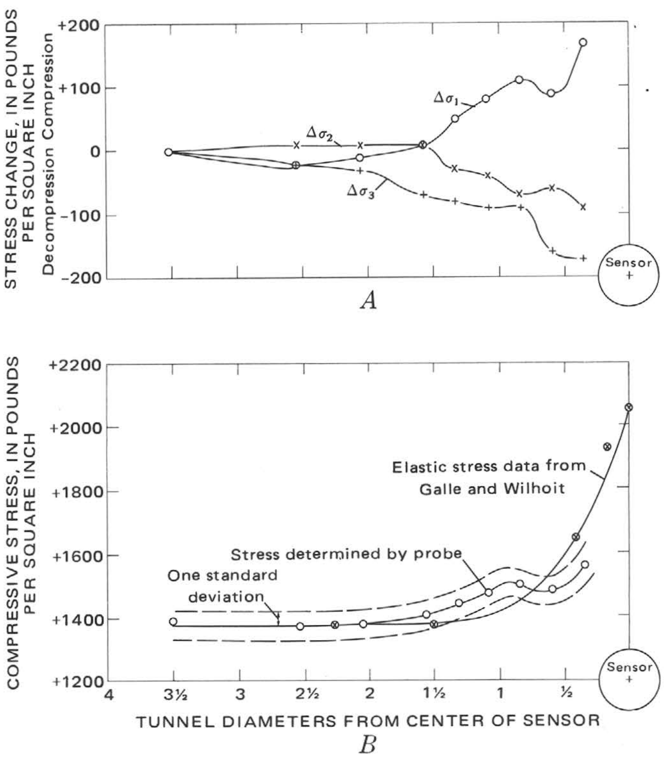

FIGURE 22.—Changes of magnitude in principal stresses (*A*) and maximum principal stress (*B*) compared to the results of Galle and Wilhoit (1962, p. 148, fig. 7b) in granite model.

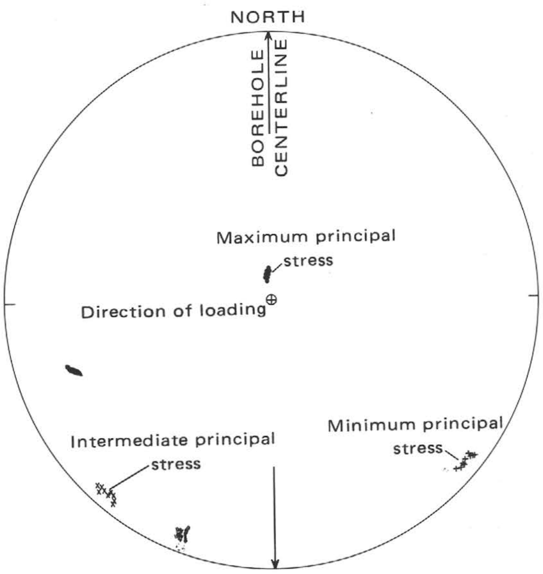

FIGURE 23.—Bearing and plunge of principal stress changes in granite model (lower hemisphere equal-area projection).

vancing tunnel is slightly lower and this region of stress concentration is not as extensive. The region of tunnel-induced stress concentration is limited to approximately 2 diameters ahead of the tunnel face for the granite compared to more than 4 tunnel diameters for the acrylic model and more than 2.50 tunnel diameters for the concrete model (figs. 16*B*, 19*B*, 22*B*).

These differences probably result from the differences between the model materials (table 10). The acrylic is essentially elastic but of low modulus. The concrete is locally heterogeneous, owing to composition and grain size, but in bulk it is elastically isotropic with a modulus between those of acrylic and granite. Physical tests of the granite showed it to be elastically anisotropic, possibly because of mineral orientation, but it is homogeneous in composition and of high Young's modulus.

TABLE 10.—*Summary of model material properties*

Model	Young's modulus (10^6 lb/in^2)	Poisson's ratio	Compressive strength (lb/in^2)	Tensile strength (lb/in^2)
Host material properties				
Acrylic	0.327	0.39	18,000	12,000
Concrete	3.30	.26	7,580	485
Granite	4.50	.23	27,500	880
Sensor properties				
Acrylic	30.5 (steel)	0.285	60,000	
Concrete	15.0 (brass)	.285	30,000	
Granite	30.5 (steel)	.285	60,000	
Grout properties				
Acrylic	1.55 (steel filler)	0.39		
Concrete	.45 (carborundum filler)	.28		
Granite	.45 (carborundum filler).	.28		

EVALUATION OF MODEL RESULTS

Three aspects of the test results warrant critical evaluation; namely, (1) prior to tunneling the maximum principal stress at the sensor exceeded the average applied stress, (2) the magnitude of and variation in the tensile stresses normal to the applied compressive stress, and (3) the compressive stress concentration that was measured ahead of the onset of the predicted, tunnel-related, elastic stress rise. These aspects are primarily related to the differences and similarities between the stress patterns obtained from the three models.

STRESS AT PROBE IN EXCESS OF AVERAGE APPLIED STRESS

Prior to the onset of stress changes related to the model tunneling, the maximum principal compressive stress sensed by the probe in the acrylic model was 2,100 lb/in^2 compared to an average applied compressive stress of 1,950 lb/in^2; in the concrete model 1,420 lb/in^2 was sensed compared to 1,310 lb/in^2 applied; and in the granite model 1,380 lb/in^2 was sensed compared to 1,155 lb/in^2 applied. This is a 7.7-percent stress increase for the acrylic model, a 8.4-percent increase for the concrete, and a 19.5-percent increase for the granite.

These increases can be explained as the result of destressing at the unrestrained surfaces of the models. Destressing measured on the surface of the acrylic model has been described previously (Nichols and others, 1968, p. C20). That report showed a stress decrease of approximately 30 percent from the center of a face to the corner of the model. Galle and Wilhoit (1962, p. 148–149) showed a similar surface-destressing phenomenon in their photoelastic model (fig. 24). The decrease in load-carrying capability at the unrestrained surfaces and edges of the models had to be compensated by a corresponding increase in load-carrying capability elsewhere in the model. This loss of load was transferred to the more confined interior of the models where the spherical sensors were placed. The acrylic model, which had the lowest stiffness of the three model materials, had the lowest increase in maximum principal stress concentration. The granite, the stiffest model material, had the greatest maximum stress concentration increase. The sizable jump in the maximum stress concentration for the granite may be the result of greater anisotropy and of decreased linearity of the stress-strain relationship for the natural rock (granite) in comparison to the more linear stress-strain curves for artificial rock (concrete) and the amorphous material (acrylic).

STRESSES PRECEDING THE ADVANCING TUNNEL

According to elastic theory and the experiments of Galle and Wilhoit (1962), the stress concentration ahead of an advancing tunnel in an elastic material should be confined to a zone within, at most, 2 diameters ahead of the advancing tunnel. It can be seen in figures 16B, 19B, and 22B that the experimental data correspond reasonably well to those obtained by the photoelastic techniques employed by Galle and Wilhoit for approximately 1 diameter ahead of the model-tunnel face (fig. 24). Between 1 and 3 diameters ahead of the advancing model-tunnel faces, a zone of anomalously high compressive stress concentration was measured.

These zones of anomalously high compressive stress in the models cannot be ascribed to instrument error. An indication of the maximum potential instrument error can be obtained from the standard deviations of the intermediate and minimum principal stresses. The pooled standard deviations of the intermediate and minimum principal stresses were 39 lb/in^2 for the acrylic model, 70 lb/in^2 for the concrete model, and 52 lb/in^2 for the granite model. The plots of these standard deviations in figure 16*B*

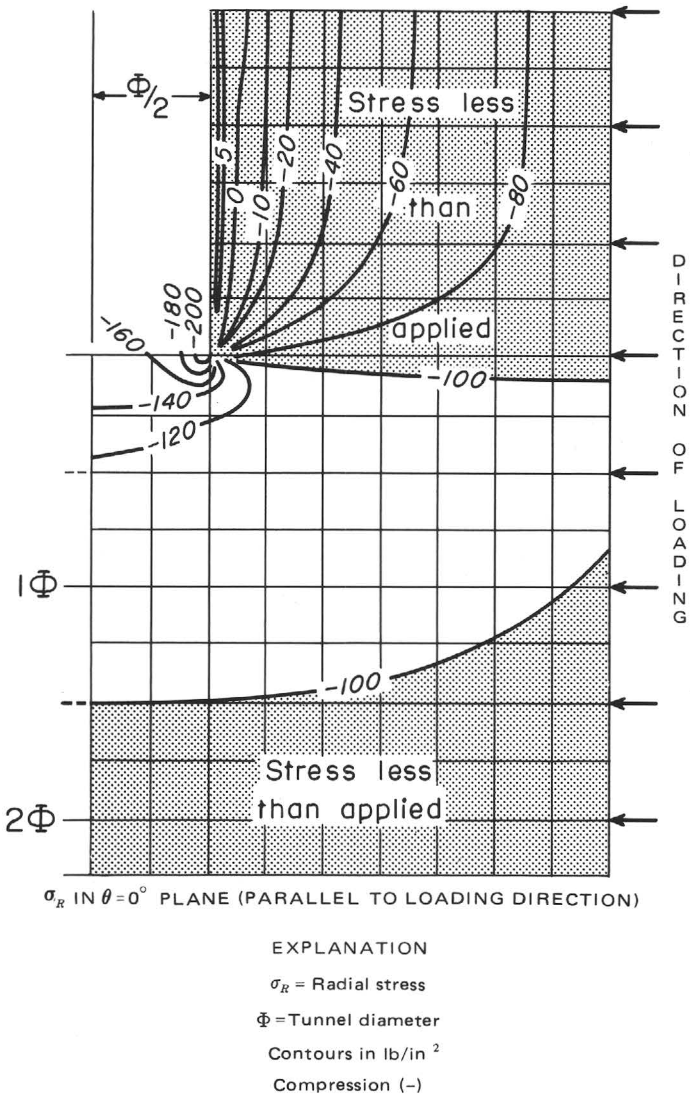

FIGURE 24.—Stress distribution adjacent to model tunnel in photoelastic material modified from Galle and Wilhoit, 1962, p. 148).

for the acrylic model, in figure 19*B* for the concrete model, and in figure 22*B* for the granite model suggest that these subsidiary higher stressed zones owe their existence to a real stress concentration and not to instrument error. Our field evidence agrees approximately with an onset of stress increase at about 2-5 tunnel diameters ahead of a model-tunnel face. The model used by Galle and Wilhoit (1962) may have been of too limited an extent to show this stress peak because their models extended only 2.25 diameters ahead of their model-tunnel face (fig. 24). These tests suggest that model geometry and dimensions strongly influence elastic solutions.

The anomalous vertical compressive stress concentrations which were measured from 2 to 5 diameters ahead of the model tunnels did not continuously increase to the predicted stress of approximately 1.50 times the average before-tunneling stress. A decrease in vertical compressive stress occurs prior to the final stress rise ahead of the tunnel face. In order to explain this phenomenon, one must consider that a decrease in confinement in the direction of the advancing tunnel would produce a decrease in stress (reduction of restraint) in the direction of tunnel advance. The increase in maximum principal compressive stress in the direction of loading results in small additional increases in the intermediate and minimum tensile stresses acting perpendicular to the loading direction (figs. 16*A*, 19*A*, 22*A*).

A small increase in tensile stress in the direction of the approaching tunnel in the acrylic model accompanying a small decrease in the maximum principal compressive stress occurs between 1 and 2 tunnel diameters ahead of the tunnel (table 7; figs. 16*A*, 17). The tensile stress perpendicular to the direction of the approaching tunnel decreases slightly.

In the concrete model a small increase in the lateral tensile stresses occurs in the direction of the approaching tunnel, accompanied by a decrease perpendicular to the approaching tunnel, within the zone of decreased maximum principal compressive stress from 0.75 to 1.25 tunnel diameters ahead of the advancing tunnel (table 8; figs. 19*A*, 20). These results are similar to those obtained from the acrylic model.

In the granite model the minimum principal stress increases in tension between 3.50 and 1.50 tunnel diameters ahead of the tunnel face, whereas the intermediate principal stress remains slightly compressive (table 9; figs. 22*A*, 23). The average lateral tensile stress $((\sigma_3+\sigma_2)/2)$ increases throughout the zone ahead of the advancing tunnel. The granite model differs from the other two models in that the intermediate and minimum principal stress directions are not oriented perpendicular to and parallel to the tunnel axis.

The granite was anisotropic in the horizontal plane, having a specimen modulus of 4.89×10^6 lb/in² and a Poisson's ratio of 0.210 in the intermediate principal stress direction and a specimen modulus of 4.85×10^6 lb/in² and a Poisson's ratio of 0.244 in the minimum principal stress direction. The influence of the anisotropy in Poisson's ratio could account for a difference in horizontal stress of approximately 80 lb/in² between the intermediate and minimum principal stresses in the granite. The average actual difference was approximately 590 lb/in², or about seven times larger than can reasonably by explained by elastic anisotropy. No obvious explanation exists for the magnitude of the nonsymmetric lateral stress in the granite model. The directions of the intermediate and minimum principal stresses are, however, in agreement with those calculated from the elastic anisotropy, with the stiffer member carrying the greater stress.

The average horizontal-to-vertical stress ratio determined for the granite model agrees reasonably well with the plane-strain predicted stress ratio (table 11). The ratio

TABLE 11.—*Change in lateral tensile stress in granite model*

[Mean difference=2.9 percent; standard deviation=7.5 percent: 95-percent confidence interval=2.9 to 8.7 percent]

Diameters from sensor	Measured ratio Avg. $\sigma_{hor.}/\sigma_{vert.}$	Predicted ratio[1] Avg. $\sigma_{hor.}/\sigma_{vert.}$	Percent difference[2]
3.53	0.275	0.295	−6.8
2.57	.282	.295	−3.4
2.09	.286	.295	−3.0
1.61	.300	.295	+1.7
1.37	.306	.295	+3.7
1.13	.307	.295	+4.1
.89	.308	.295	+4.4
.65	.335	.295	+13.6
.41	.331	.295	+12.2

[1] Based on absence of restraint, plane-strain elastic relations, and physical specimen tests.

[2] $\frac{\text{Measured ratio} - \text{predicted ratio}}{\text{Predicted ratio}} \times 100.$

of average horizontal stress ($(\sigma_2+\sigma_3)/2$) to average vertical stress increased with the increased longitudinal stress resulting from tunnel advance. This implies a change in Poisson's ratio with either the change in confinement or increasing uniaxial stress. During testing of granite specimens, an increase in Poisson's ratio from 0.20 to 0.24 was measured from 0 to 10,000 lb/in². No change in Poisson's ratio could, however, be detected over the small stress range measured in the granite model (1,370–1,560 lb/in²).

The release of confinement, induced by the approaching tunnel, appeared to be the dominant factor in the behavior of the acrylic model. Poisson's strain was apparently more important in the concrete model, but release in confinement was present. The response of the granite appeared to be related more to anisotropic variations in the granite than to release of restraint related to tunneling.

In all three models, the maximum tensile stress developed in the material most capable of carrying it: the stiffer epoxy grout in the case of the acrylic model, the stiffer concrete in the case of the concrete model, and the direction of lower Poisson's ratio and greater stiffness of rock in the case of the granite model. Indicated anomalous stresses cannot be ascribed to instrument error. But an anomalous condition exists that cannot be supported by available elastic theory or by measurements.

DISCUSSION OF LATERAL DEFORMATION

The before-tunneling load-induced horizontal tensile stresses in the acrylic model were approximately 1,820 lb/in² parallel to the direction of the emplacement borehole and approximately 1,000 lb/in² normal to the emplacement borehole. The induced horizontal tensile stresses in the concrete block 2.50 tunnel diameters ahead of the sensor were approximately 150 lb/in² parallel to the direction of the emplacement hole and approximately 500 lb/in² normal to the borehole. The induced horizontal tensile stresses in the granite block, in the zone from 1.50 to 3.50 tunnel diameters ahead of the sensor, were approximately 90 lb/in² 42° clockwise from the axis of the emplacement hole and approximately 700 lb/in² 49° counterclockwise from the axis of the emplacement hole.

The existence of internal lateral tensile stresses in a uniaxial test specimen has been observed or has been postulated by other investigators. Conway (1963, p. 131) used photoelastic freezing techniques to observe high lateral tensile stresses in uniaxial tests conducted on CIBA epoxy, with both low-friction end conditions and high-friction end conditions. With the low-friction end condition, Conway observed a nearly uniform radial tensile stress across all longitudinal sections of the specimen, with a stress discontinuity at the external boundary. With the high-friction end condition, he again observed a nearly uniform radial tensile stress across all longitudinal sections to within one-tenth of the specimen length from the ends. Conway stated (p. 131) that these tensile stress components directly contradict elastic theory and that (p. 149) they are approximately equal to one-half the axial principal stress.

Brown and Trollope (1967, p. 234), using the principle of superposition, postulated that there are effective stresses (stresses induced perpendicular to the uniaxial loading direction) within a loaded body which are related by the expressions:

$$\sigma_x' = \sigma_x - \nu'(\sigma_y + \sigma_z), \tag{8}$$

$$\sigma_y' = \sigma_y - \nu'(\sigma_x + \sigma_z), \tag{9}$$

and

$$\sigma_z' = \sigma_z - \nu'(\sigma_x + \sigma_y), \tag{10}$$

where ν' is a parameter dependent upon the structure of the material, σ_x', σ_y', and σ_z' are internal effective stresses, and σ_x, σ_y, and σ_z are boundary stresses. From these expressions it may be seen that internal tensile horizontal effective stresses are present in a uniaxial test.

Judging from our experimental results and those of Conway (1963), the concept of effective stresses seems to be real and in disagreement with elastic theory. If we use equations 8, 9, or 10 to solve for effective internal stress components, then we must determine the value of ν' and its physical significance. Brown and Trollope (1967, p. 234) stated that ν' for ideal linear materials may be equal to Poisson's ratio (ν), but our data do not confirm this. The acrylic model and Conway's epoxy model probably are as close to ideal linear materials as any real material can be. The concrete and granite models probably are anisotropic with local stress concentrating structures (pebbles and grains), but they have a nearly linear response. Our data, however, indicate that ν' more nearly approximates $\nu/(1-\nu)$, and Conway's data also indicate that the same relationship may exist.

The restraining stress necessary to prevent elastic tensile strains from developing in such uniaxially loaded isotropic elastic bodies is equal to $\nu/(1-\nu)$ times the applied uniaxial stress (Obert and Duvall, 1967, p. 474). In the case of the acrylic model, the restraining compressive stress necessary to prevent that model from deforming laterally should be

$$\left(\frac{0.39}{1-0.39}\right)(2{,}100 \text{ lb/in}^2)=1{,}340 \text{ lb/in}^2.$$

Similarly, the restraining lateral, or horizontal, stress in the concrete model should have been about 500 lb/in^2 in tension and uniform in all directions:

$$\left(\frac{0.26}{1-0.26}\right)(1{,}420 \text{ lb/in}^2)=500 \text{ lb/in}^2.$$

The granite model would be subject to a restraining stress of 395 lb/in^2 in all lateral directions:

$$\left(\frac{0.23}{1-0.23}\right)(1{,}320 \text{ lb/in}^2)=395 \text{ lb/in}^2.$$

The average lateral stress components measured in the acrylic-epoxy model, the granite model, and the concrete model prior to tunneling were, respectively, -1,410, -395, and -325 lb/in^2 (all in tension). The absolute values of the effective lateral tensile stress components in a uniaxial test, therefore, approximately agree with the compressive lateral stresses required for perfect lateral confinement.

Our test results are similar to Conway's (1963), and indicate a sharp stress discontinuity at the boundary of the model. This is necessary to account for the difference between σ' and σ.

In addition to the effects of material structure, ν' may also depend on the geometry and the degree of confinement afforded by the body, and possibly on the intrinsic characteristics of the body which determine the nature of the elastic constants ν and E. The variation of the elastic constants may well determine the value of ν'.

The average lateral stress, 1,410 lb/in^2 in tension, measured in the acrylic-epoxy model prior to the start of model tunneling is greatly exceeded by the tensile strength of the acrylic (12,000 lb/in^2). The tensile strength of the high-compressive-strength concrete was estimated to exceed 800 lb/in^2 (Portland Cement Assoc., 1952, p. 5-6). Tensile tests performed on concrete cored from this model indicated a tensile strength of 485 lb/in^2, considerably greater than the average lateral tensile stress of 325 lb/in^2 measured in the anisotropic concrete model before tunneling. The average lateral tensile stress measured by the probe in the granite prior to tunneling, 395 lb/in^2, was much less than the 880-lb/in^2 tensile strength determined by physical specimen testing.

CONCLUSIONS FROM MODEL STUDIES

The model studies increased our confidence in the borehole probe and justified its further use. These results showed that the borehole probe could accurately determine changes in stress magnitude and direction. Both compressive and tensile changes were correctly observed. The reproducibility of stress determinations was shown over a range of known applied stresses within three materials of contrasting physical properties. The influence of boundary conditions was clearly detected by the borehole probe. These studies indicated the areas of application and limitation of elastic theory to predict stress distribution related to the tunnel excavation in rock.

The model-tunnel studies revealed two surprising findings: first, that stress changes occur considerably farther ahead of an advancing tunnel face than theoretically expected, and second, an anomalous stress concentration effect preceding (one or more tunnel diameters ahead of) the anticipated stress buildup near the tunnel face.

These tunnel effects were useful in the interpretation of the field-tunneling studies which are reported in the following section.

FIELD INVESTIGATIONS

ROCK MECHANICS INVESTIGATIONS AT THE COLORADO SCHOOL OF MINES EXPERIMENTAL MINE

The analysis of stress changes related to underground excavation requires a knowledge of the in situ stress field and the significant geologic properties of the rock mass. These significant geologic properties primarily include rock-mass structural discontinuities and compositional features. Knowledge of these properties is necessary because stresses commonly have geologic controls (Bielenstein and Eisbacher, 1969; Lee and others, 1969). The deformation of a rock mass is never strictly homogeneous, in part because geologic materials are, as a rule, heterogeneous and discontinuous. The scale of significant geologic properties may range in size from individual mineral grains to mountain chains to tectonic provinces. Therefore, a satisfactory understanding of the stress field in one part of a mine usually requires knowledge of the geologic history and geologic features over a larger area.

SCOPE OF FIELD STUDIES

The field investigations were carried out in the experimental mine of the Colorado School of Mines, located at Idaho Springs, Colo., 45 km (28 mi) west of Denver in the Front Range of the Rocky Mountains (fig. 25). R. S. Culver of the Colorado School of Mines helped to coordinate the initial U.S. Geological Survey instrumentation program

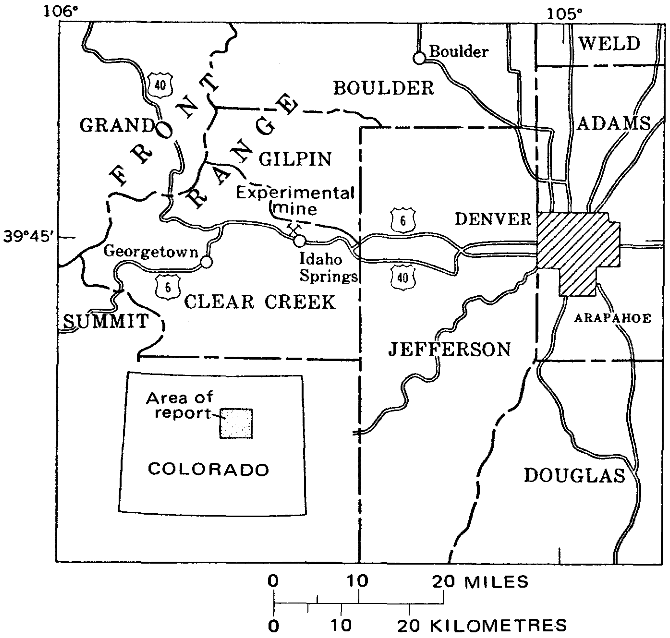

FIGURE 25.—Location of Colorado School of Mines experimental mine at Idaho Springs, Colo.

with the excavation schedule and with rock mechanics studies of other groups in the mine. This coordination provided more information from several types of instruments than otherwise would have been available. These results will be mentioned, where pertinent, in the following sections.

The purpose of our field investigations was to determine what geologic properties cause deviations from gravitational stresses and, in turn, the relation of stress changes produced by tunneling to specific significant geologic properties.

GEOLOGIC SETTING OF THE IDAHO SPRINGS AREA

The general geology of the Idaho Springs area has been described comprehensively by several investigators, including Spurr and Garrey (1908), Bastin and Hill (1917), and Lovering and Goddard (1950). Various features of the Precambrian bedrock have been treated in recent, more detailed studies; structural geology and rock units have been reported by Moench (1964), joint patterns by Harrison and Moench (1961), wallrock alteration by Tooker (1963), general economic geology by Moench and Drake (1966a), and uranium deposits by Sims and Sheridan (1964). Moench, Harrison, and Sims (1962) and Tweto and Sims (1963) gave comprehensive summaries of igneous relationships, tectonic activity, and structural geology.

The Precambrian bedrock in the Idaho Springs area comprises a generally conformable series of folded metasedimentary gneisses and metaigneous and igneous rocks (Harrison and Moench, 1961). Most of the gneissic rocks are thought to represent clastic sedimentary rocks that have been deformed, recrystallized, and partly reconstituted at considerable depth and at high temperatures. Most investigators believe that the ubiquitous foliation represents bedding planes.

Three varieties of granitic rocks have been recognized in the Idaho Springs area. These rocks were intruded into the metasedimentary gneisses during Precambrian time and include granodiorite, quartz diorite, both evidently related to the Boulder Creek batholith, and biotite-muscovite granite, related to the Silver Plume Granite. The granitic rocks form many small bodies that are generally concordant but may be locally discordant. Bodies of granodiorite and quartz diorite have gneissic border zones that are parallel to the foliation and lineation in the gneissic country rocks, suggesting that these rocks were deformed and metamorphosed after their emplacement. The biotite-muscovite granite is rather massive and was emplaced after the principal gneiss-forming metamorphic event.

The Precambrian geologic history of the Idaho Springs area has been summarized by Harrison and Moench (1961, p. B2). The major events recognized by these authors are as follows:

1. Precambrian sediments were deeply buried and reconstituted into high-grade gneisses.
2. The foliated metasedimentary rocks were plastically deformed into major folds with north-northeast-trending axes. The deformation was accompanied by the intrusion of granodiorite, and then minor amounts of quartz diorite and associated hornblendite.
3. Biotite-muscovite granite was intruded near the end of the period of plastic folding.
4. Uplift and erosion of several thousand feet of cover occurred.
5. The Precambrian rocks were deformed locally. Where deformed, the more massive rocks were crushed and granulated; the more foliated gneissic rocks were formed into small terrace, monoclinal, or chevron folds; also some foliated metasedimentary rocks were cataclastically deformed.

The generally deformed condition of most rocks in central Colorado is testimony that this area has been a region of crustal activity throughout much of geologic time. The gneisses show strong foliation, drag folds, mineral alinements, and slickensides, as well as high-grade metamorphic mineral assemblages. These rocks belong to the sillimanite-almandine-orthoclase subfacies of the almandine-amphibolite facies of Turner and Verhoogen (1960, p. 550). The same authors stated (p. 553) that rocks such as these were metamorphosed in an environment having a temperature range of 550°–750°C and pressures of between 60,000 and 120,000 lb/in^2.

During the Tertiary Laramide orogeny, a sequence of porphyry dikes and irregular plutons was intruded into the Precambrian metamorphic and igneous terrane in the Idaho Springs area. These rocks constitute part of a belt of porphyries that extends northeastward across the Front Range and, together with Tertiary mineral deposits, constitutes the Front Range mineral belt (Moench and Drake, 1966a, p. 25). The porphyries were intruded along preexisting planes of weakness in the Precambrian rocks: along joints, foliation surfaces, contacts, faults, and axial planes of folds (Tweto and Sims, 1963). Most of the dikes trend northeastward, but some strike northwest and a few short ones strike east.

Faulting occurred on a grand scale during Tertiary time. Early Miocene to Pliocene faulting displaced mountain versus valley blocks as much as 12,200 m (40,000 ft) vertically (Scott, 1973). Some of the youngest (vein) deposits have been offset in places by movement along faults or fractures (Lovering and Goddard, 1950, p. 170–171), indicating that Laramide stresses were significantly affecting the rock long after the major Laramide igneous (porphyry) intrusions.

The bedrock in the Idaho Springs area indicates a complex geologic history, and the stress field associated with the bedrock of this area has changed in response to geologic events. The regional geologic events have produced the existing geologic and stress conditions present at the field site. These conditions significantly influenced the behavior of the excavations made in the experimental mine.

Field experiments by the U.S. Geological Survey in the Colorado School of Mines experimental mine began in December 1966, when two three-dimensional borehole probes were installed (fig. 26). This date also marked the first field test of the borehole probe. At later dates, 12 additional probes were installed at several locations in the mine. Five instruments were strain-relief overcored in order to determine the in situ stress field. Nine probes were used to monitor time-dependent changes of rock stress related to an active excavation. These were monitored periodically for as long as 4 years. The methods used to install the three-dimensional borehole probe were described by Lee, Nichols, and Abel (1969).

The experimental excavation involved two large rooms (1 and 2) and a central access crosscut between drifts B Left and C Left. Plate 1 is a map of rooms 1 and 2 showing the geologic structures and the locations of the probes. Figure 26 shows the mining sequence in each room and in the central crosscut. The overburden in this part of the mine is about 107 m (350 ft).

Geologic mapping was done throughout the period of field investigations. This procedure allowed us to record rock-mass information as new excavations were made near previously mapped locations. The detailed mine maps of Moench and Drake (1966b) provided helpful background information on the major geologic structures in the experimental mine.

In the vicinity of the two rooms, most of the rock is biotite or hornblende gneiss and gneissic granite with lesser pegmatitic granite and amphibolite. Geologic structural features include two major through-going subparallel faults, three major joint sets, and a conspicuous gneissic foliation (pl. 1; fig. 29). The faults trend east-northeast with a shallow southeast dip and intersect nearly at right angles with the steeply dipping east-northeast-trending foliation. Fault 1 (the southern fault) intersects room 1; fault 2 (the northern fault) intersects the extended central crosscut (pl. 1). Fault 1 has as much as 0.03 m (0.1 ft) of associated gouge and as much as 0.6 m (2 ft) of sheared, mineralized rock on both the hanging wall and the footwall. Fault 2 has 0.02–0.12 m (0.05–0.4 ft) of gouge and as much as 3.7 m (12 ft) of sheared and altered rock—mainly confined to the hanging wall. Both faults are exposed in other openings, as much as 30.5 m (100 ft) away, where they have similar attitudes. One of the major joint sets parallels the generally steeply northwest-dipping, east-northeast-trending foliation usually; another major joint set strikes northwest and dips steeply to the northeast; and a third set dips steeply and strikes northeast approximately perpendicular to the excavation direction.

Mapping of joints in the study area included a visual assessment of the amount of alteration associated with the joint as well as significance (rank) and average spacing of joints. This information was helpful in understanding the complex deformation behavior of the rock mass during and after excavation. For example, where there was strong decompression ($\Delta\sigma_3$) coincident with the orientation of a joint set the information recorded on the geologic map adjacent to each joint symbol (pl. 1) was examined. If gouge, or intense fracturing were associated with the joint surfaces and if the joints were closely spaced, we would expect the rock to be more compressible perpendicular to such joints than parallel to them. This directional anisotropy, if marked, should be detectable from analysis of the three-dimensional stress changes. Indeed, the rock mass seldom responded uniformly to excavation-induced stress changes. Differences in stiffness, controlled by the properties of joints, were important, particularly in the behavior of the rock mass around room 2.

IN SITU STRESS FIELD

Five determinations of the in situ stress field were made in the study area by overcoring probes B-3, 17, 18, 21, and 22 at various locations (pl. 1). The three-dimensional stress field was determined by stress-relief overcoring at five sites, three approximately 4.6 m (15 ft) northwest of room 2 and two approximately 7.6 m (25 ft) west of room 1. Figure 27 and table 12 show the stresses determined.

The composite results of these in situ principal stress determinations show a consistent clustering of orientations (fig. 27). These clusters of preferred principal stress orientations each contain five principal stress determinations. Cluster σ_A contains three maximum and two intermediate principal stress determinations; cluster σ_B contains two maximum, two intermediate, and one minimum principal stress determinations; and cluster σ_C contains four minimum and one intermediate principal stress determinations. Figure 28 suggests that there may be

FIGURE 26.—Plan of field site at Colorado School of Mines experimental mine, showing general arrangement of workings, excavation sequence, borehole probe locations, and major faults.

TABLE 12.—*Calculated in situ stresses*

	Probe B-3			Probe 17			Probe 18			Probe 21			Probe 22		
	Magnitude (lb/in²)	Bearing (degrees)	Plunge (degrees)	Magnitude (lb/in²)	Bearing (degrees)	Plunge (degrees)	Magnitude (lb/in²)	Bearing (degrees)	Plunge (degrees)	Magnitude (lb/in²)	Bearing (degrees)	Plunge (degrees)	Magnitude (lb/in²	Bearing (degrees)	Plunge (degrees)
Principal stresses:[1]															
σ_1	620	N. 68 E.	16	1,805	N. 47 E.	20	1,415	S. 8 E.	38	1,440	S. 74 E.	53	1,020	N. 15 E.	28
σ_2	515	S. 17 E.	17	1,225	S. 16 E.	51	930	N. 66 E.	20	1,045	N. 0 E.	10	770	S. 73 W.	53
σ_3	420	N. 62 W.	66	690	N. 56 W.	32	870	N. 46 W.	45	510	S. 86 W.	35	480	S. 62 E.	22
Near-horizontal stress components along probe axes:															
σ_y	540	S. 54 E.	10	1,115	N. 15 W.	0	960	N. 63 E.	0	1,015	N 75 E.	10	715	N. 72 E.	10
σ_z	585	N. 36 E.	2	1,480	N. 75 E.	2	1,190	S. 27 E.	2	1,010	N. 18 W.	2	810	N. 18 W.	2
Near-vertical stress component along probe axis:															
σ_x	430	N. 66 W.	80	1,125	S. 75 W.	88	1,065	N. 27 W.	88	970	S. 62 W.	80	745	S. 62 W.	80
Horizontal stress components with respect to central crosscut axis:															
σ_{parallel}	555	N. 36 W.	0	1,085	N. 36 W.	0	1,140	N. 36 W.	0	1,085	N. 36 W.	0	675	N. 36 W.	0
$\sigma_{\text{perpendicular}}$	600	N. 54 E.	0	1,680	N. 54 E.	0	995	N. 54 E.	0	795	N. 54 E.	0	810	N. 54 E.	0
Vertical stress component:															
σ_{Vertical}	435		90	1,145		90	1,080		90	1,115		90	785		90

[1] All stresses compressive.

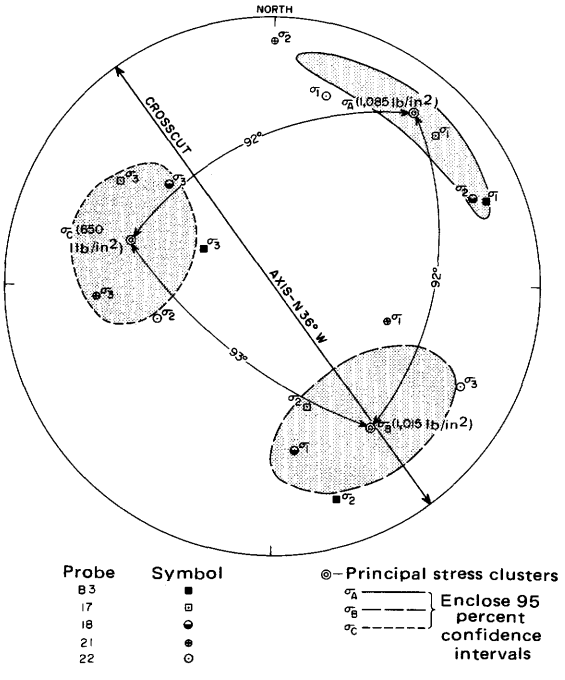

FIGURE 27.—Principal in situ stress orientation determinations (lower hemisphere equal-area projection).

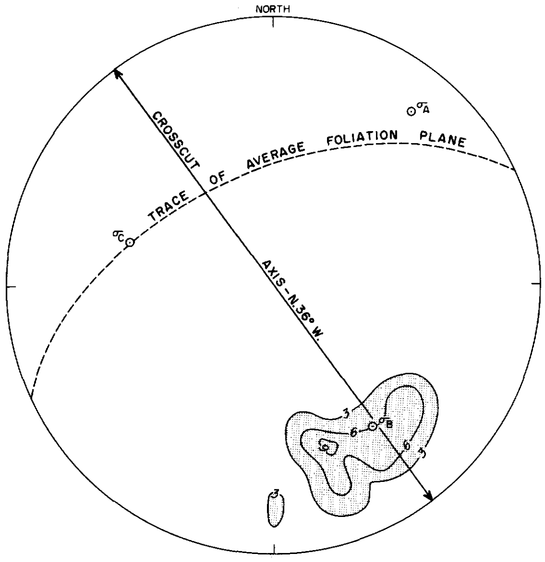

FIGURE 28.—Foliation joints in study area. Lower hemisphere equal-area projection; contoured on 3, 6, and 9 poles per 1-percent area; 51 poles. σ_A, σ_B, and σ_C are centers of principal stress clusters shown in figure 27.

a significant relationship of stress to foliation. The 95-percent confidence interval for the orientations of cluster σ_B covers the full variation of the poles of the foliation present in the study area. The average orientations of the other two principal stress clusters, σ_A and σ_C, lie on and close to the trace of the average foliation plane (fig. 28). The average maximum principal stress cluster (σ_A) is oriented approximately perpendicular to a joint set present in room 2 (SW. quadrant, fig. 29).

The apparent relationship of the present stress-field orientation to much older geologic features, the foliation and jointing, is indicative of the importance of previous geologic events to the orientation of the principal stresses.

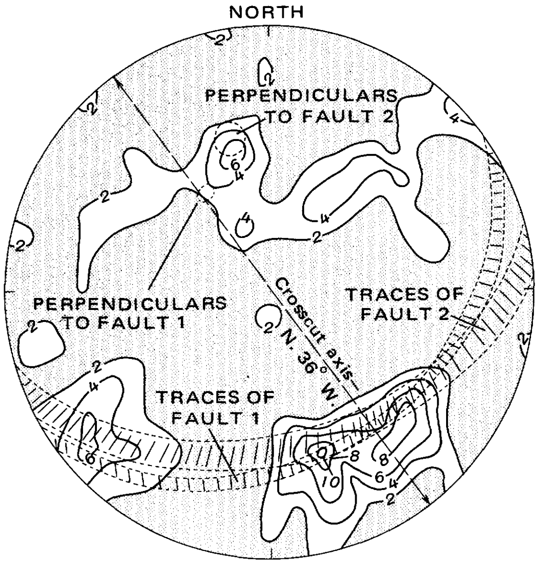

FIGURE 29.—Equal-area diagram of 159 joints in study area. Lower hemisphere projection, contoured on 2 poles per 1-percent area; 159 poles. Also shown are stress-change orientations around room 2.

The foliation is the most persistent geologic structural feature in the study area (pl. 1; fig. 28).

Faults 1 and 2 appear to exert considerable local influence on the stress-field orientation. Figures 27 and 29 show that the average intermediate principal stress direction lies close to the planes of faults 1 and 2. Also, the principal stress orientations determined at probe 17 (located 3.7 m (12 ft) in the footwall northwest of fault 1) were rotated into or toward the trace of fault 1 and toward and perpendicular to fault 1 relative to the principal stresses determined at probe B-3 in the hanging wall of fault 1.

The variations in the magnitudes and orientations of the principal stresses included in the individual clusters may be related to variations in stiffness between foliation layers and to joints perpendicular to the foliation. An accuracy of about 3 percent for the average of each cluster of stress orientations is indicated by the independent check for orthogonality shown in figure 27.

The influence of anisotropic changes in modulus across foliated lithologic contacts or across and along faults and joints apparently caused large local variations in the background stress field. A nearby stress-field determination was used, in preference to the average condition, for analysis of rock behavior throughout this report whenever available. A nearby stress-field determination should be more accurate near the site of determination. Because of the complexity of the geologic environment and the small number of in situ stress determinations, extrapolation of a local stress-field determination, particularly stress magnitudes, over more than a few feet can be grossly misleading (table 12). When a nearby stress-field determination was not available, the average in situ stress field was used for analysis.

The U.S. Bureau of Reclamation made nine biaxial plane-strain overcore stress-relief measurements in one borehole with an instrument similar to the U.S. Bureau of Mines borehole deformation gage at the location shown in figure 26. The average results in a vertical plane oriented N. 80° W. were 850 lb/in^2 vertical compressive stress, 680 lb/in^2 horizontal compressive stress acting N. 80° W., and a shearing stress of +170 lb/in^2 acting in the plane. The comparable average stresses calculated from the composite stress-cluster data (fig. 27) are 780 lb/in^2 vertical compressive stress, 890 lb/in^2 horizontal compressive stress acting N. 80° W., and a shearing stress of +180 lb/in^2 acting in the plane. The stress values of the U.S. Bureau of Reclamation lie within the variations of the principal stress clusters (table 13).

The magnitudes and orientations of the principal stresses and principal stress clusters cannot be explained on the basis of the 106.7 m (350 ft) of overburden present. Overburden can account for only approximately 385 lb/in^2 of vertical stress and 115 lb/in^2 of horizontal restraining stress. Nor were we convinced that active tectonic boundary forces produced these stresses. In order to determine whether residual stresses (Varnes, 1970; Varnes and Lee, 1972) might provide an explanation for the observed stress magnitudes and orientations, several laboratory tests were performed.

Six-inch-diameter core samples of gneiss were taken from the Idaho Springs Formation in the study area, placed in a temperature-humidity-controlled room, strain gaged, and overcored. Relieved residual extensional

TABLE 13.—*Principal in situ stress clusters determined in field study area*

Principal stress cluster	Bearing (degrees)			Plunge (degrees)			Magnitude[1] (lb/in^2)		
	Average	95-percent confidence interval		Average	95-percent confidence interval		Average	95-percent confidence interval	
		From	To		From	To		From	To
A	N. 39 E.	N. 5.8 E.	N. 72.2 E.	19	11.4	26.6	1,085	583	1,587
B	S. 35 E.	S. 2.0 E.	S. 68.0 E.	36	17.1	57.9	1,015	463	1,567
C	N. 73 W.	N. 43.0 W.	S. 77.0 W.	44	23.9	64.1	650	437	863

[1] All stresses are compressive.

strains measured by six overcored strain gages stabilized from + 1 to +554 μin./in, 1,050 hours after overcoring. The average residual strain measured was 175 μin./in. The indicated equivalent stored compressive stress prior to release ranged from 8 to 4,350 lb/in².

Thus, sufficient residual strains are present in some rocks of the Idaho Springs Formation to account for the stress magnitudes measured by in situ stress-relief overcoring and to provide the driving stresses indicated by the magnitudes of decompression during long term stress monitoring, which are discussed in the following sections. The range of magnitudes of the residual strains would favor an in situ stress field containing residual components in addition to those induced from other sources.

EXPERIMENTAL ROOM 1

Prior to excavation of room 1, two three-dimensional borehole probes, 5 and 8, were installed (fig. 26). Probe 5 was in the southwest wall of the future room, approximately 0.9 m (3 ft) above floor level, and probe 8 was in the northeast wall. Both installations were completed before section 2 of the room excavation began. Figure 26 shows the sequence and date of the sections removed. The room, primarily excavated for rock-bolt performance studies, was to have been 7.3 by 12.2 m (24 by 40 ft). Access was provided to the room from B-Left drift by a smaller central crosscut. Additional strain information was available from single- and multiple-position extensometers and from instrumented rock bolts that had been installed in the roof of the room by R. S. Culver, Colorado School of Mines, as excavation proceeded. Some of these extensometers were positioned across fault 1; thus, displacements along the fault were well documented (Culver, 1967).

The relationships of fault 1 and of the foliation to stresses determined at probes 5 and 8 are shown in figure 30, both instruments being approximately 3.7 m (12 ft) (normal distance) from the fault plane, probe 5 in the hanging wall and probe 8 in the footwall. Excavation proceeded northwesterly, beginning in the hanging wall of fault 1. When the excavation of section 3 (fig. 26) intersected the fault surface, measured displacements of as much as 0.01 cm (0.004 in.) occurred across the fault (Culver, 1967). Vertical decompression (that is, a tensile stress change) followed on footwall probe 8, and at the same time hanging wall probe 5 experienced moderate increase of compression. Figure 31 shows the vertical components of time-dependent stress changes determined by data monitored on probes 5 and 8. The beginning of a large decompression on probe 8 (fig. 31) coincided with measured displacements of as much as 0.5 cm (0.2 in.) across the fault (Culver, 1967), which occurred after the last round (14) was excavated from the room. In the footwall at probe 8, a vertical decompression of approximately 3,500 lb/in² took place during a period of a little more than a month, indicating continuing displacement along the fault plane accompanied by stress readjustments in the rock mass. During this time, there was no excavation activity, but the loosening of slabs of rock from the roof and wall above probe 8 became serious and caused the excavation plan to be abandoned. Remedial bolting and subsequent renewed excavation of the central crosscut in July (fig. 31) resulted in further adjustments in the stress field around probe 8. Load-carrying ability of the rock was effectively increased by the rock reinforcement, as shown by the 3,200-lb/in² increase in compression in the rock. The renewed excava-

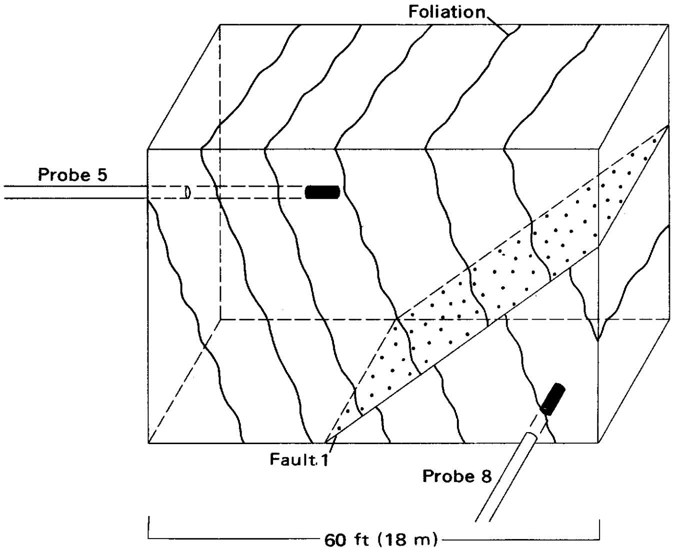

FIGURE 30.—Generalized view showing relationship of hanging wall and footwall of fault 1 (stippled) to foliation and to probes 5 and 8.

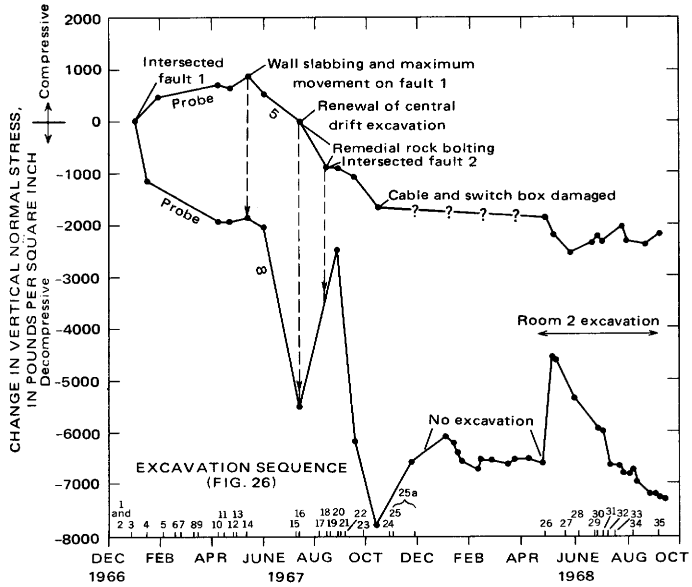

FIGURE 31.—Vertical normal stress in rock adjacent to probes 5 and 8 as excavation advanced. For clarity, only data at inflection points have been used.

tion activity and rock bolting were apparently too far away from probe 5 to greatly affect the stress conditions in its vicinity; however, a slow decompression continued, probably caused by continued adjustment along fault 1. When the central crosscut penetrated fault 2 in July and August 1967, another large time-dependent decompression was produced in the footwall around probe 8 (fig. 31), and a smaller decompression was produced on probe 5.

In late July 1967, probes 9 and 10 were installed approximately 15.8 m (52 ft) ahead of the face of the central crosscut (fig. 26). These probes, which are discussed in detail later, were subjected to increased compression during the period of fault 2-related decompression of probes 5 and 8 (fig. 31). Fault 2 was partially exposed in the lower right-hand corner of section 16 and was fully exposed around the entire section of the central crosscut with the removal of section 17. Apparently, the intersection of fault 2 caused a time-dependent transfer of compression stress from the rock in the vicinity of probes 5 and 8 to the rock in the vicinity of probes 9 and 10. Such time dependence can be reasonably explained by slow adjustments of individual joint blocks responding to changing stress conditions along and adjacent to excavation-activated faults.

When viewed in three dimensions, the stress-change orientations reveal even more strikingly their relation to geologic features and excavation activity. Figure 32 shows the traces of the plane of fault 1 and the average foliation plane in the same vicinity, the poles of the fault, and perpendiculars to the foliation planes. The other poles in the figure represent 10 principal stress changes at probe 8 obtained from daily measurements over a 2-week period beginning at the time excavation intersected fault 1. The attitudes of the three principal stress changes are shown by the indicated symbols. The data show that the intermediate principal stress changes consistently are oriented nearly horizontally in a plane parallel to the fault and that they bear to the southwest, nearly at right angles to the dip of the fault and foliation planes. Both the maximum and the minimum principal stress changes are oriented either approximately in the plane of the fault or approximately perpendicular to the fault. The poles of the maximum and minimum stress changes exchange positions from time to time, as shown by their alternations in readings 4 through 10. Later measurements (fig. 33) showed that the poles shown in the north half of the diagram migrated with time to form a maximum perpendicular to the fault. For the 2-week period, all poles in the southeast sector (on or near the fault plane) represent the greatest absolute stress changes—changes of either maximum compression or maximum decompression. This fact indicates that, as excavation in the footwall continued, the rocks bordering the fault were expending strain energy—rebounding—in a series of contractions and dilations having an almost daily periodicity. This behavior is attributed to the sudden removal of natural rock support across fault 1 by movement along fault 1. Movement on the fault appears to have allowed stored (potential) energy to be gradually expended, as indicated by the overall decompression in the rock around probe 8 during this 2-week period (fig. 32).

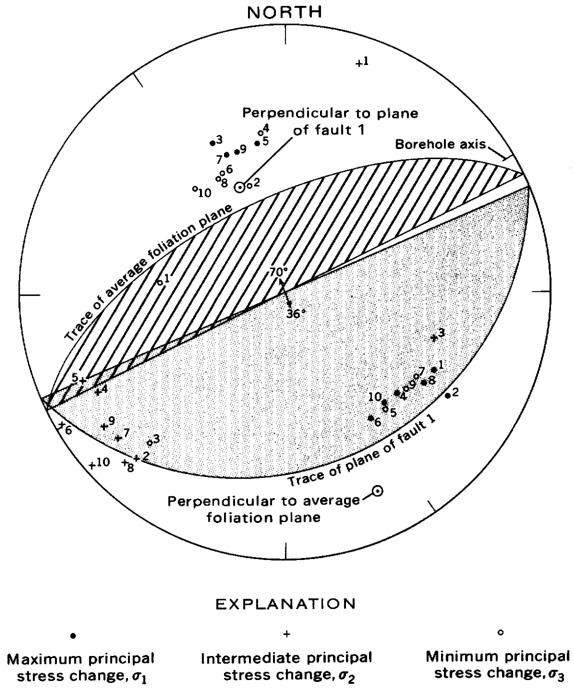

FIGURE 32.—Equal-area lower hemisphere diagram of poles of principal stress changes, as determined from probe 8. Shown are 10 readings taken over a 2-week period, beginning when mining intersected fault 1 (fig. 26).

Figure 33 shows equal-area diagrams for the directions of all 219 principal stress changes ($\Delta\sigma_1$, $\Delta\sigma_2$, and $\Delta\sigma_3$ not differentiated) measured by probes 8 and 5 during room 1 excavation. Contours represent percent of intercepts in a 1-percent area. Also shown in the equal-area plots are planes representing the attitude of fault 1 and the average attitude of foliation. Orientations of the three principal stress changes during the period are concentrated within small intercept areas. However, the individual orientations of $\Delta\sigma_1$, $\Delta\sigma_2$, and $\Delta\sigma_3$ shifted from time to time from one intercept area to another, but at any one time one principal stress-change intercept is present within each area of concentration.

The plots for both probes show very strong concentrations that are related to geologic features or to excavation direction and excavation procedures. Probe 8 in the footwall shows a very strong concentration of stress-change directions in the southeast quadrant, on the trace of the fault plane. A second concentration in the northwest quadrant lies near the trace of the average foliation plane and includes the direction perpendicular to the fault. The third concentration coincides with the pole of a major joint set (not shown in the diagram). The plots of stress-change directions for probe 5 in the hanging wall are dif-

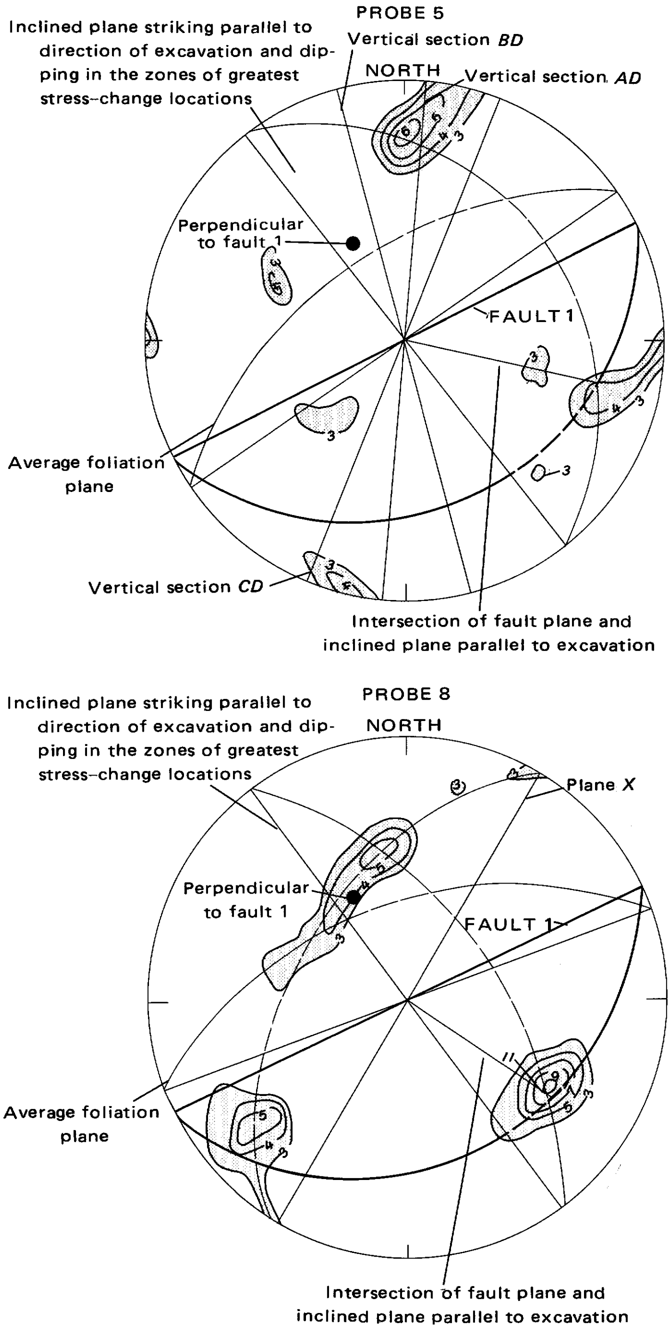

FIGURE 33.—Comparative equal-area lower hemisphere diagrams of undifferentiated principal stress-change directions ($\Delta\sigma_1$, $\Delta\sigma_2$, $\Delta\sigma_3$) determined at probes 5 and 8. Probe 5; 219 poles, Jan. 5 to June 6, 1967; probe 8; 225 poles, Dec. 12, 1966, to June 6, 1967. Contours represent percent of stress-change directions per 1-percent area. See figure 34 for location of lines of vertical sections *AD*, *BD*, and *CD*.

ferent from those of probe 8 in that only one concentration is strongly related to geologic features. There is a concentration in the southeast quadrant that lies across the trace of the fault plane, but it is weaker and does not have the same orientation as the similar concentration for probe 8. The strong stress-change clusters for probe 5 in the northeast and southwest quadrants are not clearly associated with any geologic features, but they are alined very closely with the average strike of the vertical section through probe 5 that corresponds to the longest dimension of the room during that particular stage in the excavation sequence. Figure 34 shows the average strike (*AD*) of the longest vertical section through the room and the strike *CD* and *BD* of the vertical sections, which show the limits of migration of this plane during excavation. These same sections, *CD* and *BD*, can be seen to limit the boundaries of the strong concentration of stress changes (fig. 33). The weak concentration seen in the northwest quadrant is not clearly associated with any known geologic or excavation feature, although it approximates the direction perpendicular to the fault.

The data from probe 8 (fig. 33) show that within the footwall of fault 1 the directions of principal stress changes, which are nearly all decompressive, aline closely with geologic structures. Without exception, the major and minor principal stress changes for any long-term, large-magnitude change are either perpendicular to the intersected fault or lie within that fault plane. The same long-term changes are not so strongly related to the folia-

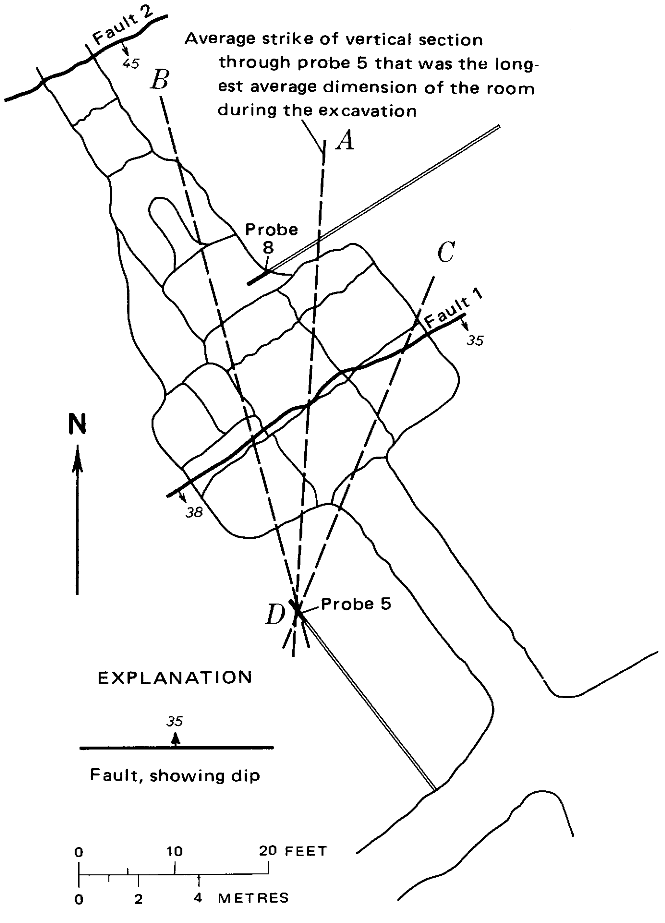

FIGURE 34.—Map of room 1 in Colorado School of Mines experimental mine showing strike of vertical sections *AD*, *BD*, and *CD*.

tion. The fact that the foliation and the nearby fault planes are practically at right angles tends to obscure the role played by foliation.

At probe 8, the directions of stress changes appear to be controlled by geologic structure, and directional influences of excavation procedures are obscured. However, the equal-area plot indicates that the direction of excavation may have some influence because two of the largest stress-change clusters lie on the trace of a plane that strikes parallel to the general direction of excavation. One of these clusters lies nearly at the intersection of this plane and the fault plane. Another plane, *X*, whose intercept on the lower hemisphere coincides with a great circle cutting through the two smallest clusters, has no apparent relation to the geologic structure or to the excavation.

The data for probe 5 indicate that room geometry exerts more influence on the changing stress field in the hanging wall than in the footwall of fault 1. The majority of stress changes are compressive, and the largest cluster lies in the vertical plane containing the longest average dimension of the room during that particular stage in the excavation sequence. Also, similar to probe 8, two of the largest stress-change clusters for probe 5 occur on the trace of a plane parallel to the direction of excavation, and one of the clusters occurs at the intersection of traces of the excavation plane and the fault plane. Excavation directions appear to exert a significant influence on the orientation of stress-change directions.

An explanation other than one dependent on a gravity-load elastic analysis is needed to provide a reasonable understanding of the changing stress field. The natural (in situ) stress-field information (obtained after room 1 was excavated) was helpful in this respect.

The directions of the measured maximum principal in situ stresses in both the hanging wall(probe B-3) and the footwall (probe 17) are alined approximately parallel to the strike of fault 1 (table 12 and fig. 35). The maximum principal stress in the footwall is nearly three times the subparallel maximum principal stress in the hanging wall. The direction of the intermediate principal stresses in both the hanging wall and the footwall is approximately down the dip of fault 1. The intermediate principal stress in the footwall is approximately 2½ times the subparallel intermediate stress in the hanging wall. The minimum principal stresses in both the hanging wall and the footwall are roughly normal to the plane of fault 1. The minimum principal stress in the footwall is 1½ times the subparallel minimum principal stress in the hanging wall. These differences in magnitude occur over a distance of only 7.6 m (25 ft) across fault 1, and, assuming that the rock at these locations was unaffected by the excavation, these stresses represent the preexcavation stress field. During faulting, more energy may have been released in the hanging wall than in the footwall, owing to less confining pressure on the hanging wall than on the footwall.

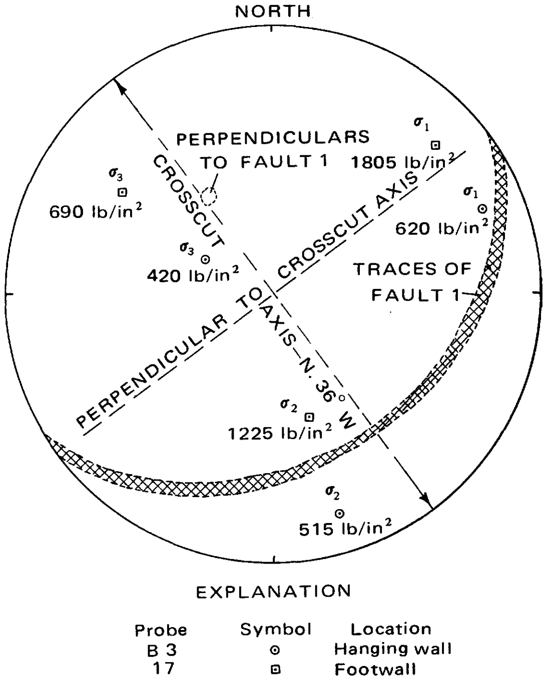

FIGURE 35.—Orientation of in situ stresses determined in walls of fault 1. Equal-area lower hemisphere projection.

The vertical normal stress component is 435 lb/in^2 in the hanging wall, a figure that corresponds approximately to the stress produced by the estimated 107 m (350 ft) of overburden. However, the vertical normal stress component in the footwall was 1,145 lb/in^2, almost three times that in the hanging wall, too high to be explained by the same 107 m (350 ft) of overburden. As the result of the principal stress differences across fault 1, rather large shear stresses must have been present within the rock mass surrounding fault 1. When downdip confinement along fault 1 was reduced during the excavation of room 1, the shear strength of the rock material in the fault was exceeded. Movement occurred in the fractured rock zone around fault 1, and further enlargement of room 1 had to be stopped.

EXPLANATION OF STRESS CHANGES IN ROOM 1

In the initial stages of excavation, the access drift was advanced toward fault 1 and the natural high level of stress within the footwall was further concentrated. When the advancing opening penetrated the fault displacement occurred and stresses in the footwall were partially relieved; but the stresses in the hanging wall continued to build up. As can be seen in figure 36, when the room was excavated beyond the fault (first row of excavation) the hanging wall apparently began to act as a support member for the roof load (commonly called arch load), as evidenced by increased compressive stress in probe 5. The effective ovaloid room cross section intersecting probe 5 and parallel to the longest ceiling support distance should contain the highest magnitude tangential stresses. The major principal stress-change directions occur in or near this plane, as demonstrated in figure 33. If an ovaloid section represented by a hypothetical line of zero change in stress level, as shown in figure 36, is used to represent the longest effective section of the excavated room, a tangential stress concentration at probe 5 would be approximately three times the vertical normal stress of the theoretical stress field (Obert and others, 1960, p. 12). The hypothetical zero stress-change line was approximately located using extensometer data obtained by Culver (1967). The vertical normal stress, as determined from overcoring in the hanging wall near probe 5, was 435 lb/in^2 (table 12) as compared to approximately 900 lb/in^2 increase in vertical normal stress at probe 5 caused by excavation during the first 5 months. At the end of this period the total vertical stress on probe 5 was approximately 1,335 lb/in^2 or slightly greater than three times the original vertical stress, which agrees with the stress concentration predicted by the ovaloid opening analysis.

None of the principal stress-change directions shown in figure 33 are vertical, but all are shallow plunging. This information agrees with the finding that the plunge of the major principal stress direction of the natural stress field was 16° in the hanging wall and 20° in the footwall. The low-angle, high-magnitude tangential stress at the curved corner of the ovaloid opening is, therefore, further increased by the relatively high horizontal stress component of the in situ stress field. Continued fault movement and decreased shear resistance along the fault caused the roofload and, hence, the line of zero stress level to progressively shift upward and northward, allowing the footwall support section in which probe 8 is located to be relieved of its load (fig. 36). However, probe 5 continued to show a net increase in compressive stresses related to the arching roofload. Decompressive stress changes then began, probably as a result of fault movement that caused a redistribution of the roofload over an even wider span extending beyond probe 5. Probe 8 showed large decompressive stress components parallel to and perpendicular to the fault surface, indicating a decrease of compressive stress in these directions. Apparently the stresses in the footwall were decreasing because the footwall near probe 8 was no longer supporting the roofload and because the confinement of this highly prestressed rock had been removed. The wall, relieved of its load, was deflecting into the room.

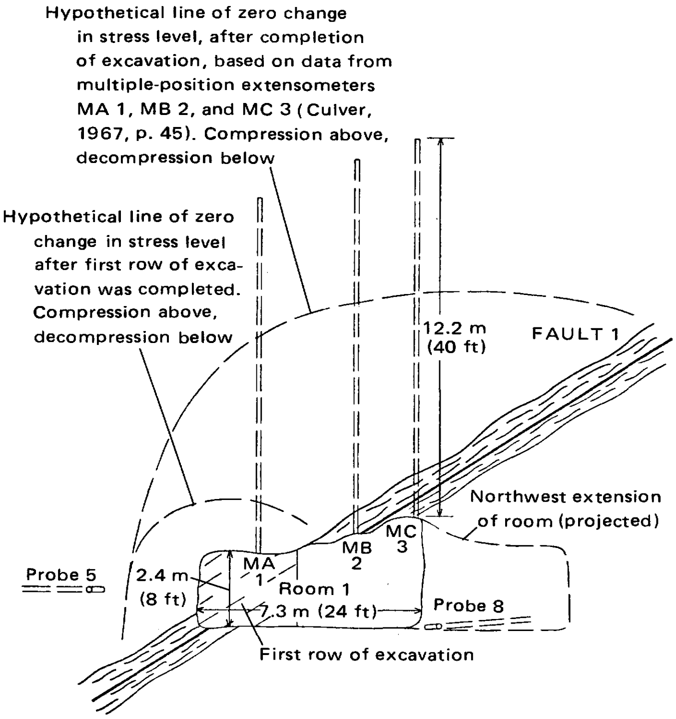

FIGURE 36.—Cross section *AD* (fig. 34) containing probe 5, constructed parallel to the longest average dimension of room 1 during most of the excavation, showing hypothetical lines of zero change in stress level after two stages of excavation.

Decompression continued on probe 5 during July, August, September, and October 1967 (fig. 32), apparently resulting from the advancing excavation and continued disturbance of the existing fault and joint system.

STRESS CHANGES AHEAD OF THE CENTRAL CROSSCUT EXTENSION

Most field measurements of rock response axially behind an advancing face differ from the anticipated elastic response. For example, in the Straight Creek pilot bore in Colorado (Abel, 1967, p. 16) rock-mass deformations took place over a zone 6–60 tunnel diameters behind the advancing face. Field measurements generally agree, however, with the extent of the radial influence zone around a tunnel as predicted elastically and photoelastically (for example, see Abel, 1967, p. 19).

The distance ahead of the tunnel face in which the stress distribution is affected by the advancing tunnel is essentially unknown. To our knowledge, no measurements of deformation, strain, or stress have been reported for the rock ahead of a tunnel. There are obvious physical difficulties in instrumenting this region.

A number of European investigators, however, have made convergence measurements ahead of advancing longwall mining faces. A longwall face, normally on the order of 183–914 m (600–3,000 ft) long and 0.9–2.7 m (3–9 ft) high, approximates the geometry of a tunnel in the plane perpendicular to the longwall face. The divergence of the reported results is informative in anticipating the zone of influence in the rock ahead of a tunnel where a strain sensor could conceivably detect stress changes associated with the tunnel excavation. Various investigators at the International Conference on Strata Control in Paris, France, in 1960 reported on their findings on the extent of the zone of influence ahead of longwall mining faces as follows:

Potts (1961), Kolar Schist, India: Onset >4.6-6.1 m (>15-20 ft).

Denkhaus and Hill (1961, p. 247-248), Quartzite, South Africa: Onset >6.1 m (>20 ft), peak 4.6-6.1 m (15-20 ft).

Leeman (1961, p. 308), Quartzite, South Africa: Onset at 7.6 m (25 ft), peak <3.7 m (<12 ft).

de Reeper and Bruens (1961, p. 328), Coal, Belgium: Onset at 4.6 m (15 ft) (approximately five thicknesses of seam ahead of face).

Carter (1961, p. 471), Coal, Great Britain: Onset <66 m (<216 ft), peak <14 m (<46 ft).

Spackeler (1961), Coal, East Germany: Peak <5.5 m (<18 ft) (probably <3.7 m (<12 ft)).

Henshaw (1961), Coal, Great Britain: Onset >14 m (>46 ft).

The wide variation in these field measurements, showing onset of stress from 5 to 25 seam thicknesses ahead of the face, and peak stress from 0 to 8 seam thicknesses, departs markedly from the theoretical prediction of the onset of such stress changes 1 diameter ahead of the tunnel face.

Following the termination of excavation of room 1, as the result of bad roof and wall conditions associated with fault 1, the central crosscut was extended on the same N. 36° W. bearing until it intersected C-Left drift (pl 1; fig. 26). Probes 9 and 10 were installed ahead of the advancing tunnel and were monitored starting on July 28, 1967, following excavation of section 16 (fig. 26). The results of this field sutdy of the stress changes occurring ahead of an advancing tunnel were compared with the laboratory model-tunnel studies.

The stress-change histories for probes 9 and 10 from August 4 until they were destroyed by advance of the central crosscut are presented in figure 37. They demonstrate an initial increase in compressive stress followed by a large decrease in compressive stress. The magnitudes of the stress changes measured by probe 10 were consistently less than those measured by probe 9.

The onset of stress changes associated with the advancing tunnel took place as early as or before the probes were installed because stress changes were recorded upon installation of the probes. This change occurred more than 7 diameters ahead of the advancing tunnel face (figs. 27, 37). Elastic analysis predicts the onset of stress change at 1 tunnel diameter ahead of the tunnel face. In the elastic acrylic model the onset occurred more than 4 tunnel diameters ahead of the model tunnel, in the heterogeneous isotropic concrete model it occurred at more than 2½ tunnel diameters ahead, and in the anisotropic homogeneous granite model it occurred at more than 2 tunnel diameters ahead. The results of studies of longwall behavior mentioned above indicate that the onset of stress influences related to longwall mining could be detected from 5 to more than 25 seam thicknesses ahead of the advancing face.

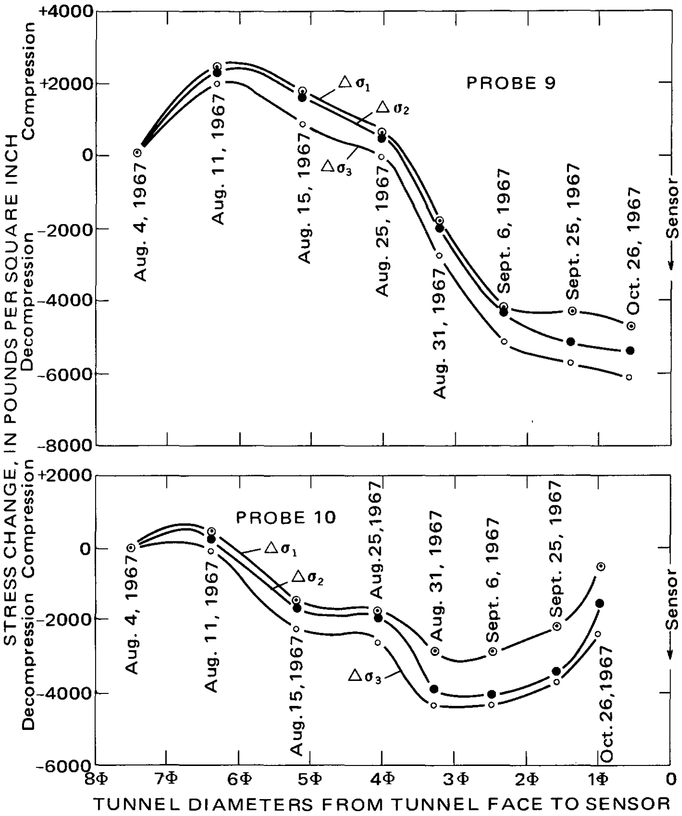

FIGURE 37.—Principal stress changes caused by advance of central crosscut. Date of excavation is shown.

A compressive stress peak was measured by probes 9 and 10 between approximately 6 and 6½ tunnel diameters ahead of the advancing tunnel face (fig. 37). No such stress peak is predicted by elastic theory. The absolute stress of this peak is not known, because probes 9 and 10 sensed stress changes relative to an initial reading without reference to a known premining in situ stress field. A similar compressive stress peak was observed in each of the tunnel models, at 2 tunnel diameters for the acrylic model, at 1¼ tunnel diameters for the concrete model, and at 1 tunnel diameter for the granite model. The results from the longwall measurements indicate a peak of from less than four seam thicknesses to somewhat more than eight seam thicknesses ahead of the advancing longwall face.

The results from probes 9 and 10 of our field study approximately agree with the available field data but disagree in magnitude with the laboratory results and disagree with elastic theory.

The orientation of the average maximum principal background stress cluster (σ_A) in the study area is flat lying and trends northeast-southwest, and the orientation of the mean intermediate principal background stress is gently plunging and trends northwest-southeast. Because

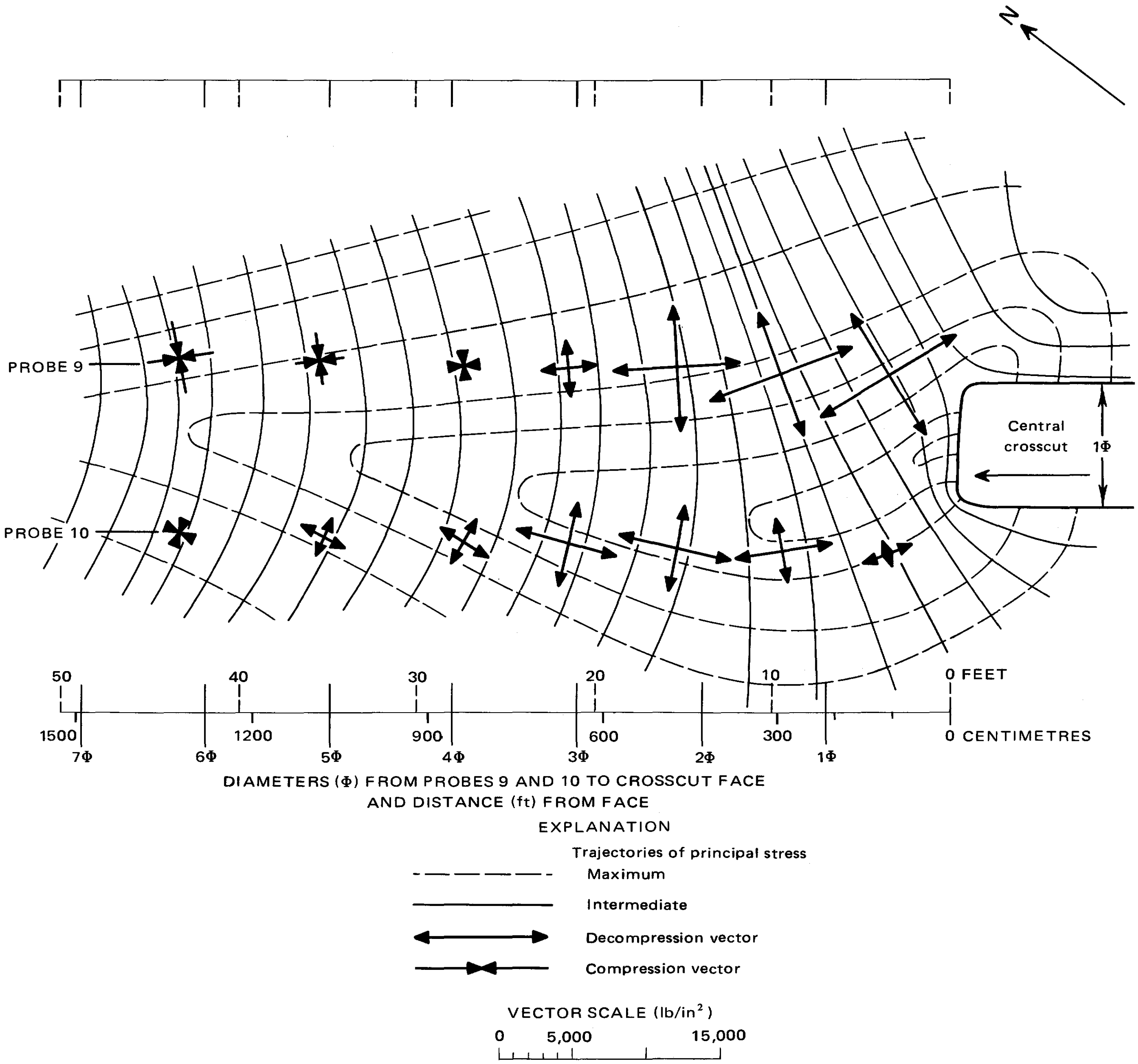

FIGURE 38.—Plan view of stress-change trajectories and stress-change vectors. Follow vectors and trajectory lines from left to right across diagram to simulate the effect of approaching excavation.

the maximum and intermediate stress changes near probes 9 and 10 were also nearly flat lying, a plan view containing these near-horizontal principal stress-change vectors could be constructed (fig. 38) which would show the stress response as the crosscut advanced. This diagram shows stress changes with respect to distance and to crosscut diameters ahead of the face. The locations of the stress-change vectors are related to their distance from the face of the crosscut after each increment of advance and therefore do not represent a typical plan illustration.

The pattern of the stress-change trajectories suggests: (1) the stress orientations are influenced by foliation and fault attitudes, (2) the onset of tunnel-excavation-induced stress response is at least 7 diameters ahead of the tunnel, (3) the orientation of the minor asymmetry of stress trajectories ahead of the advancing crosscut is grossly similar to the orientation of in situ stresses, which suggests an interaction between stress changes induced by mining and the mean maximum principal background stress cluster (σ_A), and (4) the tensile stress changes progressively increase in all directions as the central crosscut approaches the probes.

The departure of the stress change versus distance relationship from elastic predictions, laboratory model measurements, and photoelastic measurements suggests that rock-mass properties controlled the rock-mass response. The central crosscut was driven normal to the strike of the major geologic weakness in the rock mass, the foliation. This rock-mass weakness could allow extensional strain relief parallel to the crosscut axis and normal to the plane of foliation. Apparently the rock expanded preferentially perpendicular to these discontinuities, toward the crosscut face.

The influence of fault 1 on the nearby stress field, as previously discussed, directed our attention to the possible similar influence of fault 2 on probes 9 and 10. The relative locations of fault 2 and probes 9 and 10 are shown in figure 26. Initial compression, followed by large decompression, occurred on the lower stressed (footwall) side of fault 2 (fig. 37) as the tunnel advanced, a behavior similar to that of fault 1 (fig. 31). The advance of the excavation toward probes 9 and 10 provided a means for the stress to be transferred from the higher stressed hanging wall to the lower stressed footwall of fault 2. This decompressive stress release dominated the response of probes 9 and 10. The overall effect of crosscut advance was to decompress the rock ahead of and to the side of the crosscut.

EXPERIMENTAL ROOM 2

Room 2 was excavated after the central crosscut had been driven to the intersection with C-Left drift. The excavation of room 2 was accomplished by widening the central crosscut to 7.3 by 18.3 m (24 by 60 ft). The sequence of excavation is shown in figure 26. R. M. Cox of the Colorado School of Mines designed the room and supervised its excavation for rock-bolt performance studies (Cox, 1971). Prior to excavation, probes 15, 19, 24, and 25 were installed in the roof of the central crosscut at the locations shown in figure 26. Probes 15 and 24 were installed 5.5 m (18 ft) above the ceiling, whereas probes 19 and 25 were only 1.2 m (4 ft) above the ceiling. The location of probe B-5, also shown in figure 26, was in the northwest wall, about 5.5 m (18 ft) from the central crosscut.

Multiple-position borehole extensometers (MPBX's) were installed by Cox (1971) at locations shown in figure 39. These MPBX's were placed so that they extended 12.2 m (40 ft) above the roof of the central corsscut. Figure 39 shows the relationships of probes 15, 19, 24, and 25 and MPBX's 1, 2, and 3 to fault 2, all being located in the footwall. The roof probes were spaced from 7.6 to 14.2 m (25–46.5 ft) from the fault surface, probe 15 being the closest and probe 25 the farthest. It is doubtful that any of the MPBX installations intersect the plane of fault 2 unless the dip of the fault above the roof decreases to less than the 45° dip measured in the central crosscut. The 12.2-m (40 ft) anchor of MPBX-1 would be located very close to the fault plane and probably is in locally sheared rock adjacent to the fault. Probe B-5, which lies northwest (to the right)of the area of the cross section shown in figure 39, is approximately 18.9 m (62 ft) from the surface of fault 2.

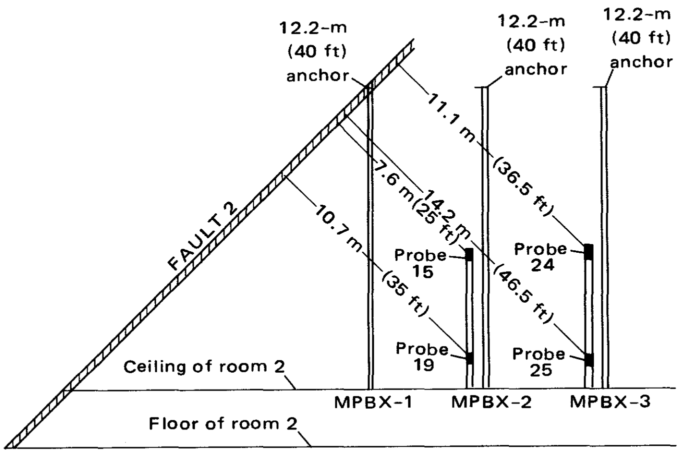

FIGURE 39.—Generalized section showing relation of borehole probes, multiple-position borehole extensometers (MPBX's), and fault 2. In order to show true dip of fault, horizontal distances are exaggerated.

The excavation of room 2 began in April 1968 and proceeded essentially by excavating four 1.2- by 2.4-m (4- by 8-ft) slabs the length of the 15.2-m (50 ft) room, two on each side of the central crosscut (fig. 26). The room was successfully completed in September 1968. Other smaller excavations were made as needed to trim the ends (transitions) of the room. The extensometers and stress probes were read by Cox (1971) before and after excavation of each slab. The data used in the following discussions were compiled from the borehole stress probes and the MPBX installations before, during, and after each slab was excavated from the room, during the period April 4, 1968, through January 1, 1969.

Figure 40 shows principal stress changes with time for probes 15,19, 24, and 25 above room 2 and probe B-5 to the west of room 2. Figure 41 is a similar plot of the total strains that occurred between anchors of each MPBX installation. Prior to May 26, 1968, some small excavations were made in the transition zone on the right side and the first slab was presplit. During this period the rock near deep probe 24 compressed and the rock near shallow probe 25 decompressed (fig. 40). The equal-area plot (fig. 42*A*) from deep probe 24 over the five intervals prior to May 26 shows that the principal stress-change directions ($\Delta\sigma_1$,$\Delta\sigma_2$, $\Delta\sigma_3$) cluster in three small groups that are related to the orientation of the in situ stress field, the excavation direction, and fault 2. The orientation of these clusters is very close to that of the average principal stresses and to the principal stresses determined from overcoring nearby probe 18. Two stress concentration clusters lie in or close to the vertical plane striking in the direction of the central crosscut axis and normal to the foliation. One of these clusters (fig. 42*A*) appears to be related to the intersection of the vertical plane and the trace of the plane of fault 2, and the other cluster is nearly perpendicular to the fault. The third cluster (consisting only of $\Delta\sigma_2$) is nearly hori-

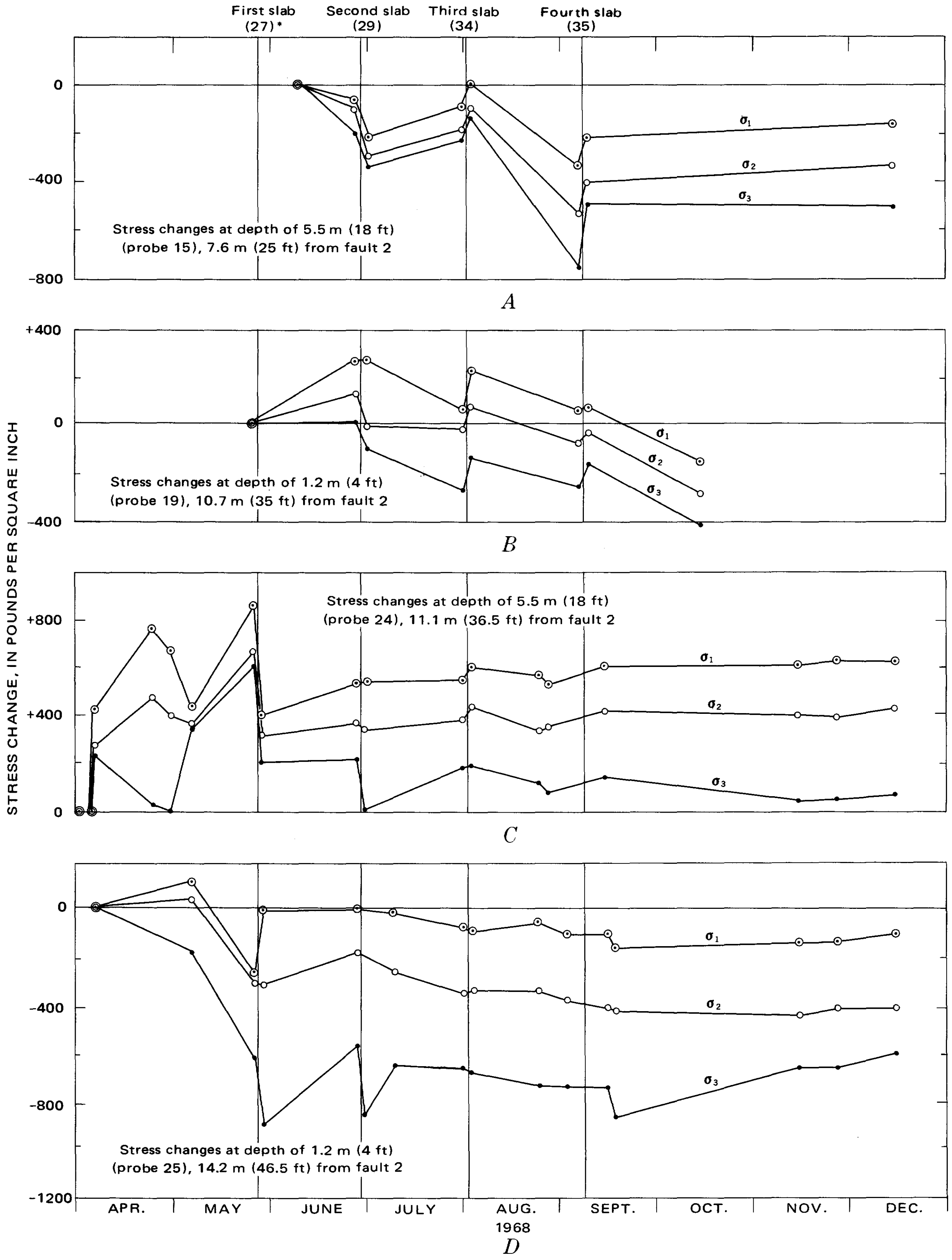

FIGURE 40.—Principal stress changes in roof during excavation of room 2. *, see figure 26 for location of slabs. +, compression; -, tension.

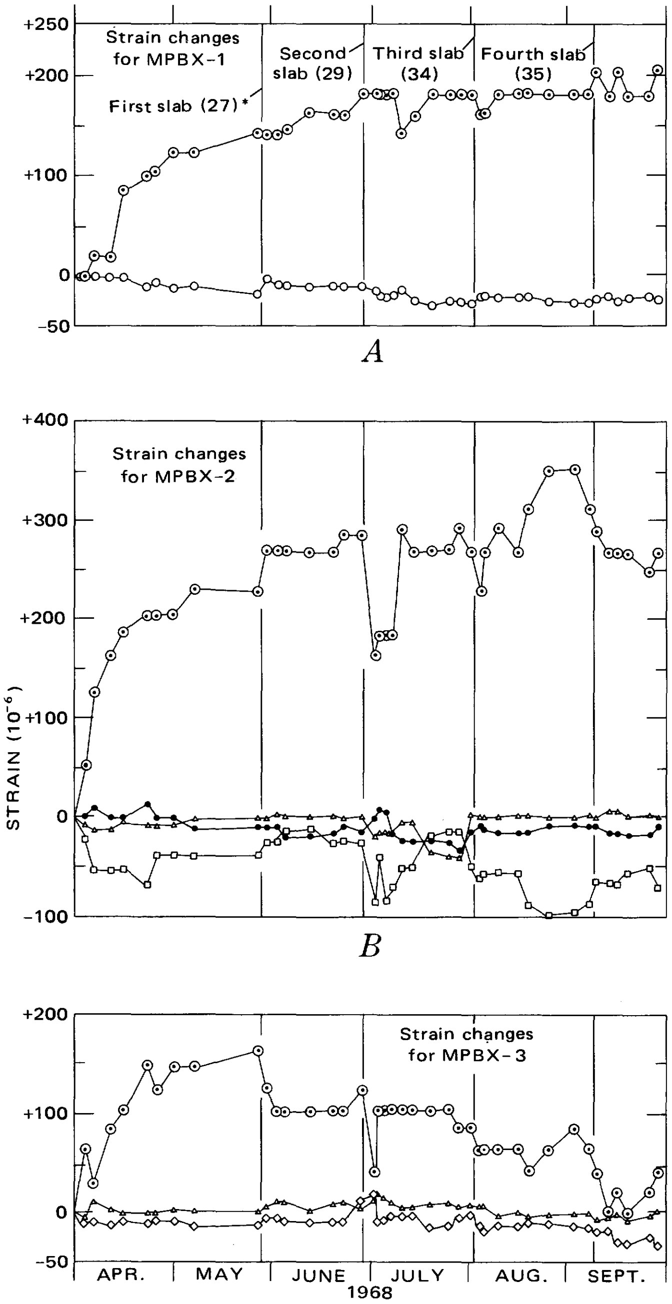

EXPLANATION

Strain changes for borehole intervals, measured from collar of borehole

	m	ft
⊙	0- 1.2	0- 4
▫	1.2- 3.0	4-10
◇	1.2- 6.1	4-20
○	1.2-12.2	4-40
•	3.0- 6.1	10-20
▵	6.1-12.2	20-40

FIGURE 41.—Strain changes for multiple-position borehole extensometers in roof of room 2. *, see figure 26 for location of slabs. +, compression; =, tension. Strains are based on anchor displacements.

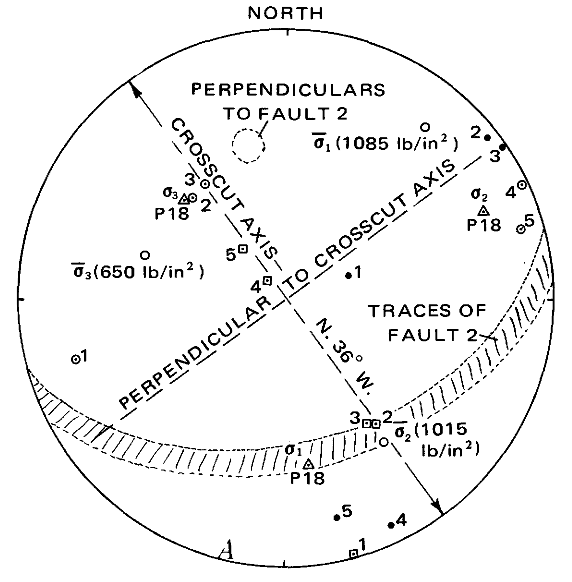

Probe 24 (5.5 m or 18 ft depth)

TIME		INTERVALS
1		Apr. 5, 1968
2		Apr. 23, 1968
3	Apr. 3, 1968 to	Apr. 30, 1968
4		May 7, 1968
5		May 26, 1968

$\Delta\sigma_1$ ⊙ }
$\Delta\sigma_2$ • } Probe 24
$\Delta\sigma_3$ ⊡ }
$\bar{\sigma}$ ○ Average principal stresses
σ △ Probe 18 principal stresses

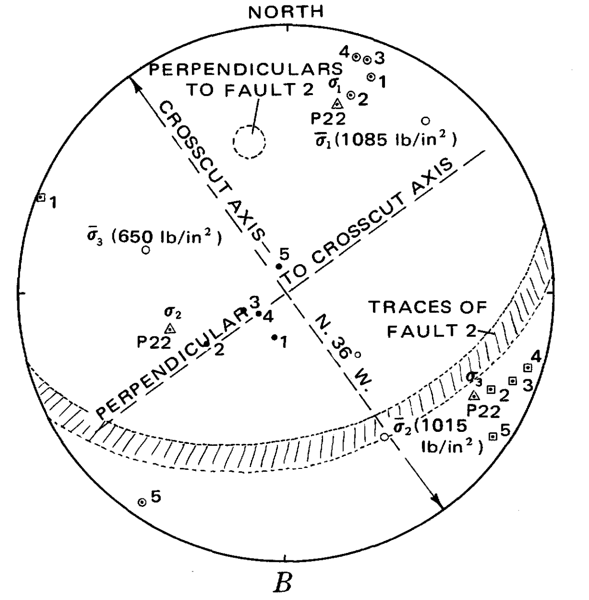

Probe 25 (1.2 m or 4 ft depth)

TIME		INTERVALS
1		Apr. 11, 1968
2		Apr. 15, 1968
3	Apr. 5, 1968 to	Apr. 23, 1968
4		May 7, 1968
5		May 26, 1968

$\Delta\sigma_1$ ⊙ }
$\Delta\sigma_2$ • } Probe 25
$\Delta\sigma_3$ ⊡ }
$\bar{\sigma}$ ○ Average principal stresses
σ △ Probe 22 principal stresses

FIGURE 42.—Principal stress changes of probes 24 (*A*) and 25 (*B*) before room 2 excavation.

zontal and approximately perpendicular to the crosscut axis and parallel to the strike of fault 2. The data show an exchange of positions of $\Delta\sigma_1$, $\Delta\sigma_2$, and $\Delta\sigma_3$ with time, indicating alternation of stress axes. We observed a similar behavior when fault 1 was penetrated during the excavation of room 1 (figs. 32, 33). The data from probes 24 and 25 suggest that there was movement along fault 2 prior to May 26 that disturbed the stress field.

A similar plot (fig. 42*B*) of stress-change data before room widening from shallow probe 25, which was more remote from fault 2 than probe 24, shows the principal stress-change directions also clustering in three small areas. These changes, unlike the stress-change directions at probe 24, do not appear to be related to either the plane of fault 2 or the direction of the excavation. Figure 42 also has plotted on it the average principal stress directions and magnitudes of the in situ stress field and the orientations determined by the overcoring of probes 18 and 22 (fig. 28). The correspondence of the average in situ principal stress directions with the principal stress-change directions at probe 25 suggests that the orientation and magnitude of in situ stresses at this location are probably the controlling factors on stress changes taking place before major room 2 excavation.

During this time, MPBX-3 (fig. 41*C*) showed vertical compressive strains from 0 to 1.2 m (0–4 ft) above the roof, low-magnitude tensile strains from 1.2 m to 6.1 m (4–20 ft), and nearly zero strain from 6.1 to 12.2 m (20–40 ft). MPBX's 1 and 2 (figs. 41*A*, 41*B*) showed similar strains during this interval. MPBX-1, the closest instrument to fault 2, showed compressive strain from 0 to 1.2 m (0–4 ft), and slight tensile strain from 1.2 to 12.2 m (4–40 ft). MPBX-2, adjacent to probes 15 and 19, (figs. 40*A*, 40*B*) showed compressive strain from 0 to 1.2 m (0–4 ft), tensile strain from 1.2 to 3.0 m (4–10 ft), and nearly zero strain from 3.0 to 6.1 m (10–20 ft) and from 6.1 to 12.2 m (20–40 ft). These data suggest that the initial transition rounds and presplits on the southeast side of room 2 triggered additional adjustment along fault 2, which in turn distrubed the stress field in the footwall of fault 2.

The in situ stress data for probes 18, 21, and 22, located 9.4–11.3 m (31–37 ft) west-northwest of probe 25 (table 12), show that the horizontal stresses are similar in magnitude to the vertical stresses, and the vertical stresses are about two to three times greater than can be explained by the overburden load. The principal stress directions determined from probes 18 and 22 are included in figure 42.

The changes that took place during the excavation of the northeast side of the transition zone can be explained by considering figure 43, a vertical section along the central crosscut. Figures 43*A* and 43*B* are a sketch of the probable orientation of maximum and minimum subsidiary principal stress trajectories before fault movement and of the subsequent mining-induced principal stress changes measured by probes 24, 25, 15, and 19. Figure 43*C* shows a sketch suggesting the effect on the stress field of movement along fault 2 and the probable stress-relieved zones and stress-increased zones in the footwall. The fault movement apparently decreased the compressive stress acting parallel to the crosscut axis in approximately the first 1.2 m (4 ft) of roof rock in the footwall. This roof-load had to be shifted upward along the fault until these stresses could be carried by the still-confined (stiffer) parts of fault 2.

Probe 24, closer to the fault than probe 25 and in a section of the footwall not relieved by fault movement, has superposed principal stress changes that are oriented perpendicular to and parallel to the fault plane. These stress changes correspond approximately to the in situ stress directions (fig. 44). The increased loads in the vicinity of probe 24 consisted of an initial substantial stress increase normal to the fault plane, followed in a month by a similar increase parallel to the fault plane.

The rock adjacent to probe 25, on the other hand, showed principal stress decreases which were nearly horizontal and vertical (fig. 42*B*). This probe, at a depth of 1.2 m (4ft) in the ceiling, is in a thin zone of rock that was partially destressed by fault movement and excavation. The components of stress changes (figs. 42*B*, 43*B*, 43*C*) represent decreases in the magnitudes of the in situ stresses in directions of decreasing confinement. Using relations shown in 1960 by Obert, Duvall, and Merrill (p. 12, fig. 5*c*), and approximation of the stresses in the vicinity of probe 25 prior to the fault movement was made. Excavation of the central drift in rock having approximately equal magnitude in situ horizontal and vertical stress components (table 12) probably moderately increased these stress magnitudes. As we explain in the following section, the theoretical tangential stress (σ_t) at the top of the drift is about two times the vertical (σ_v) or the horizontal (σ_h) stress. The maximum and minimum stress-change directions (fig. 42*A*) were rotated perpendicular and parallel, respectively, to the axis of the crosscut. This behavior suggests that there was a loss of confinement of the rock and a release of stress that was greatest approximately parallel to the central crosscut axis (σ_3 of in situ stress field). The presplit blasting on April 4, 1968, and the transition round blasting on April 23 and 27, 1968, may have triggered a stress release along fault 2. This stress release, accompanied by a confinement loss, could have caused the stress reorientation. Maximum confinement was then in a direction intermediate between the normal to the crosscut axis and σ_A of the in situ stress field. Intermediate confinement was approximately vertical. The stress-change directions (fig. 42*B*) are closely alined to corresponding directions of in situ stress confinement; that is, the least decompression, $\Delta\sigma_1$, is in the direction of maximum confinement, the intermediate decompression, $\Delta\sigma_2$, is in the

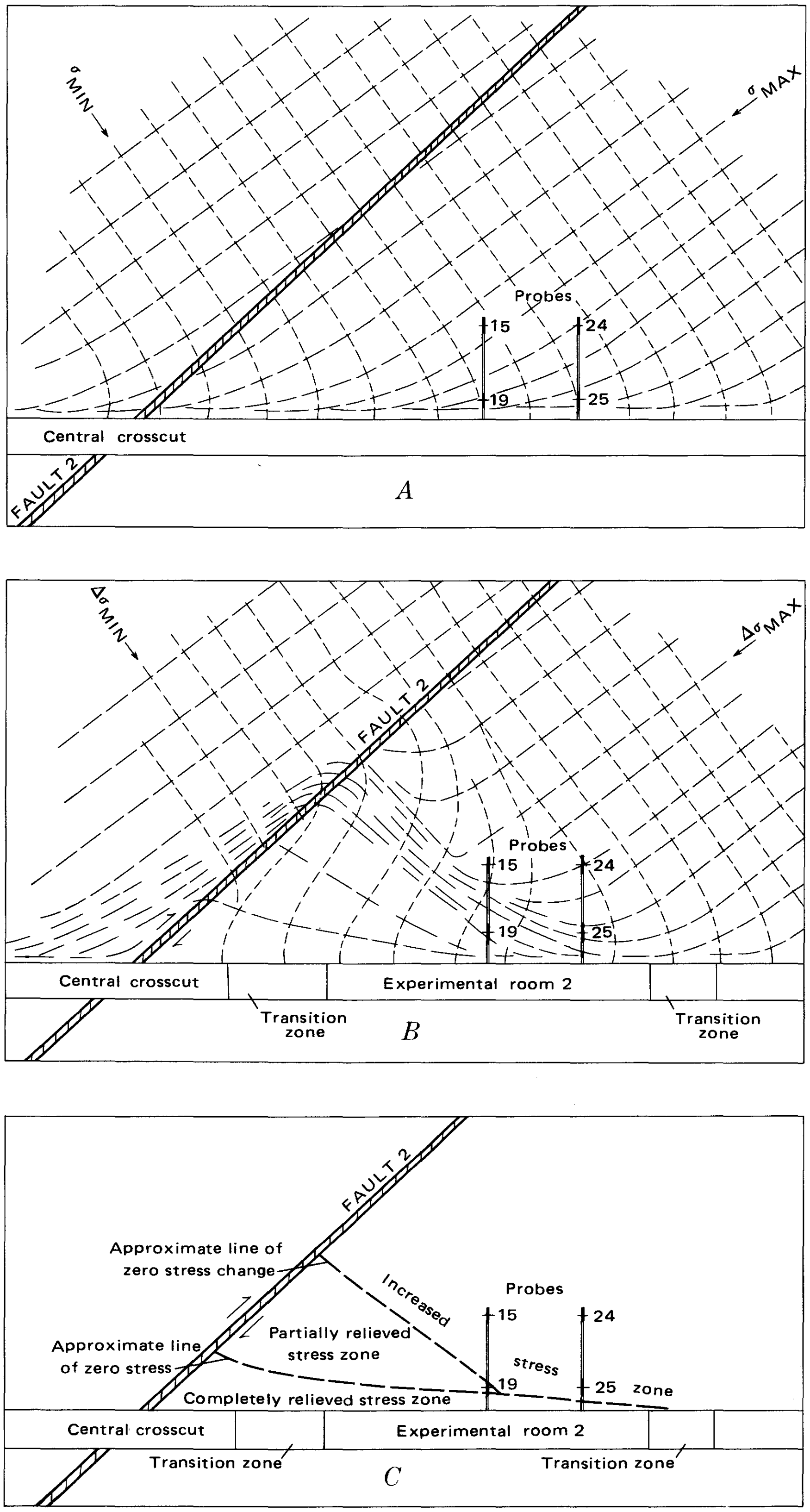
σ MIN
σ MAX
Probes
15
24
19
25
Central crosscut
FAULT 2
A
Δσ MIN
Δσ MAX
FAULT 2
Probes
15
24
19
25
Central crosscut
Experimental room 2
Transition zone
Transition zone
B
FAULT 2
Approximate line of zero stress change
Increased stress zone
Probes
15
24
Partially relieved stress zone
Approximate line of zero stress
19
25
Completely relieved stress zone
Central crosscut
Experimental room 2
Transition zone
Transition zone
C

◀ FIGURE 43 (facing page).—Generalized in situ stress conditions at several stages in the excavation of room 2. Excavation triggered fault movement, which in turn caused changes in the stress field. No stress scale is implied.

- *A*. Approximate orientation of maximum and minimum principal stress trajectories before excavation of room 2 and before movement along fault 2.
- *B*. Inferred orientation of maximum and minimum principal stress trajectories after movement along fault 2 and after excavation of room 2.
- *C*. Stress zones resulting from deformations and stress field shown in *B*, above.

direction of intermediate confinement, and maximum decompression, $\Delta\sigma_3$, is in the direction of minimum confinement.

The vertical compressive strain increase measured between 0 and 1.2 m (0 and 4 ft) at all MPBX installations prior to the excavation of room 2 (fig. 41) also can be explained by reverse movement on fault 2. Such movement would produce a decrease in compression in the roof rock parallel to the crosscut axis near the fault. Decompression was facilitated by the unrestrained roof at the boundary of the central crosscut (fig. 43). At this boundary the horizontal compressive stress acting parallel to the crosscut axis would be reduced. The vertical compressive strain (Poisson's effect from the horizontal decompression) would be greatest where restraint was least, in the near-roof rock.

The low-magnitude vertical tensile strains that occurred above 1.2 m (4 ft) at all MPBX installations were probably caused by minor downward adjustments of the rock above the 1.2-m- (4 ft) thick near-roof partially stress-relieved zone.

Major slabbing for room enlargement started on May 26, 1968, after the preliminary transition rounds were excavated. The four main slabs were taken at about monthly intervals, and the excavation of the room was finished by September 19 of the same year.

Data presented in figure 40 show that after the first slab was taken in room 2, and until the room was finished, the stress levels on all the probes generally became less compressive with time. After each slab was taken, sudden stress changes occurred that recovered rapidly. During the same interval, the MPBX data presented in figure 41 show that the 0- to 1.2-m (0–4 ft) intervals either were stable or underwent tensile strain, the 1.2- to 6.1-m (4–20 ft) intervals underwent tensile strain, and the 6.1- to 12.2-m (20–40 ft) intervals were nearly stable. It would appear that the rock mass up to 6.1 m (20 ft) above the central crosscut was decompressing as the room was widened. Deeper than 6.1 m (20 ft), negligible change occurred in the rock mass as the result of the excavation.

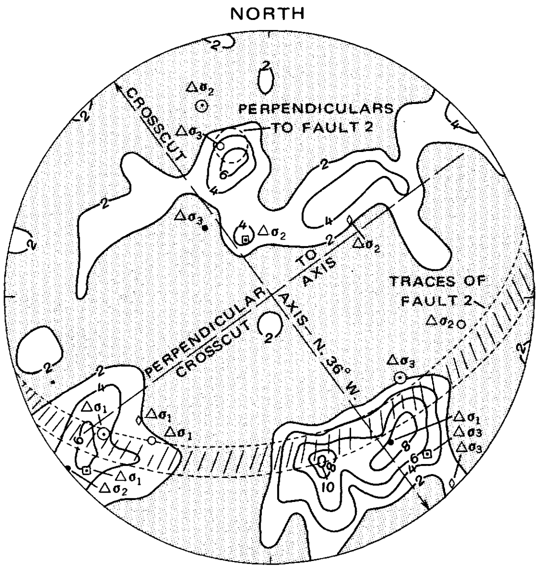

EXPLANATION

Probe	Symbol	Distance from room 2 into the roof (wall*) ft	m	Distance from fault 2 ft	m
15	○	18	5.5	25	7.6
19	⊙	4	1.2	35	10.7
24	•	18	5.5	36.5	11.1
25	⊡	4	1.2	46.5	14.2
B5	◊	16	4.9*	62	18.9

FIGURE 44.—Stress-change orientations determined from borehole probes around room 2: equal-area lower hemisphere projection showing joints, fault 2, and excavation orientation. Contour interval of joints is 2 poles per 1-percent area; 159 poles.

Rock-mass response, reflecting prolonged structural controls and high stress levels, such as we have just described, is probably most likely in massive rock rather than severely fractured rock. Indeed, room 2, the largest room in the mine, was excavated in some of the most competent rock in the study area (pl. 1) and required no artificial support.

An elastic analogy helps to illustrate our interpretations. The excavation of room 2 by enlarging the central crosscut can be compared to the plane-strain approximation of widening a nearly circular (ovaloidal) opening within a semi-infinite plate having a width-to-height ratio of slightly less than unity (W_0/H_0=0.8), to a rectangular opening with rounded corners having a width-to-height ratio of 3 (W_0/H_0=3). Again using the relationships developed by Obert, Duvall, and Merrill (1960, p. 9, 10, 12, 14), we can compare the initial central crosscut to an ovaloid opening in a hydrostatic stress field having a horizontal stress component nearly equal to the vertical component; thus, $\sigma_h/\sigma_v \approx 1 = M$ (table 12). The tangential stress concentration at the center top surface of the nearly circular (ovaloid) opening would be approximately twice the horizontal or vertical stress component; that is, $\sigma_t \approx 2\sigma_h \approx 2\sigma_v$. In widening the opening to a rectangular opening with $W_o/H_o=3$, the tangential stress on the center top surface would then be about three-quarters of the horizontal or vertical stress; that is, $\sigma_t \approx \frac{3}{4}\sigma_h \approx \frac{3}{4}\sigma_v$. The tangential stress at the center of the roof of the rectangular opening was then less than half what it was before the opening was widened. Thus, the elastic response of the tangential stress in the roof of the central drift should have been to decompress as the widening of room 2 proceeded. The decompressive stress changes should and did reach a maximum within the completely relieved zone, as shown in figure 43, decreasing upward and becoming negligible at approximately 6.1 m (20 ft) above the roof of the room in the undisturbed in situ stress field. This decompression above the ceiling indicates that the roofload or abutment load caused by lateral excavation was being transferred upward and was arching progressively higher above the excavation. Probes 15 and 24, approximately 4.3 m (14 ft) above the initial completely relieved zone, partially reflect this progressive upward transfer of load. Probe 24, which had a preroom-excavation monitoring period, showed an initial increase in compression before room excavation. Both instruments showed a net decompression in all directions during room excavation, followed by stabilization. Probes 19 and 25, on the other hand, being within the 1.2-m (4 ft) relieved zone, should have undergone only minor decompression during room widening. The data for probe 25 indicate that this did happen. The net change was slightly compressive after excavation ceased. The zone probably was not completely relieved in all directions by the initial fault movement, and some components of decompression were observed in directions of decreased confinement. Probe 19, however, showed a progressive net decompression in all directions throughout the period of measurement. Perhaps continued fault adjustments caused localized stress relief of rock during excavation.

The concentration centers of the principal stress-change directions for probes 15, 19, 24, and 25 are shown in figure 29. Superposed on the diagram are major geologic features and excavation orientation that appear to exert varying degrees of control upon the stress field. The geologic features include the orientation of fault 2 and contours of poles of major joint sets. The most prominent joint set is that of foliation joints which are oriented nearly perpendicular to the fault plane, a common relation in this part of the mine.

The stress changes that occurred at probes 15 and 19 appear to be strongly influenced by fault 2 in that the principal stress-change directions ($\Delta\sigma_1, \Delta\sigma_2, \Delta\sigma_3$) either lie within the fault plane or nearly coincide with the perpendicular to the fault. The stress changes occurring at probes 24 and 25 may have been more strongly influenced by the room orientation and joint sets than by the fault. The principal stress-change directions aline closely with these features. The $\Delta\sigma_1$ direction for probes 15, 19, and 25 and the $\Delta\sigma_2$ direction for probe 24 are nearly perpendicular to the room axis or in the same direction as the widening of the crosscut. One of the major joint sets is nearly perpendicular to this direction and parallel to the room axis.

The least decompression occurs normal to the room axis for three of the four probes in the roof and only intermediate decompression for the fourth probe; it is inferred that the greatest constraint to deformation (confinement) is perpendicular to the room axis. The joint set parallel to the room axis (fig. 29) does not significantly affect confinement across these joints, probably owing to their tightness and lack of alteration. Although the room excavation proceeded perpendicular to the crosscut axis, the room was always longer parallel to the crosscut axis. Maximum confinement was horizontal and perpendicular to the room axis. Accordingly, minimum decompression in the rock in the roof of the room occurred as anticipated by elastic theory, perpendicular to the room axis.

The long axis of the room should be parallel to the direction of least confinement of the roof rock. For probe 25, in the lower partially relieved zone, this appears to be true. In addition, the greater compressibility of the rock perpendicular to the foliation and prominent foliation joints acts to decrease confinement along the room axis. However, probe 24, which is 4.3 m (14 ft) above the relieved zone, was still compressed by the arched roofload. The fact that more rock has been excavated in the direction of the room axis than in other directions may explain why the roofload at depth is greatest in this direction. As the room was widened the compressive roofload was transferred higher into the rock and a strong constraint was thereby maintained in the direction of the room axis. A minimum decompression along the crosscut axis was observed at deep probe 24 after postexcavation stability was achieved.

The maximum decompression direction at deep probe 24 and the intermediate decompression direction at shallow probe 25 are nearly coincident. They dip steeply parallel to the room (crosscut) axis and normal to a strong joint set (fig. 29). The deep probe 24 had the least confinement in the direction of decreasing overburden to the ground surface and apparently confinement was reduced by the strong joint set, which is approximately parallel to the ground surface. At probe 25 the intermediate confinement was apparently controlled by the same joint set.

In summary, the compressive stress concentration in the rock mass in the roof of the room at probe 24 migrated upward and southerly—a direction that coincides with the minimum overburden thickness, with the joint set normal, and with the room axis. The resulting decompression was maximum in this direction. On the other hand, probe 25, in rock that was partially relieved prior to room excavation, was not so much affected by the upward migration of the roofload as it was affected by reduced confinement in the direction of the room axis. Foliation joints had the greatest influence on decreasing restraint in this zone.

Fault 2 had a great influence upon the principal stress-change directions of probes 19 and 15. Deep probe 15, which is in the unrelieved zone, underwent maximum decompression normal to the fault, accompanied by minimum and intermediate decompression in directions parallel to the fault surface. The minimum decompression direction was nearly normal to a major joint set and to the room axis. It would appear that as the roofload migrated upward during room excavation fault 2 provided the least constraint, whereas the short room dimension provided the maximum constraint. Other joints were not effective in reducing constraint perpendicular to the room axis. The intermediate constraint was parallel to the fault surface but does not appear to be related to other geologic or excavation factors.

Probe 19, in the shallow, partially relieved zone, behaved in a manner similar to deep probe 15 above it in that the principal stress-change directions were nearly parallel to or perpenducular to the surface of fault 2. As seen in figure 29, $\Delta\sigma_1$, the least decompression, was parallel to the surface of fault 2 and perpendicular to a major joint set and the room axis. The intermediate decompression, $\Delta\sigma_2$, was nearly perpendicular to fault 2, and the maximum decompression, $\Delta\sigma_3$, which lay in the fault plane, was approximately perpendicular to the foliation joints and approximately parallel to the room axis.

The constraint near shallow probes 19 and 25 in the relieved zone was similar, except that probe 19 was influenced more by fault 2 than was probe 25. Both the maximum and minimum stress-change directions sensed by probe 19 are parallel to fault 2. The intermediate stress-change direction sensed by probe 19 lay closer to the perpendicular to fault 2 than the intermediate stress-change direction sensed by probe 25, which was more influenced by foliation joints.

DISCUSSION OF STRESSES IN THE EXPERIMENTAL MINE

Harrison and Moench (1961) and Moench and Drake (1966a) have distinguished both Laramide and Precambrian regional joint systems in the Idaho Springs area. Moench and Drake (1966a, p. 43) suggested, on the basis of data on faults, joints, and veins, that the stress field was compressive and was oriented east-northeast in early Tertiary time. Later in Tertiary time, these authors postulated that the region was subjected to tensional stress also oriented east-northeast. R. H. Moench (written commun., 1974) found that the youngest fault movements (postmineralization) were noted on faults that trend north and northwest, appropriate for σ_1 oriented about N. 12°W. and σ_3 about N. 78°E. (both presumably horizontal). Our measurements throw little light on these generalities. In fact, the five in situ stress determinations were marginally adequate to describe the stress field in one section of a mine in the Idaho Springs district. If one considers the effects of residual stresses in addition to tectonic and gravitational forces and the complex tectonic history, as well as variations in rock composition, it is perhaps reasonable to expect variation, rather than consistency, in stress magnitudes and orientations. Boundary stresses could change with depth and, in the case of most near-surface measurements in mountainous regions, they would be influenced by topography.

We have, therefore, resisted the temptation to apply the data gained in this investigation to areas remote from the field site. We believe that to do so, without intermediate measurement locations, would oversimplify, perhaps incorrectly, regional structural relations. We can interpret the rock behavior encountered in the experimental mine with greater confidence.

The unequal compressive stresses measured in opposing walls of fault 1 are difficult to explain by either overburden or tectonic loading; likewise, the high-magnitude vertical decompressive stresses associated with the excavation of room 1 do not fit these conventional loading conceptions. It is unlikely that such large stress concentrations (differences) could be due to the geometry of the opening or to contrasting material properties. The magnitudes of vertical stresses approximate those of horizontal stresses at a given location and, at the shallow depth of the mine, are probably too large to be produced by either a gravitational or a tectonic boundary load. The experimental mine is situated well above the nearby surface drainage to the south and east, which would reduce the magnitudes of transmitted boundary loads.

In addition to the overburden load, and possibly tectonic stress components, the rock mass at the field site contains releasable residual ("locked-in") stresses that are in turn related to past geologic processes. The presence of unequal compressive stresses in the walls of faults suggests to us that ancient fault movement preferentially relieved stresses, or concentrated more compression in one wall than in another. The effect would be to store more strain energy in the less relieved block while releasing part of the strain energy in the adjacent block. Rock near several probe locations showed early stress changes alined with foliation and later changes alined with fault orientation. Drilling and blasting apparently disturbed the fault equilibrium, triggering a release of residual stress. The resulting stress change imposed a new orientation on the stress field at several locations.

Stress changes can also be activated by overcoring. The strain energy released can be large, as shown by the 4,350-lb/in^2 compressive stress released by coring a rock sample after it was removed from the mine. Residual stresses of these magnitudes, locked in the rock fabric during past episodes of deeper burial and more active tectonism, can account for the magnitude of the stress changes measured in the vicinity of the excavations.

Stress changes occurred as much as seven tunnel diameters ahead of the face, suggesting that releases of residual strain energy may act for considerable distances along faults and foliation.

Decompressions, such as were monitored by probes 5 and 8 in the walls of room 1, the roof of room 2, and ahead of the advancing crosscut, may be reasonably explained by the release of residual strain energy. An expected and observed concentration of compression at shallow depths in the walls was caused by load transfer due to removal of rock. Then, as excavation removed confinement, the walls of the excavations progressively deflected and deteriorated. The result was a large docompression.

The laboratory model-tunnel studies were only partly successful in predicting the stress changes encountered at the field location. The overriding influence of faults, joints, and foliation was not predictable from our simple unit-block models. The presence and behavior of residual stresses were not anticipated, and such a complex natural stress field would be extremely difficult or impossible to accurately simulate in a model. The models did, however, anticipate the underground findings of stress changes as much as two diameters ahead of the advancing tunnel face, but much less than the actual distance.

Continued effort will be required to improve our knowledge of geologic structures and associated stresses. A better understanding should come as investigators are able to distinguish overburden, boundary-tectonic, and residual components of the in situ stress field and then establish their relative importance.

REFERENCES CITED

Abel, J. F., Jr., 1967, Tunnel mechanics: Colorado School Mines Quart., v. 62, no. 2, 88 p.

Bastin, E. S., and Hill, J. M., 1917, Economic geology of Gilpin County and adjacent parts of Clear Creek and Boulder Counties, Colorado: U.S. Geol. Survey Prof. Paper 94, 379 p.

Bielenstein, H. U., and Eisbacher, G. H., 1969, Tectonic interpretation of elastic-strain-recovery measurements at Elliot Lake, Ontario: Ottawa, Dept. Energy, Mines and Resources, Mines Br. Research Rept. R 210, 64 p.

Brown, E. T., and Trollope, D. H., 1967, The failure of linear brittle materials under effective tensile stress, *in* Rock mechanics and engineering geology: Vienna, Springer-Verlag, v. 5, no. 4, p. 219-241.

Carter, W. H. N., 1961, A review of strata control experience in longwall working in Great Britain, *in* Internat. Conf. Strata Control, 3d, Paris 1960, Rev. de l'Industrie Minerale: p. 471-482.

Conway, J. C., 1963, An investigation of the stress distribution in a circular cylinder under static compressive load for varying boundary conditions: Pennsylvania State Univ. M. S. thesis, 201 p.

Cox, R. M., Jr., 1971, Rock behavior during experimental room excavation in Idaho Springs gneiss: Colorado School Mines D. Sci. thesis T-1283, 215 p.

Culver, R. S., 1967, Evaluation studies on rock bolts and rock mechanics instruments, phase 1: Omaha Dist. Corps Engineers Tech. Rept. 4, 74 p.

Denkhaus, H. G., and Hill, F. G., 1961, The conditions of the ground around excavations in hard rock at great depth, *in* Internat. Conf. Strata Control, 3d, Paris 1960, Rev. de l'Industrie Minerale: p. 243-251.

Edwards, R. H., 1951, Stress concentrations around spheroidal inclusions and cavities: Jour. Appl. Mechanics, v. 73, p. 19-30.

Galle, E. M., and Wilhoit, J. C., Jr., 1962, Stresses around a well bore due to internal pressure and unequal principal geostatic stresses: Soc. Petroleum Engineers Jour., v. 2, no. 2, p. 145-155.

Goodier, J. N., 1933, Concentration of stress around spherical and cylindrical inclusions and flaws: Jour. Appl. Mechanics, Am. Soc. Mech. Engineers Trans., v. 55, p. 39-44.

Harrison, J. E., and Moench, R. H., 1961, Joints in Precambrian rocks, Central City-Idaho Springs area, Colorado: U.S. Geol. Survey Prof. Paper 374-B, 14 p.

Henshaw, H., 1961, *Discussion of* Carter, W. H. N., A review of strata control experience in longwall working in Great Britain, *in* Internat. Conf. Strata Control, 3d, Paris 1960, Rev. de l'Industrie Minerale: p. 484.

Lee, F. T., Nichols, T. C., Jr., and Abel, J. F., Jr., 1969, Some relations between stress, geological structure, and underground excavation in a metamorphic rock mass west of Denver, Colorado, *in* Geological Survey research 1969: U.S. Geol. Survey Prof. Paper 650-C, p. C127-C132.

Leeman, E. R., 1961, Measurement of stress in abutments at depth, *in* Internat. Conf. Strata Control, 3d, Paris 1960, Rev. de l'Industrie Minerale: p. 301-311.

———1964, The measurement of stress in rock; I, The principles of rock stress measurement; II, Borehole rock stress measuring instruments; III, The results of some rock stress investigations: South African Inst. Mining and Metallurgy Jour., v. 65, p. 45-114, 254-284.

Lovering, T. S., and Goddard, E. N., 1950, Geology and ore deposits of the Front Range, Colorado: U.S. Geol. Survey Prof. Paper 223, 319 p. [1951].

Medearis, Kenneth, 1974, Numerical-computer methods for engineers and physical scientists: Fort Collins, Colo., KMA Research, 275 p.

Moench, R. H., 1964, Geology of Precambrian rocks, Idaho Springs district, Colorado: U.S. Geol. Survey Bull. 1182-A, 70 p. [1965].

Moench, R. H., and Drake, A. A., Jr., 1966a, Economic geology of the Idaho Springs district, Clear Creek and Gilpin Counties, Colorado: U.S. Geol. Survey Bull. 1208, 91 p.

———1966b, Mines and prospects, Idaho Springs district, Clear Creek and Gilpin Counties, Colorado—Descriptions and maps: U.S. Geol. Survey open-file report, 214 p.

Moench, R. H., Harrison, J. E., and Sims, P. K., 1962, Precambrian folding in the Idaho Springs-Central City area, Front Range, Colorado: Geol. Soc. America Bull., v. 73, no. 1, p. 35-58.

Nichols, T. C., Jr., Abel, J. F., Jr., and Lee, F. T., 1968, A solid-inclusion borehole probe to determine three-dimensional stress changes at a point in a rock mass: U.S. Geol. Survey Bull. 1258-C, 28 p.

Obert, Leonard, and Duvall, W. I., 1967, Rock mechanics and the design of structures in rock: New York, John Wiley & Sons, Inc., 650 p.

Obert, Leonard, Duvall, W. I., and Merrill, R. H., 1960, Design of underground openings in competent rock: U.S. Bur. Mines Bull. 587, 36 p.

Portland Cement Association, 1952, Design and control of concrete mixtures [10th ed.]: Portland Cement Assoc., 68 p.

Potts, E. L. J., 1961, *Discussion of* Denkhaus, H. G., and Hill, F. G., The conditions of the ground around excavations in hard rock at great depth, *in* Internat. Conf. Strata Control, 3d Paris 1960, Rev. de l'Industrie Minerale: p. 252.

Reeper, F. J. M. de, and Bruens, F. P., 1961, Measuring the loads on roadway supports by means of strain gauges, *in* Internat. Conf. Strata Control, 3d, Paris 1960, Rev. de l'Industrie Minerale: p. 321-337.

Scott, G. R., 1973, Tertiary surfaces and depsoits of the Southern Rockies and their recognition [abs.]: Geol. Soc. America Abs. with Programs, v. 5, no. 6, p. 510.

Sims, P. K., and Sheridan, D. M., 1964, Geology of uranium deposits in the Front Range, Colorado, *with sections by* R. U. King, P. B. Moore, D. H. Richter, and J. D. Schlottmann: U.S. Geol. Survey Bull. 1159, 116 p.

Spackeler, G., 1961, *Discussion of* Carter, W. H. N., A review of strata control experience in longwall working in Great Britain, *in* Internat, Conf. Strata Control, 3d, Paris 1960, Rev. de l'Industrie Minerale: p. 483.

Spurr, J. E., and Garrey, G. H., 1908, Economic geology of the Georgetown quadrangle (together with the Empire district), Colorado, with general geology, by S. H. Ball: U.S. Geol. Survey Prof. Paper 63, 422 p.

Tooker, E. W., 1963, Altered wallrocks in the central part of the Front Range mineral belt, Gilpin and Clear Creek Counties, Colorado: U.S. Geol. Survey Prof. Paper 439, 102 p. [1964].

Turner, F. J., and Verhoogen, John, 1960, Igneous and metamorphic petrology [2d ed.]: New York, McGraw-Hill Book Co., Inc., 694p.

Tweto, Ogden, and Sims, P. K., 1963, Precambrian ancestry of the Colorado mineral belt: Geol. Soc. America Bull., v. 74, no. 8, p. 991-1014.

Varnes, D. J., 1970, Model for simulation of residual stress in rock, *in* Symposium on rock mechanics, 11th, Proc.: New York, Soc. Mining Engineers, AIMMPE, p. 415-426.

Varnes, D. J., and Lee, F. T., 1972, Hypothesis of mobilization of residual stress in rock: Geol. Soc. America Bull, v. 83, no. 9, p. 2863-2865.

☆ U.S. GOVERNMENT PRINTING OFFICE 1976—777-034/21